Università degli Studi di Milano - Bicocca
Facoltà di Scienze Matematiche, Fisiche e Naturali
Corso di Dottorato di Ricerca in Scienze Chimiche
XXII ciclo

Charging phenomena of supported metal clusters and effects on chemical reactivity: a DFT study

A.A. 2008/2009

Ph.D. dissertation
Sabrina Sicolo

Supervisor
Prof. Gianfranco Pacchioni

Acknowledgements

This work wouldn't have been possible without the aid and the guide of the members of my research group: Prof. Gianfranco Pacchioni, Dr. Livia Giordano, Dr. Cristiana Di Valentin and quasi-Dr. Umberto Martinez, a friend more than a colleague.

Contents

Chapter 1

Introduction

Change starts when someone sees the next step.

William Drayton

1.1 The gold rush of heterogeneous catalysis

Gold is certainly the metal which in the past decade has attracted more interest in the field of catalysis by supported metal clusters. The pioneering work of Masatake Haruta shed a new light on the chemical properties of gold, contradicting the commonplace about its noble nature, and ultrasmall gold particles have begun to garner attention for unique and unexpected catalytic properties.[1–9] This unusual catalytic activity has been proved to hold for a variety of different reactions, amongst which the very well known and studied low temperature CO oxidation,[10] the selective oxidation of propene to propene oxide,[11] the water gas shift,[13] the NO reduction,[14] the selective hydrogenation of acetylene and butadiene,[15] the hydrochlorination of ethyne to vinyl chloride[16–18] and as a bimetallic component of vinyl acetate monomer production catalysts.[19,20] In particular, the low temperature CO oxidation is important both as a model system and for applications in indoor air quality[21] and as a guard bed catalyst to prevent CO poisoning of proton exchange membrane fuel cells.[22–24] Several experimental and theoretical efforts are currently being performed, aiming at understanding such a different chemical reactivity of nanometer-sized gold particles with respect to the massive phase.

Gold is a unique element even in the atomic form, as it exhibits larger relativistic effects than its neighbours and any other element with $Z < 100$, Z being the atomic number. Relativistic effects can qualitatively be attributed to the high speeds of all electrons if they move nearby a heavy nucleus. The relativistic effects on valence-shell properties increase down a column of the periodic table roughly like Z^2. The

subsequent mass increase leads to an energetic stabilization and radial contraction of the s and p orbitals. The contraction of those orbitals leads in turn to a stronger screening of the nuclear attraction, and hence to a destabilization and expansion on the d and f orbitals.[25] Relativistic effects explain many of the differences and some of the similarities between the 5th and 6th row of the Periodic System. A well-known example is the difference between silver and gold. A relativistic bond-length contraction exists, which also correlates roughly with Z^2. According to this contraction, Au-based single bonds are at the same time shorter and stronger than the corresponging Ag-based bonds. The higher cohesive energy of gold as compared to silver can be explained by the increased participation of the d orbitals in metal-metal bonding. Gold also has the highest electronegativity (2.54) any metal and is only slightly more electropositive than such non-metals as sulfur and iodine. Gold possesses an extremely high electron affinity (2.31 eV) and ionization potential (9.22 eV) as well.[26]

On the experimental side, the catalytic activity of supported gold clusters was discovered in 1987 by Haruta *et al.*:[1] a variety of gold catalysts was used to catalyze the oxidation of carbon monoxide at temperatures as low as 200 K. The novel catalysts, prepared by coprecipitation, were composed of ultra-fine gold particles and one of the oxides of 3d transition metals of group VIII, namely, Fe, Co, and Ni.

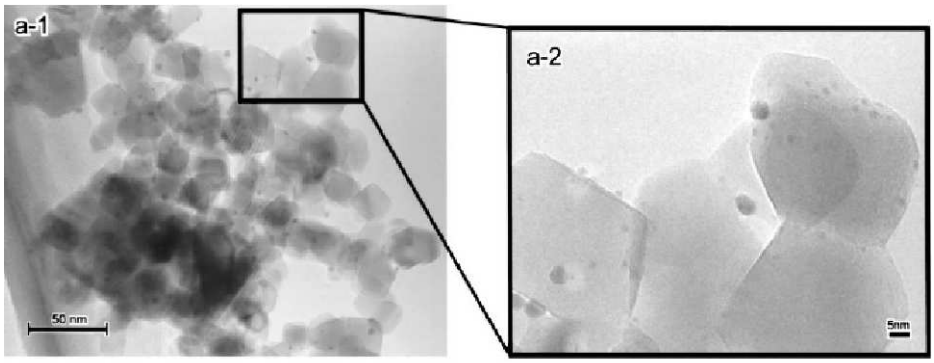

Figure 1.1: TEM images of Au/TiO_2 catalysts calcined at 473 K taken at a magnification of 200,000. Partially enlarged image of section a is shown in the inset.[27]

By way of illustration, Figure 1.1 shows TEM images of a Au/TiO_2 catalyst prepared by deposition-precipitation followed by calcination at 473 K; the catalyst is

active in the low temperature oxidation of CO, and the TEM image gives an overall impression over the mean particle size of such an active sample, which turned out to be about 2.5 nm.[27]

A few models and explanations have been suggested for rationalizing the catalytic activity of gold particles, which is supposed to be ascribed to the interplay between several factors. In the first place, the appearance of activity as a function of the dimension of the particles (Figure 1.2)[11,12] may be related either to new electronic properties of sub-nanometer sized clusters which don't have a counterpart in the bulk[28,29] (Figure 1.3a) and/or to the availability of under-coordinated sites, like corners and edges, that by definition exhibit a more pronounced reactivity with respect to regular sites of the surface and bulk (Figure 1.3b).[30]

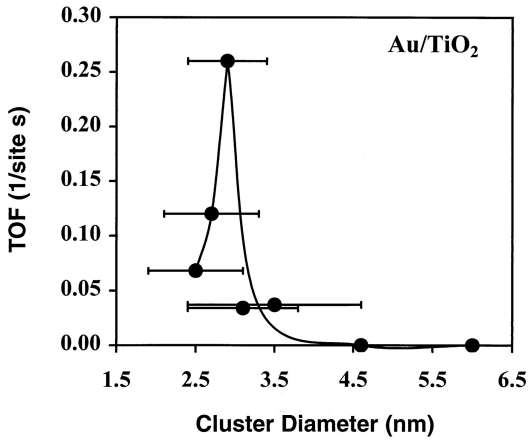

Figure 1.2: CO oxidation turnover frequencies (TOFs) at 300 K as a function of the average size of the Au clusters supported on a high surface area TiO_2 support.[12]

Besides the dimension, also the shape of the particles seems to play a decisive role in determining the catalytic activity of gold clusters.[35] The experimental evidence that semi-spherical supported particles are more active then spherical ones, the shape being determined by the synthesis technique,[5] points toward the role of the substrate in the reactivity of the particles. On one side, the perimeter of the semi-spherical islands provides adsorption and reaction sites for adsorbed molecules (perimetral model); on the other side, the maximized contact area between the particle and the substrate suggests an extra-stabilization arising from the interaction

between the metal and the support. A strong interaction of the metal with the support also prevents the coalescence of the particles, resulting in smaller and more dispersed clusters. This condition fulfills at the same time the requirements on the size of the clusters – the smaller, the better – and on the surface area, which for a catalyst must be high.

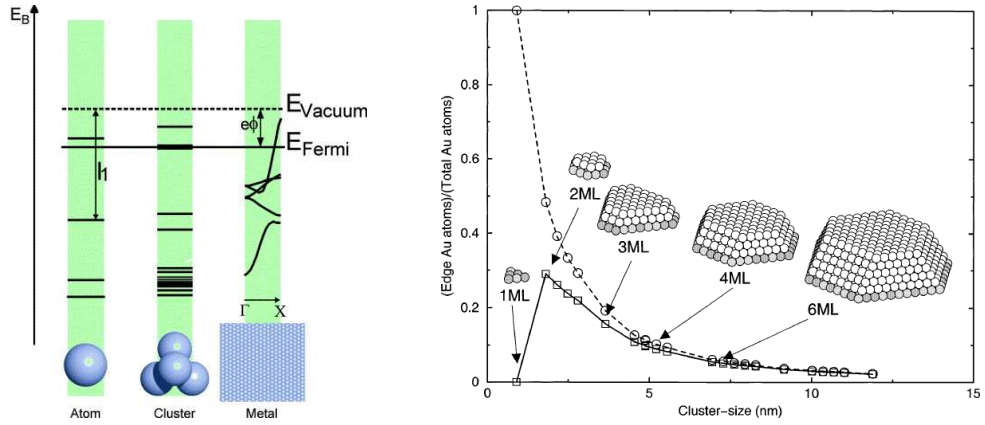

a b

Figure 1.3: a) Diagram illustrating the transition from an atom to a metal (E_B, binding energy; I_1, first ionization energy; e: electron charge; φ: work function; Γ, X: symmetry points in the Brillouin zone);[36] b) Calculated step density for Au particles on TiO_2 as a function of particle size. (○) and (□) correspond to the total and free step sites on the Au particles. Free are the step sites not in direct contact with the support. Lines through the two sets of points are only drawn as a guide to the eye. Insets illustrate the corresponding Wulff constructions for selected particle sizes.[30]

Recently, aberration-corrected scanning transmission electron microscopy has been used to analyze several iron oxidesupported catalyst samples, ranging from inactive ones to others with high activities.[31] It has been found that high catalytic activity for carbon monoxide oxidation is related to the presence of bilayer clusters that are $\sim$ 0.5 nanometer in diameter and contain only $\sim$ 10 gold atoms (Figure 1.4). This result regarding the activity of bilayer clusters is consistent with modellistic studies, involving both theoretical simulations and experimental model catalyst systems.[32–34]

How to take advantage of the influence of the support for the stabilization and activation of metal clusters is indeed the topic of this work. It must be pointed out

that the gold is not the only metal which has been taken into account in the course of this work.

Late transition metals – whose role in catalysis is undiscussed – have often been considered, mainly within the framework of comparative studies, but it is a matter of fact that gold has always emerged as a peculiar and strikingly reactive case, and for this reason many projects dealing with chemical reactivity more than phenomenology have been focused on it.

The thesis is organized as follows. Later in this chapter an overview of the motivation is given: the concept of functionalized support is introduced through one of

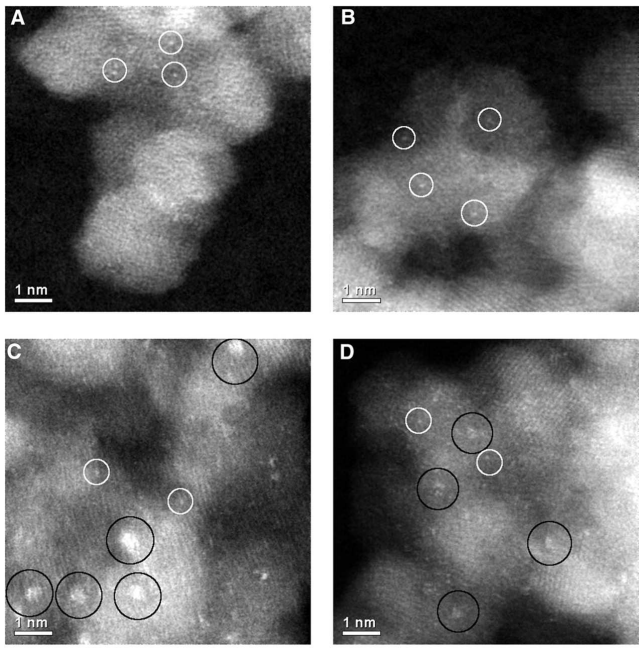

Figure 1.4: High-magnification STEM-HAADF images of (A and B) the inactive and (C and D) the active Au/FeO_x catalysts acquired with the aberration-corrected JEOL 2200FS. The white circles indicate the presence of individual Au atoms, whereas the black circles indicate subnanometer Au clusters consisting of only a few atoms. Note the presence and image intensity difference of two distinct cluster-types: In (C) there are 0.5 nm higher-contrast clusters, whereas in (D) 0.2- to 0.3-nm low-contrast clusters dominate. This difference indicates that bilayer and monolayer subnanometer Au clusters are present in the active catalyst[31]

the most important reactivity studies of supported clusters available in the literature (Sec. 1.2). Making use of the conceptual importance of this aforementioned work, two alternative methods have been proposed by our group in order to improve the mechanism that seems to be at the basis of the enhanced catalytic activity of supported metals. The principles of these methods are given in the following sections (Secs. 1.3 and 1.4).

The second chapter deals with the computational models employed in the simulation of surfaces.

The last part of the thesis gives an account of the results achieved in this work. The results are sorted depending on the functionalization method (Parts I and II).

1.2 Metal clusters on oxides

The structure and properties of small metal particles represent a field of research which has attracted a lot of attention during the last years: as an intermediate state of matter between atoms in the gas phase and the solid state, they often exhibit exceptional physical and chemical properties which are not scalable from those of the corresponding bulk materials (*non-scalable regime*). While these properties are essentially determined by the size of the particle in the case of free unsupported clusters, the interaction with a substrate turns out to be crucial for supported systems, modifying, introducing or strengthening certain features.

One of the areas where deposited metal particles are technically employed to a large extent is heterogeneous catalysis. In real catalytic devices, an active component such as a transition metal is dispersed over a suitable support material, usually an oxide. In the first place this allows to achieve the highest possible surface area of the active phase. Because of the high degree of dispersion, however, particle size effects together with metal-substrate interactions can influence the catalytic behaviour significantly. Of course, how these effects can be exploited to improve the catalytic activity or the selectivity of a supported catalyst has always been a central issue in catalytic research.[37]

A key aspect of the stabilization (and activation) of metal atoms and clusters on the surface of an oxide is the role of point defects. Several chemical reactions taking place at an oxide surface are directly or indirectly connected to the presence of defects. Under-coordinated sites as well as point defects of the Schottky type

exhibit a peculiar reactivity that distinguishes them from the behaviour of a flat surface and thus opens the possibility to functionalize an oxide surface by creating defects in a controlled and tailored fashion.

One of the most interesting examples of the importance of surface point defects is the reactivity of oxygen vacancies (see also Sec. 1.3). There is general consensus about the fact that surface oxygen vacancies act as shallow traps for metal atoms diffusing on MgO.[38–45] Investigations on size-selected small gold clusters soft-landed on a well-characterized MgO(001) surface with and without oxygen vacancies revealed that gold octamers bound to oxygen vacancies of the magnesia surface are the smallest known gold heterogeneous catalysts that can oxidize CO into CO_2 at temperatures as low as 140 K. The same cluster bound to a MgO surface without oxygen vacancies is catalytically inactive for CO combustion (Figure 1.5).[34]

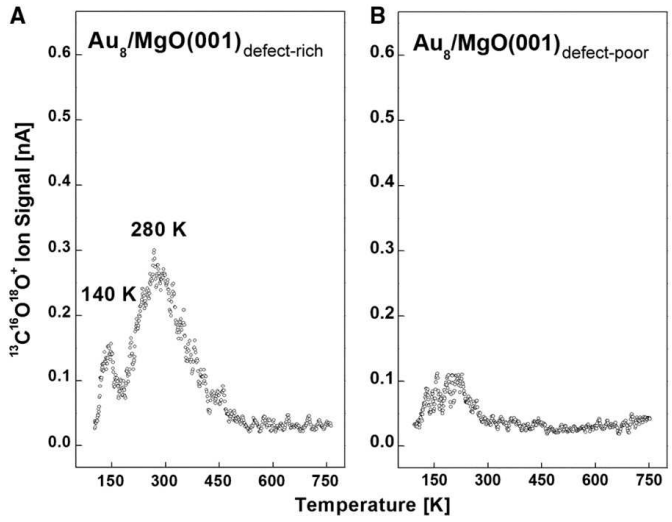

Figure 1.5: Mass spectrometric signals pertaining to the formation of CO_2 on Au_8 deposited on (A) oxygen vacancies rich and (B) oxygen vacancies free MgO(001) thin films.[34]

Quantum-mechanical ab initio simulations, in juxtaposition with laboratory experiments, indicate that charging of the metal cluster caused by partial transfer of charge from the substrate oxygen vacancy into the deposited cluster underlies the catalytic activity of the gold clusters. These investigations predicted that (i) the oxygen vacancies on the metal oxide support surface play the role of active sites, (ii)

these sites serve to anchor the deposited clusters more strongly than sites on the undefective surface, thus inhibiting their migration and coalescence, and, most important, (iii) these active sites control the charge state of the gold clusters, thus promoting the activation of adsorbed reactant molecules. The role of oxygen vacancies in the adsorption properties of metal particle has also been acknowledged by using adsorbed CO as probe molecule.[46]

The number of intrinsic surface oxygen vacancies on alkaline-earth oxides is however too small to be practically useful, and higher concentrations of these defects must be created via electron bombardment, using high-energy radiations or controlling the sample preparation to enhance their abundance.[47] Moreover, the general assumption that sees oxygen vacancies as nucleation sites has been recently questioned for the case of Pt and the transition metals at the right of the periodic table.[55,56] Furthermore, even the interaction with oxygen vacancies may not be sufficient to enhance the chemical activity: it has been discussed already that the gold octamer bound to oxygen vacancies of the MgO surface is the smallest cluster that can oxidize CO into CO_2,[34] despite the inactivity of smaller clusters like Au_4.

The motivation of this work has thus been the need for more viable and efficient methods for the generation of electron-rich surfaces and the subsequent stabilization of charged metal clusters. In particular, the stabilization and charging of metal clusters on electron-rich surfaces produced with two methods based on different chemical and physical principles has been studied.

The first method deals with the functionalization of an alkaline-earth oxide surface by exposure of polycrystals to hydrogen, alkali metals, or in general, to electron donors. This procedure results in the spontaneous ionization of the donor and the subsequent localization of electrons on under coordinated sites of the surface (electron traps), as it has been proved by experimental synthesis and characterization.[47] These trapped electrons act as efficient sites for nucleation and charging of metal nanoclusters from diffusion of deposited adatoms, and the activation toward the CO oxidation has been checked for gold by means of ab initio calculations in the framework of this work.

Charging of supported metal clusters can also be achieved basing on a different mechanism when an ultrathin oxide film (MgO, AlO_x, SiO_2) is grown on a metal substrate (Mo, Ag, NiAl).[48] When special conditions are fulfilled, electrons can tunnel through the thin oxide film to the supported cluster, resulting in a cluster anion.

The shape of these charged clusters differ substantially from those of the neutral counterparts: a dimensionality crossover and a corresponding enhanced wettability are observed as a result of the electrostatic interaction between the charged cluster and the metal support,[49–54] and it may be expected that this feature will also result in a different chemical reactivity.

1.3 Excess electrons stabilized on ionic oxide surfaces

Excess electrons can be generated in the bulk of ionic solids, where they are responsible for a characteristic absorption band in the visible region and, hence, are appropriately named color centers or F centers (abbreviated from the German word for color, farbe).

The stabilization of excess electrons by a two-dimensional array of ions, such as the surface of an ionic oxide, is an important issue, since charge localization and transport at oxide surfaces and interfaces are crucial phenomena in several fields of science and technology, ranging from photocatalysis to sensors and electronic devices. The earliest model of the surface electron trapping on oxides, proposed by Tench in the 1960's,[57] is the natural extension of the bulk anionic vacancies and it consists of a pyramidal hole generated on the (100) surface by removal of an O^{2-}_{5c} ion. This vacancy, labeled F^{2+}_{s}, can trap one or two electrons, producing surface F^{+}_{s} (paramagnetic) and F_{s} color centers, respectively. Recently, the model has been refined after the prediction,[58,59] later proven,[60,61] that oxygen vacancies form preferentially at low-coordinated sites such as steps, edges and corners of the surface.

Surface anionic vacancies are present on MgO powders subjected to extreme activation conditions (1073 K heat treatment), although their overall number is far lower than generally thought, even below the detection limit of EPR (5×10^{11} centers/cm^2).[61] Thus, to be observed, oxygen vacancies must be created either by electron bombardment or by changing the preparation method (and the stoichiometry) of the film.

EPR traditionally played a leading role in the study of point defects in materials and specifically excess electron centers in condensed matter.[62] This is true also for surface-trapped electrons. This highly sensitive technique provides an unsurpassed source of information of spin doublet electronic states. In favorable circumstances, the symmetry (point group) of the center can be ascertained and the distribution of

the unpaired electron spin density over the nuclei constituting the trapping site can be deduced. Generally, the most informative parameters derived from EPR come from the electron-nuclear (or hyperfine) interaction. Because analysis of the hyperfine coupling tensor provides a direct measure of spin density on the nearby nuclei, a realistic chemical and structural description of the surface traps can be achieved.[58]

Recent EPR and theoretical evidence has instigated a completely new debate on the whole idea of oxygen vacancies as electron-trapping sites, showing how other morphological features, commonly found on high-surface-area alkaline-earth oxides, can also trap electrons. These surface electrons can be stabilized by strong local potentials of positive and negative ions in particular arrays and in some cases even by single low-coordinated cations. In this way, the surface of the solid can be modified by the addition of electrons (creating an electron-rich surface), thereby opening up realistic possibilities to tune the optical, electronic, chemical and magnetic properties of these materials.

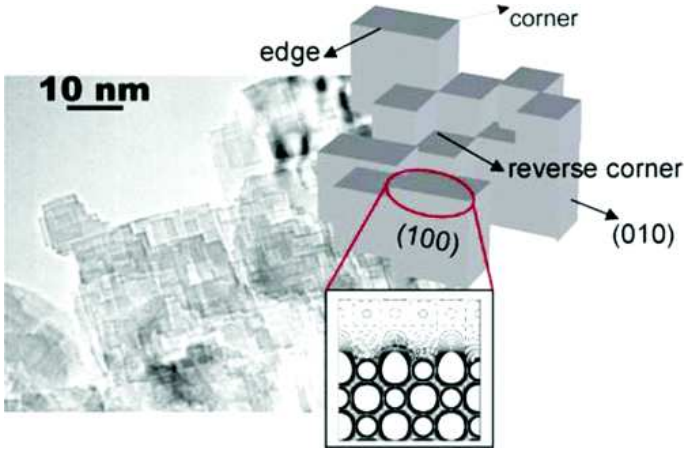

Figure 1.6: High-resolution transmission electron microscopy (HR-TEM) micrography of a high-surface-area polycrystalline MgO sample. A schematic model indicating the relevant surface sites discussed in the text is also shown. In the inset, the electrostatic potential in the xy plane through the edge is shown.[47]

Polycrystalline MgO, like the other alkaline-earth oxides, exhibits a NaCl-type structure and a morphology based on cubic crystals with extended (100) planar faces. Both Mg^{2+} and O^{2-} ions at these crystal facets are surrounded by five ions of

opposite charge in square pyramidal coordination and are chemically inert. Finely divided MgO materials are built up by assemblies of extremely small interpenetrated cubes with edges of approximate lengths ranging from 4 to 8 nm (Figure 1.6). Depending on the preparative method, specific surface areas of up to 1000 $m^2\ g^{-1}$ can be produced. As a result, the number of low-coordinated ions – primarily located at the edges (four coordinated (4c)), corners (3c) and other irregularities, such as steps and kinks – becomes more abundant. It is mainly at these low-coordinated, highly reactive sites that the formation of surface excess electron centers occurs by chemical doping.

Exposure of MgO[63] or CaO[64] surfaces to hydrogen atoms results in the spontaneous ionization, at temperatures as low as 77 K, of H· with the subsequent formation of excess electrons and extra protons on the surface, as schematically represented in eq. 1.1.

$$Mg_n^{2+}O^{2-} + H\cdot \longrightarrow Mg_n^{2+}(e^-)(OH^-) \tag{1.1}$$

The electron-trapping site can either be a single low-coordinated cation ($n = 1$) or a small array of surface cations ($n > 1$), while the proton is stabilized by a single O^{2-} anion in the form of a surface hydroxyl group. The formation of excess electrons may be regarded as a dissolution process, whereby hydrogen undergoes ionization despite its high ionization energy (13.6 eV). The reason for this unusual hydrogen chemistry is due to the strong proton affinity of the very basic O^{2-} surface ions coupled with the energy gain by trapping the electron near low-coordinated Mg^{2+} cations. The intriguing consequence of eq. 1.1 is that it provides a viable way of dropping excess electrons on specific surface sites.

A major point of interest concerns the precise description or nature of the surface-trapping sites. At least three different sites have been identified on the MgO surface that are able to spontaneously ionize H· atoms and stabilize the resulting products in the form of $(H^+)(e^-)$ pairs, according to eq. 1.1; these sites are illustrated in Figure 1.7. The sites consist of an electron trapped near an adsorbed proton (surface OH group): the plot of the spin density of an edge site (Figure 1.8) clearly shows that the electron is separated from the OH group, the electron density being localized on the low-coordinated cations of the surface (Mg_{lc}).
These trapped electrons are thermally very stable, as their ionization energies are of the order of 3 eV and more.[65] Although EPR spectroscopy has been fundamental in the reassignment of these new surface excess electron-trapping sites, important

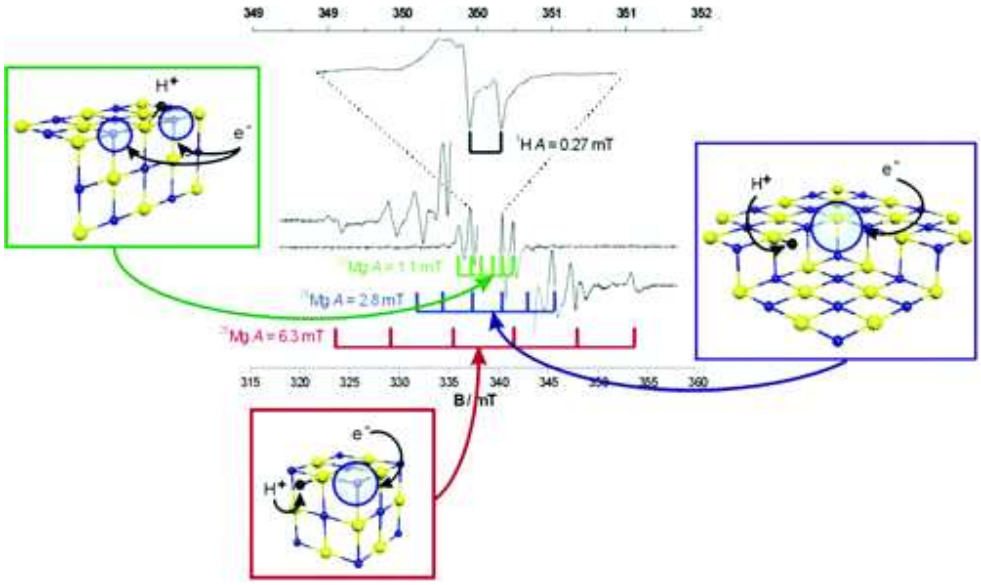

Figure 1.7: EPR spectrum and atomistic models of $(H^+)(e^-)$ centers on MgO.[47]

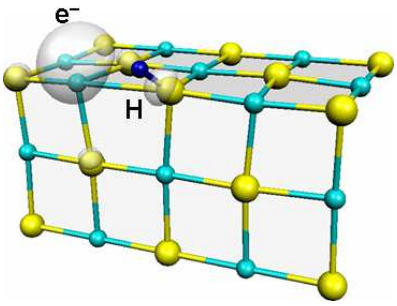

Figure 1.8: Spin density plot of a $(H^+)(e^-)$ center formed at an edge site of the MgO surface. The electron (e^-) resides on the Mg^{2+} cation near the adsorbed proton (H^+) of an OH group.

contributions have been also obtained by IR[66] and UV-vis[67] studies.

The chemical reactivity of electron-rich surfaces could offer new avenues for research in heterogeneous catalysis. As we have discussed in the previous section, enhanced catalytic properties were observed for selectively charged deposited metal nanoparticles on oxide surfaces. The number of intrinsic surface F centers

on alkaline-earth oxides is however too small to be practically useful, and higher concentrations of these defects must be created by means of severe experimental techniques. On the contrary, the viable and controlled chemistry involved in the formation of the $(H^+)(e^-)$ surface ion pairs by atomic hydrogen or via UV irradiation of MgO in molecular hydrogen could potentially provide alternative canditates to achieve the charging of metal clusters at specific sites and thereby open unprecedented pathways for the design and synthesis of a new class of supported catalysts.

1.4 Spontaneous charging of supported clusters on ultra thin films

Oxide thin films have been extensively used in the last two decades as model systems to unravel properties of supported metal catalysts, with the aim to provide an atomistic view of the processes governing the complex reactions which occur on heterogeneous catalysts.[36,68–70]

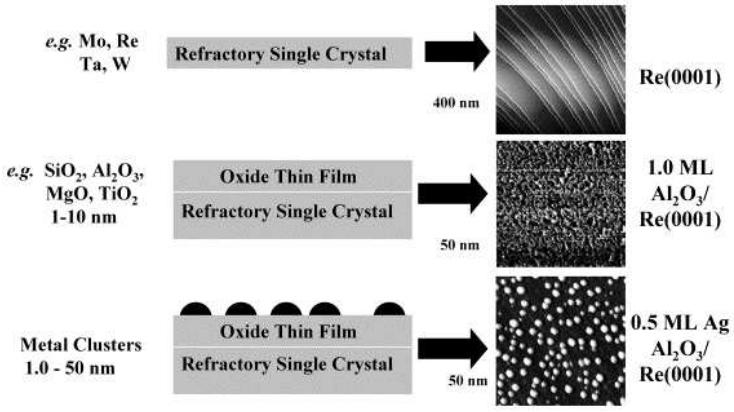

Figure 1.9: Schematic of a planar oxide-supported model catalyst preparation procedure with the corresponding STM images of each stage.[71]

Figure 1.9 shows the basic steps of the preparation of such systems, involving the chemical vapour deposition (CVD) of the oxide film followed by the deposition of metal clusters by means of physical or chemical methods. Oxide films were born with the purpose to mimic the features of bulk oxides, allowing at the same time

the use of surface science characterization tools, such as electronic spectroscopies and microscopies, that cannot be used on insulating materials. In most cases these films behave as the bare oxide surfaces; however, when the film thickness decreases to 1 nm or below, new unexpected properties can be observed. For instance, it has been predicted theoretically[72–75] and then experimentally confirmed[76,77] that a spontaneous charging of metal atoms and clusters adsorbed on ultrathin MgO films supported on Mo(100) or Ag(100) substrates can occur by means of direct electrons tunneling through the oxide layer. The same phenomenon has been predicted and later observed for electronegative molecular species, like NO_2.[78–81]

There is already a considerable amount of studies in the literature, regarding the peculiar reactivity of ultra-thin films that distinguishes them from the corresponding bulk oxides. A few studies, both experimental and theoretical, focused the attention on the dimensionality crossover that occurs for small gold clusters deposited on MgO ultrathin films.[49–54]

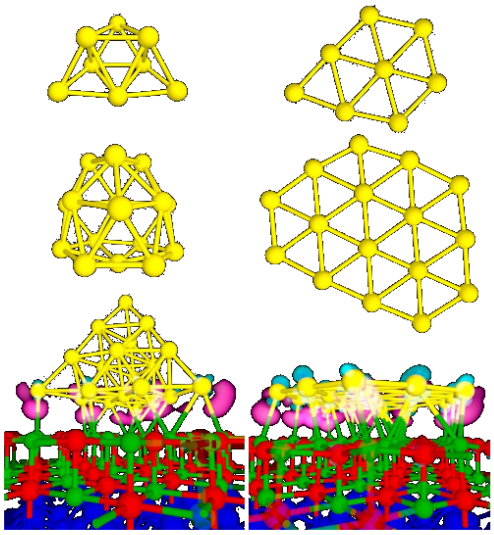

Figure 1.10: Relaxed atomic configurations of isolated Au_n cluster isomers and upon adsorption on MgO/Mo(100). For the clusters adsorbed on MgO/Mo(100) the charge density at the cluster-oxide interface is displayed: charge accumulation in pink and charge depletion in light blue.[51]

In fact, it has been observed that, due to the interaction with the thin film, gold

clusters adopt different geometries with respect to the ones observed in the gas-phase or on bare MgO surfaces; in particular, the clusters experience a reduction in the dimensionality, arranging in 1-dimensional chains whereas 2-dimensional islands are expected,[50] and in 2-dimensional flat clusters whereas 3-dimensional bulky structures should be observed (Figure 1.10).[51] The driving force for this cross-over is the stabilizing electrostatic interaction with the substrate, which arises from a net charge accumulation at the interface between the cluster and the support. This unexpected feature opens the possibility to employ ultra-thin films as functionalized materials in their own right, instead as mere models for oxide surfaces, since the charging of metal clusters is one of the possible mechanism to increase the chemical activity of a supported particle (see Sec. 1.2). The activity of gold clusters supported on ultra-thin films toward the combustion of carbon monoxide has indeed been tested on clusters of different dimensionality.[82,83]

Charging phenomena on ultrathin films do not depend on the presence of defects and are only related to some fundamental parameters of the metal/oxide interface and of the adsorbed species. In a recent paper by Grönbeck *et al.*,[84] the authors provide a picture of the several contributions involved in the stabilization of an adsorbate on an oxide thin film supported on a metal. The adsorption energy of a species (A), be it an atom, a cluster or a molecule, on an oxide surface (MO) supported by a metal (M) can be decomposed into:

$$\mathrm{E_{ads}} \sim \mathrm{E_{pol}} + \mathrm{E_b[A/MO]} + \mathrm{E_{adh}[MO/M]} + (\mathrm{EA} - \Phi) + \mathrm{E[A/A]} \qquad (1.2)$$

where $\mathrm{E_{pol}}$ is the electrostatic contribution owing to the polarization of the oxide and the image charge in the metal due to the presence of a charged adsorbate, $\mathrm{E_b}$ is the chemical interaction between the adsorbate and the oxide, $\mathrm{E_{adh}[MO/M]}$ is the oxide/metal interface energy, $\mathrm{EA} - \Phi$ is the difference between the electron affinity of the adsorbate and the work function of the combined oxide/metal system and $\mathrm{E[A/A]}$ is the interaction between the charged adsorbates, which in turn depends on the coverage. The (change in the) work function of the metal, in particular, has been object of several studies.[86–90] In Figure 1.11 a schematic picture of energetic states involved in a metal/dielectric system is shown.

According to the Schottky model[85] when a metal and a dielectric are brought into contact, charge transfer across the interface is not allowed and the Schottky barrier height is given by the difference between the work function of the metal in vacuum, $\Phi_{\mathrm{m,vac}}$, and the top of the dielectric valence band, $\mathrm{E_v}$. However, the Schottky model

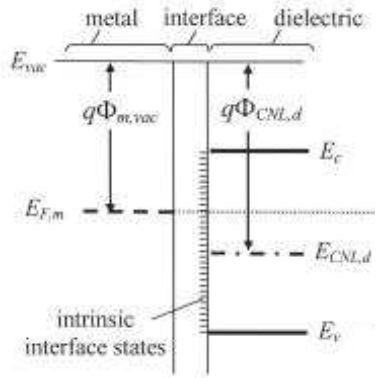

Figure 1.11: Schematic picture of energetic states involved in a metal/dielectric system.[86]

is not generally obeyed. One reason is that the metal wave function decays into the oxide in the energy range where the metal conduction band overlaps with the oxide band gap, giving rise to metal-induced gap states (MIGS). The MIGS can be divided into two main categories: conventional MIGS, simply due to the spatial penetration of the tails of the metal work function into the oxide, and states due to chemical bonding at the interface.[87] These latter can have donorlike character (close to $\mathrm{E_v}$), or acceptorlike (closer to the oxide conduction band, $\mathrm{E_c}$).[86] The energy level in the band gap at which the character of the interface states changes from donorlike to acceptorlike is the charge neutrality level, $\mathrm{E_{CNL}}$; simple MIGS models locate $\mathrm{E_{CNL}}$ roughly at the dielectric mid-gap. The presence of states due to chemical bonding at the interface induces a charge transfer (CT) across the interface creating a dipole, μ, which shifts the position of the metal Fermi energy, $\mathrm{E_{F,m}}$ with respect to $\mathrm{E_{CNL}}$. As a result, the effective metal work function of the metal/oxide system $\Phi_{\mathrm{m,eff}}$ differs from the vacuum metal work function, $\Phi_{\mathrm{m,vac}}$. Models have been proposed to relate the work function change, $\Delta\Phi$=$\Phi_{\mathrm{m,eff}}$-$\Phi_{\mathrm{m,vac}}$, to the difference between $\mathrm{E_{CNL}}$ and $\mathrm{E_{F,m}}$ or, in other word, to the metal electronegativity.[86]

However, $\Delta\Phi$ cannot be explained in the framework of the CT model only. Goniakowski *et al.*[87] have shown that MgO/metal interfaces give rise to substantial changes in work function despite a relatively small CT, an effect attributed to oxide-induced polarization of the metal electrons and proposed also for adsorbates on metal surfaces. In particular, it has been emphasized the role of the exchange repul-

sion applied by the oxide layer in pushing back the metal's spilled-out charge, thus reducing the surface dipole even in the absence of charge transfer.[88,89]

The charge transfer from or to an adsorbate is directly related to the position of the filled and empty states of the adsorbed species and the work function of the metal/oxide support. For high values of the work function, a charge transfer is expected from the adsorbate to the oxide, and viceversa. In cases where the position of the frontier orbitals of the adsorbate and of the Fermi level of the metal/oxide support are similar in energy, no charge transfer takes place. Also the thickness of the oxide film plays an important role, the charge transfer effects being related to a tunneling probability. All these parameters, work function of the metal/oxide support, electronegativity of the adsorbed species, thickness of the film, etc. can be tuned in order to determine the direction and the extent of the charge transfer.

In a recent paper by our group[90] $\Delta\Phi$ is rationalized as the sum of three main contributions:

$$\Delta\Phi = \Delta\Phi^{\mathrm{CT}} + \Delta\Phi^{\mathrm{comp}} + \Delta\Phi^{\mathrm{SR}} \tag{1.3}$$

where $\Delta\Phi^{\mathrm{CT}}$ represents the charge transfer contribution, $\Delta\Phi^{\mathrm{comp}}$ is the electrostatic compressive effect and $\Delta\Phi^{\mathrm{SR}}$ is a term due to the surface relaxation.

Amongst the systems which received more attention are MgO thin films grown on Ag(100) and Mo(100) surfaces.[36,68,69] Mo(100), in particular, can sustain high annealing temperatures, thus allowing a better quality of films containing 10-20 oxide layers. Despite the structural similarity of these two systems, both dealing with an ionic oxide as MgO grown on a metal with similar work functions (4.22 eV Ag,[70] 4.53 eV Mo[72]), there are important differences in the electronic structure. Due to the stronger adhesion energy of MgO on Mo(100) – and the subsequent shorter interface distance – there is a more pronounced decrease in the metal work function which becomes about 2 eV, whereas it is about 3 eV for MgO/Ag(100).[73] It will be shown in Chapter 5 that this difference in the work function values has relevant consequences on the adsorption properties of transition metal atoms.

1.5 Summary

Charging of metal clusters supported on oxide surfaces is an important physical effect that can improve the properties of the supported species. In particular, cluster anions exhibit enhanced catalytic properties in the course of reactions such as the

low temperature oxidation of carbon monoxide. The charging mechanism arises from the interaction of the supported clusters with functionalized oxide surfaces. Recently, the traditional functionalization of oxide surfaces based on the presence of oxygen vacancies has been debated and a new light has been shed on the drawbacks of the method, which is then less viable then it should in order to be of practical utility.

Treasuring the message emerging from the several papers dealing with oxygen vacancies and activation of metal clusters, new efforts are aiming to the synthesis of electron rich surfaces for the stabilization of metal cluster anions. The first method presented in this work enables the production of true electron rich surfaces, where electrons are localized on under coordinated sites of polycristalline alkaline-earth oxides and can act as nucleation and charging sites for metal clusters, also preventing the coalescence of the particles. However, it is not clear yet whether the charge delocalization over bigger clusters formed upon adsorption and diffusion of metal atoms will still be efficient in enhancing the catalytic properties.

The second method, instead, makes use of the tunnel effect from a metal support through an oxide thin film to supported metal clusters, and the presence of electrons at the surface of the oxide appears subsequently to the deposition of metal clusters and their interaction with the metal underneath. On one side, this ensure an accumulated charge almost proportional to the contact area between the cluster and the support, since the structure of the cluster rearranges in order to allow the maximum electrostatic interaction with the substrate. On the other side, diffusion of the particles upon heating can be a problem leading to coalescence and formation of bigger, less reactive clusters.

In this thesis, the main effects of the interaction between these functionalized surfaces and transition metal atoms and clusters will be discussed, focusing on the novel properties which characterize anionic supported clusters.

Bibliography

[1] M. Haruta, T. Kobayashi, H. Sano, N. Yamada, *Chem. Lett.* **2** (1987), p. 405.

[2] M. Haruta, *Catalysis Today* **36** (1997), p. 153.

[3] M. Haruta, M. Datè, *Appl. Catal. A* **222** (2001), p. 427.

[4] M. Haruta, *CATTECH* **6** (2002), p. 102.

[5] M. Haruta, *Chem. Rec.* **3** (2003), p. 75.

[6] G. C. Bond, D. T. Thompson, *Catalysis Reviews: Science and Engineering* (1999) **41**, p. 319.

[7] G. C. Bond, D. T. Thompson, *Gold Bull.* **33** (2000), p. 41.

[8] G. C. Bond, *Catal. Today* **72** (2002), p. 5.

[9] D. T. Thompson, *Appl. Catal. A* **243** (2003), p. 201.

[10] M. Haruta, N. Yamada, T. Kobayashi, S. Iijima, *J.Catal.* **115** (1989), p. 301.

[11] T. Hayashi, K. Tanaka, M. Haruta, *J. Catal.* **178** (1998), p. 566.

[12] G. R. Bamwenda, S. Tsubota, T. Nakamura, M. Haruta, *Catal. Lett.* **44** (1997), p. 83.

[13] D. Andreeva, V. Idakeiv, T. Tabakova, A. Andreev, R. Giovanoli, *Appl. Catal. A: General* **134** (1996), p. 275.

[14] A. Ueda, M. Haruta, *Gold Bull.* **32** (1999), p. 3.

[15] G. C. Bond, P. A. Sermon, G. Webb, D. Buchanan, P. B. Wells, *J. Chem. Commun.* **444** (1973).

[16] G. J. Hutchings, *Catal. Today* **72** (2002), p. 11.

[17] G. J. Hutchings, *J. Catal.* **96** (1985), p. 292.

[18] B. Nkosi, M. D. Adams, N. J. Coville, G. J. Hutchings, *J. Catal.* **128** (1991), p. 366.

[19] *Gold Bull.* **36** (2003), p. 21.

[20] D. J. Gulliver, J. S. Kitchen, EU Patent #654301, BP. Chem. Int. Ltd., (1995).

[21] G. Srinivas, J. Wright, C.S. Bai, R. Cook, *Studies in Surface Science and Catalysis* **101** (1996), p. 427.

[22] M. M. Schubert, M. J. Kahlich, H. A. Gasteiger, R. J. Behm, *J. Power Sources* **84** (1999), p. 175.

[23] D. Cameron, R. Holliday, D. Thompson, *J. Power Sources* **118** (2003), p. 298.

[24] T. V. Choudhary, D.W. Goodman, *Catalysis Today* **77** (2002), p. 65.

[25] P. Pyykkö, *Angew. Chem. Int. Ed.* **43** (2004), p. 4412.

[26] P. Pyykkö, *Angewandte Chemie Int. Ed.* **41** (2002), p. 3573.

[27] F. Boccuzzi, A. Chiorino, M. Manzoli, P. Lu, T. Akita, S. Ichikawa, M. Haruta, *J. Catal.* **202** (2001), p. 256.

[28] M. Valden, X. Lai, D. W. Goodman, *Science* **281** (1998), p. 1647.

[29] T. V. Choudary, D. W. Goodman, *Appl. Catal. A: General* **291** (2005), p. 32.

[30] M. Mavrikakis, P. Stoltze, J. K. Nørskov, *Catal. Lett.* **64** (2000), p. 101.

[31] A. A. Herzing, C. J. Kiely, A. F. Carley, P. Landon, G. J. Hutchings, *Science* **312** (2008), p. 1331.

[32] M. S. Chen, D. W. Goodman, *Science* **306** (2004), p. 252.

[33] H. Häkkinen, S. Abbet, A. Sanchez, U. Heiz, U. Landman, *Angew. Chem. Int. Ed.* **42** (2003), p. 1297.

[34] B. Yoon, H. Häkkinen, U. Landman, A. S. Wörz, J.-M. Antonietti, S. Abbet, K. Judai, U. Heiz, *Science* **307** (2005), p. 403.

[35] S. Tsubota, K. Tanaka, M. Haruta, *Catal. Lett.* **56** (1998), p. 131.

[36] H.-J. Freund, *Surf. Sci.* **500** (2002), p. 271.

[37] M. Che, C. O. Bennett., *Adv. Catal.* **20** (1989), p. 153.

[38] J. He, P. J. Moller, *Surf. Sci.* **189** (1986), p. 13.

[39] P. Stracke, S. Krishov, V. Kempter, *Surf. Sci.* **473** (2001), p. 86.

[40] Y. D. Kim, J. Stulz, T. Wei, D. W. Goodman, *J. Phys. Chem.* **106** (2002), p. 6827.

[41] C. T. Campbell, D. Starr, *J. Am. Chem. Soc.* **124** (2002), p. 9212.

[42] Y. F. Zhukovskii, E. A. Kotomin, P. W. M. Jacobs, A. M. Stoneham, *Phys. Rev. Lett.* **84** (2000), p. 1256.

[43] M. Frank, M. Bäumer, R. Kühnemuth, H.-J. Freund, *J. Phys. Chem. B* **105** (2001), p. 8569.

[44] S. Abbet, E. Riedo, H. Brune, U. Heiz, A. M. Ferrari, L. Giordano, G. Pacchioni, *J. Am. Chem. Soc.* **123** (2001), p. 6172.

[45] G. Haas, A. Menck, H. Brune, J. V. Barth, J. A. Venables, K. Kern, *Phys. Rev. B* **61** (2000), p. 11105.

[46] M. Sterrer, M. Yulikov, T. Risse, H.-J. Freund, J. Carrasco, F. Illas, C. Di Valentin, L. Giordano, G. Pacchioni, *Angew. Chem., Int. Ed.* **45** (2006), p. 2633.

[47] M. Chiesa, M. C. Paganini, E. Giamello, D. M. Murphy, C. Di Valentin, G. Pacchioni, *Acc. Chem. Res.*, **39** (2006), p. 861.

[48] H.-J. freund, G. Pacchioni, *Chem. Soc. Rev.* **37** (2008), p. 2224.

[49] P. Frondelius, H. Häkkinen, K. Honkala, *Phys. Rev. B* **76** (2007), p. 76073406.

[50] V. Simic-Milosevic, M. Heyde, X. Lin, T. Knig, H.-P. Rust, M. Sterrer, T. Risse, N. Nilius, H.-J. Freund, L. Giordano, G. Pacchioni, *Phys. Rev. B* **78** (2008), p. 235429.

[51] D. Ricci, A. Bongiorno, G. Pacchioni, U. Landman, *Phys. Rev. Lett.* (2006), p. 97036106.

[52] M. Sterrer, T. Risse, M. Heyde, H.-P. Rust, H.-J. Freund, *Phys. Rev. Lett.* **98** (2007), p. 206103.

[53] M. Walter, P. Frondelius, K. Honkala, H. Häkkinen, *Phys. Rev. Lett.* **102** (2009), p. 206801.

[54] N. Nilius, M. V. Ganduglia-Pirovano, V. Brázdová, M. Kulawik, J. Sauer, H.-J. Freund, *Phys. Rev. Lett.* **100** (2008), p. 096802.

[55] A. Bogicevic, D: R. Jennison, *Surf. Sci.* **437** (1999), p. L741.

[56] L. Giordano, C. Di Valentin, J. Goniakovski, G. Pacchioni, *Phys. Rev. Lett.* **92** (2004), p. 096105.

[57] A. J. Tench, R. L. Nelson, *J. Colloid Interface Sci.* **26** (1968), p. 364.

[58] E. Giamello, M. C. Paganini, D. M. Murphy, A. M. Ferrari, G. Pacchioni, *J. Phys. Chem.* **101** (1997), p. 971.

[59] G. Pacchioni, P. Pescarmona, *Surf. Sci.* **413** (1998), p. 657.

[60] M. C. Paganini, M. Chiesa, E. Giamello, S. Coluccia, G. Martra, D. M. Murphy, G. Pacchioni, *Surf. Sci.* **421** (1999), p. 246.

[61] M. Sterrer, E. Fischbach, T. Risse, H.-J. Freund, *Phys. Rev. Lett.* **94** (2005), p. 186101.

[62] P. P. Edwards, P. A. Anderson, J. M. Thomas, *Acc. Chem. Res.* **29** (1996), p. 23.

[63] D. R. Smith, A. J. Tench, *Chem. Commun.* (1968), p. 1113.

[64] M. Chiesa, M. C. Paganini, E. Giamello, C. Di Valentin, G. Pacchioni, *Chem. Phys. Chem.* **7** (2006), p. 728.

[65] D. Ricci, C. Di Valentin, G. Pacchioni, P. V. Sushko, A. L. Shluger, E. Giamello, *J. Am. Chem. Soc.* **125** (2003), p. 738.

[66] O. Diwald, E. Knzinger, G. Martra, *J. Chem. Phys.* **111** (1999), p. 6668.

[67] T. Berger, M. Sterrer, O. Diwald, E. Knzinger, *J. Phys. Chem. B* **108** (2004), p. 7280.

[68] P. L. J. Gunter, J. W. Niemantsverdriet, F. H. Ribeiro, G. A. Somorjai, *Catal. Rev – Sci. Eng.* **39** (1997), p. 77.

[69] J. Libuda, H.-J. Freund, *Surf. Sci. Rep.* **57** (2005), p. 157.

[70] C. R. Henry, *Surf. Sci. Rep.* **31** (1998), p. 231.

[71] D. W. Goodman, *J. Catal.* **216** (2003), p. 213.

[72] G. Pacchioni, L. Giordano, M. Baistrocchi, *Phys. Rev. Lett.* **94** (2005), p. 226104.

[73] L. Giordano, G. Pacchioni, *Phys. Chem. Chem. Phys.* **8** (2006), p. 3335.

[74] D. Ricci, A. Bongiorno, G. Pacchioni, U. Landman, Phys. Rev. Lett. **97** (2006), p. 036106.

[75] K. Honkala, H. Hakkinen, J. Phys. Chem. C. **111** (2007), p. 4319.

[76] M. Sterrer, T. Risse, U. Martinez Pozzoni, L. Giordano, M. Heyde, H.-P. Rust, G. Pacchioni, H.-J. Freund, Phys. Rev. Lett. **98** (2007), p. 096107.

[77] M. Sterrer, T. Risse, M. Heyde, H.-P. Rust, H.-J. Freund, Phys. Rev. Lett. **98** (2007), p. 206103.

[78] H. Grönbeck, *J. Phys. Chem. B* **110** (2006), p. 11977.

[79] P. Bronvist, H. Grönbeck, *Surf. Sci.* **600** (2006), p. L214.

[80] A. Hellman, , H. Grönbeck, *Phys. Rev. Lett.* **100** (2008), p. 116801.

[81] D. E. Starr, C. Weis, S. Yamamoto, A. Nilsson, H. Bluhm, *J. Phys. Chem. C.* **113** (2009), p. 7355.

[82] C. Zhang, B. Yoon, U. Landman, *J. Am. Chem. Soc.* **129** (2007), p. 2228.

[83] C. Harding, V. Habibpour, S. Kunz, A. Nam-Su Farnbacher, U. Heiz, B. Yoon, U. Landman, *J. Am. Chem. Soc.* **131** (2009), p. 538.

[84] P. Frondelius, A. Hellman, K. Honkala, H. Häkkinen, H. Grönbeck, *Phys. Rev. B* **78** (2008), p.085426.

[85] W. Schottky, *Phys. Z.* **41** (1940), p. 570.

[86] Y.-C. Yeo, T.-J. King, C. Hu, *J. Appl. Phys.* **92** (2002), p. 7266.

[87] J. Goniakowski, C. Noguera, *Interface Sci.* **12** (2004), p. 93.

[88] P. S. Bagus, V. Staemmler, C. Wöll, *Phys. Rev. Lett.* **89** (2002), p. 096104.

[89] L. Giordano, F. Cinquini, G. Pacchioni, *Phys. Rev. B* **73** (2005), p. 045414.

[90] S. Prada, U. Martinez, G. Pacchioni, *Phys. Rev. B* **78** (2008), p. 235423.

Chapter 2

Computational models

In so far as quantum mechanics is correct, chemical questions are problems in applied mathematics.

Henry Eyring

2.1 Basics of DFT

The Density Functional Theory (DFT) is a quantum mechanical theory for the investigation of the electronic structure – principally the ground state – of many-body systems, from atoms to the condensed phases. In the framework of this theory the total electronic energy of the system can be expressed as a functional of the ground state electron density.

DFT bases its theoretical footing on the two Hohenberg-Kohn theorems.[1] The first theorem states that the ground state properties of a many-electron system are uniquely determined by an electron density that depends on only 3 spatial coordinates. This lays the groundwork for reducing the many-body problem from $\mathcal{O}(3^N)$ (3 spatial coordinates for each of the N atoms constituting the sytem) to 3 spatial coordinates. This theorem can be extended to the time-dependent domain to develop time-dependent density functional theory (TDDFT), which can be used to describe excited states.

The second Hohenberg-Kohn theorem defines an energy functional for the system and proves that the correct ground state electron density minimizes this energy functional. Within the framework of Kohn-Sham DFT,[2] the intractable many-body problem of interacting electrons in a static external potential is reduced to a tractable problem of non-interacting electrons moving in an effective potential. Non-interacting systems are relatively easy to solve as the wavefunction can be represented as a Slater determinant of orbitals. The effective potential includes the

external potential and the effects of the Coulomb interactions between the electrons, e.g., the exchange and correlation interactions.

The major drawback of DFT is that the exact form of the functionals for exchange and correlation are not known except for the free electron gas. However, approximations exist which permit the calculation of certain physical quantities quite accurately. In physics the most widely used approximation is the local-density approximation (LDA), where the functional depends only on the density at the coordinate where the functional is evaluated. Generalized gradient approximations (GGA) are still local but also take into account the gradient of the density at the same coordinate. With this more sophisticated approximation (GGA) very good results for molecular geometries and ground-state energies have been achieved. Potentially more accurate than the GGA functionals are meta-GGA functions, which also include the Laplacian of the density.

Difficulties in expressing the exchange part of the energy can be relieved by including a component of the exact exchange energy calculated from Hartree-Fock theory. Functionals of this type are known as hybrid functionals.

In this work two different functionals have been used. The B3LYP hybrid functional[3,4] has been employed has implemented in the embedded cluster methods (see Sec. 2.2). The plane waves code (see Sec. 2.3), instead, required the use of the pure GGA functional PW91;[5] in fact, the very recent implementation of the hybrid functionals and the computational effort associated with them didn't make their use possible in the course of this work.

2.2 Embedded cluster approach

Localized phenomena such as the presence of point defects or the adsorption of molecules can be modelled in an infinite dilution regime in the framework of the cluster approach. The cluster model consists in cutting a representative portion of a given material out of the ideal infinite crystal, such that the minimum amount of atoms required to describe the property of interest is explicitly taken into account. This procedure is less trivial than it may seem, for non-physical effects due to the mere cutting of a portion of the solid can arise; in the case of an ionic oxide, the main problem is the description of the long-range electrostatic potential (Madelung potential) which is a crucial feature of ionic lattices.

The usual approach used to reproduce this potential is to generate a finite array of point charges (PCs) located in lattice potions, whose values – for a strongly ionic material – are the nominal charge of the ions. The main drawback of this approach is the non-physical polarization experienced by anions at the edge of the quantum-mechanical cluster due to presence of nearby positive point charges. This artifact can be fixed by replacing positive point charges at the interface with quantum-mechanical cluster with effective core potentials (ECPs), which simulate the exchange repulsion, preventing non-physical polarization.[6]

The shell model Another drawback of the embedding with point charges is that it doesn't take into account the long-range polarization induced by a defect or adsorbate, especially if charged or polarized. An approximate way to describe this effect is based on a classical model of a polarizable ion, the shell model, consisting in two point charges, a positive one for the core and a negative one for the shell, coupled by an harmonic potential. The displacement of the shell relative to the core simulates the polarization of a classical ion in an electric field.

P. Sushko and A. Shluger[7] introduced the shell model in the standard embedding with point charges, implementing it in their GUESS code. In their model, the quantum mechanically treated clusetr (QM) is embedded in a finite lattice (region I) of shell model polarizable ions (SM), which interact with each other and with the atoms of the QM region through classical potentials. Region I is in turn surrounded by a finite lattice of point charges (PC) which constitute the region II, whose aim is to correctly describe the electrostatic long range potential. The total energy of the system is therefore the sum of the following contributions:

- energy of the QM cluster, in presence if the external field due to charges and dipoles of the embedding scheme;
- Coulomb interaction energy between charges of classical regions (cores and shells);
- short range interaztion between shell model ions;
- harmonic potential energy between every core and its shell;
- short range Coulomb interaction between QM atoms and the ions of the embedding,

$$E_{\mathrm{tot}} = \langle\Phi|H_0 + V_{\mathrm{emb}}|\Phi\rangle + \frac{1}{2}\sum_{i,j\in\mathrm{emb}}\frac{q_i q_j}{R_{i,j}} + \frac{1}{2}\sum_{i,j\in\mathrm{emb}} W_{i,j} + \frac{1}{2}\sum_{i\in\mathrm{emb}} k_i\delta_i^2 + \sum_{i\in\mathrm{QM}}\sum_{j\in\mathrm{emb}} W_{i,j} \tag{2.1}$$

The optimization algorithm developed for the present model[8] allows the simoultaneous optimization of the coordinates of the QM and classical (region I) parts.

Localized basis set Considering that the main part of the electron density is localized around atoms and along bonds, localized atomic-like functions are a natural choice for a basis set.

Slater Type Orbitals (STO) are built like solutions of atomic hydrogen, the angular part constisting in spherical harmonics and the radial part being exponential.

Gaussian type orbitals (GTO) are instead characterized by a gaussian radial part, which is convenient for a matter of computational efficiency. However, some features such as the tipical cusp in $r = 0$, the too fast decay with r and the presence of nodes are neglected; in order to fix these lacks, linear combinations of GTOs are used (Contracted Gaussian Type Orbitals).

2.3 Periodic supercell approach

The electronic structure of solids is usually described in terms of band structure: a widely adopted approach is the use of a unit cell with appropriate dimensions periodically repeated in three-dimensions to account for the infinite nature of the crystalline solid; the Schrödinger equation is thus solved for the atoms in the unit cell, subject to periodic boundary conditions (PBC).[9] This model can also be extended to the study of surfaces, combining the PBC with the slab approach: here the unit cell is made of a given number of layers – some of which are generally constrained to resemble the bulk structure – above which a wide enough region of vacuum lays. 10 Å are usually sufficient to ensure the non-iteraction between neighbour cells.

Point defects, adsorption of molecules and in general all localized phenomena can be as well modelled in the framework of the periodic approach just considering a large enough cell (supercell approach) to avoid a non-realistic reply which would results in an extremely high concentration of defects or molecules and eventually in misleading interactions.

Plane waves formalism The periodic quantum-mechanical code used in this work is the Vienna Ab-initio Simulating Package (VASP).[11,12]
The VASP code is based on the Density Functional theory (DFT) and the wave funtion of the system is thus described in terms of Kohn-Sham orbitals.[1,2] While in the cluster approach the LCAO-MO (Linear Combination of Atomic Orbitals – Molecular Orbitals) and a gaussian-type basis set are used to describe the molecular orbitals, in the periodic approach a different basis set is chosen, which takes advantage of the periodic nature of the potential. Indeed, the Bloch theorem describes the single electron wavefunction in the Kohn-Sham equation, stating that the wave function can be written as a cell-periodic part modulated by a wave-like function:[13]

$$\psi_{n\mathbf{k}}(\mathbf{r}) = e^{i\mathbf{k}\cdot\mathbf{r}} u_{n\mathbf{k}}(\mathbf{r}) \tag{2.2}$$

where $u_{n,\mathbf{k}}(\mathbf{r})$ is the periodic function, with n band index. The single electron wave function can thus be written as:

$$\psi_{n\mathbf{k}}(\mathbf{r}+\mathbf{R}) = e^{i\mathbf{k}\cdot\mathbf{R}} \psi_{n\mathbf{k}}(\mathbf{r}) \tag{2.3}$$

where $\mathbf{R}$ is a traslational vector. The importance of such theorem is given by the fact that each electronic wave function can be written as a sum of plane waves:

$$\psi_{n\mathbf{k}}(\mathbf{r}) = \sum_{\mathbf{G}} c_{n,\mathbf{k}+\mathbf{G}}\ e^{i(\mathbf{k}+\mathbf{G})\cdot\mathbf{r}} \tag{2.4}$$

Given $\mathbf{l}$ a lattice vector of the crystal and m an integer, $\mathbf{G}$ is the reciprocal lattice vector defined as $\mathbf{G}\cdot\mathbf{l} = 2\pi m$ for all $\mathbf{l}$. From what exposed, one can evince that an infinite plane-wave basis set is, in principle, required to expand the electronic wave function. Actually, it is possible to truncate the expansion, being sure to include only the wave function with a kinetic energy under a fixed threshold. In fact, the coefficients $c_{n,\mathbf{k}+G}$ for the plane waves with small kinetic energy are more important than those with higher kinetic energy. In practice only those plane waves $|\mathbf{G}+\mathbf{k}|$ for which

$$\frac{\hbar^2}{2m_e}|\mathbf{G}+\mathbf{k}|^2 < \mathrm{E}_{\mathrm{cut}} \tag{2.5}$$

are included. Hence, the introduction of a kinetic cut-off, combined with the Bloch theroem, allows to have a finite basis set to describe the system. However, this leads to a computational error in the representation of the total energy; clearly this can be reduced by increasing the value of $\mathrm{E}_{\mathrm{cut}}$ until the energy is converged. The electronic states are allowed only for a given set of $\mathbf{k}$ vectors in the reciprocal lattice.

These vectors constitute a subspace of points, called k-points, which can sample in a significative way the first Brillouin zone.[10] To obtain an accurate approximation to the electronic potential and the contribution to the total energy from a filled electronic band, the VASP code uses the Monkhorst-Pack[14] method to generate a special set of k-points at which evaluates the electronic states. This method uses a grid of k-points, whose density depends on band dispersion. This approach provide an accurate description for the semiconductors and insulators through a very small number of k-points. To obtain a precise description of metals, however, a denser grid of k-points is needed in order to precisely define the Fermi surface. Anyway, the use of big supercells allows a reduction in the number of the k-points, because of the relation of inverse proportionality between reciprocal and direct vectors.

Pseudopotentials From a computational point of view, the Fast Fourier Transforms (FFT) method as implemented in the VASP code is extremely efficient. However, the number of required plane waves would exceed any practical limits except for Hydrogen and Lithium. Even with the introduction of the cutoff energy, too many plane waves are needed to adequately describe the core electrons. To this end, instead of exact potentials pseudopotential must be applied. This method provide a reduction in the number of electrons explicitly described and the possibility to use a lower $\mathrm{E_{cut}}$. In a classical description of the system, the electron in proximity of an ionic nucleus accelerates, gaining kinetic energy. This gain balances the potential energy loss due to the presence of the positive nucleus and the total energy holds constant. The increase of kinetic energy can be replaced with an effective repulsive potential which cancels the electrostatic potential. However, the real systems cannot be described only in terms of classical mechanics, so this deletion is not total, due to the quanto-mechanic nature of the system. The residual is called pseudopotential.[15] Most of the physical properties of the solids is strictly connected to the valence electrons, the core ones being almost unperturbed. In a quanto-mechanic description of the problem, the wavefunction oscillations hold the orthogonality between the core and the valence wavefunctions, as required by the Pauli principle. The pseudopotential acts on the pseudo-eigenfunctions, which don't present nodes and converges rapidly, instead of the real valence wavefunctions.[1] This is schematically shown in Figure 2.1.

At a first glance this approximation might seem rude, but it is very accurate,

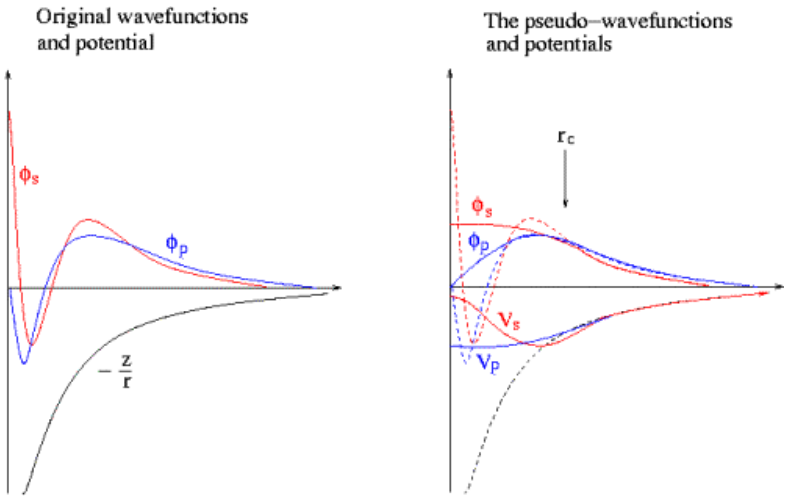

Figure 2.1: Schematic illustration of all-electron (solid lines) and pseudoelectron (dashed lines) potentials and their corrsponding wave functions. At r_c the radius at which the values of all-electrons and pseudoelectons match.

most of all in those systems whose the electrons in proximity of the nucleus don't contribute significatively to the phenomena analyzed. There are several methods to contruct pseudopotentials. In this work projected augmented waves (PAW) method pseudopotentials[16,17] have been used.

In 1994 Blöchl proposed a method to determine the electron-ion interaction, called Projector Augmented Wave (PAW). The PAW method describes the wave function as an overlap of different terms. The first part is a plane wave (the pseudo-wavefunction) and the second is an expansion on pseudoorbitals and atomic orbitals for each atom. The plane wave possesses the right flexibility to describe the bonds and the external regions of the wave function, and the correct behavior of the nodal structure of the nuclei is granted by the expansion through atomic orbitals. The PAW method combines the advantages of both representations in a well defined basis set to find the all electron wave function, the energy functional and all the other physical quantities of interest. This method is often referred to as an all-electron method, not in the sense that all the electrons are treated explicitly, but in the sense that the valence electronic wave functions are kept orthogonal to the core states.

Bibliography

[1] P. Hohenberg, W. Kohn, *Phys. Rev. B* **136** (1964), p. 864.

[2] W. Kohn, L.J. Sham, *Phys. Rev. A* **140** (1965), p. 1133.

[3] A. D. Becke, *J. Chem. Phys.* **98** (1993), p. 5548.

[4] C. Lee, W. Yang, R. G. Parr, *Phys. Rev. B* **37** (1998), p. 785.

[5] J. P. Perdew, J. A. Chevary, S. H. Vosko, K. A. Jackson, M. R. Pederson, D. J. Singh, C. Fiolhais, *Phys. Rev. B* **46** (1992), p. 6671.

[6] W. J. Stevens, H. Basch, M. J. Krauss, *J. Chem. Phys.* **81** (1984), p. 6026.

[7] P. V. Sushko, A. L. Shluger, R. C. Baetzold, C. R. A. Catlow, *J. Phys.: Condens. Matter* **12** (2000), p. 8257.

[8] P. V. Sushko, A. L. Shluger, C. R. A. Catlow, *Surf. Sci.* **450** (2000), p. 153.

[9] M. Allen, T. Tildesley, *Computer Simulation of Liquids*, Oxford University Press (Oxford 1987).

[10] M. C. Payne, M. P. Teter, D. C. Allan, T. A. Arias, J. D. Joannopoulos, *Rev. Mod. Phys.* **64**, (1992), p. 1047.

[11] G. Kresse, J. Hafner, *Phys Rev. B* **47** (1993), p. R558.

[12] G. Kresse, J. Furthmüller, *Phys. Rev. B* **54** (1996), p. 11169.

[13] N. Ashcroft, N. Mermin, *Solid State Physics*, International Thomson Publishing (Philadelphia 1976).

[14] H. Monkhorst, J. Pack, *Phys. Rev. B* **13** (1976), p. 5188.

[15] A. P. Sutton, *Electronic Structure of materials*, Clarendon Press (Oxford 1993).

[16] P. E. Blöchl, *Phys Rev. B* **50** (1994), p. 17953.

[17] O. Bengone, M. Alouani, P. E. Blöchl, J. Hugel, *Phys Rev. B* **62** (2000), p. 16392.

Part I

Charging by means of electron traps

Chapter 3

A route toward the generation of supported Au cluster anions

3.1 Abstract

On the basis of experimental evidence and DFT calculations, we propose a simple yet viable way to stabilize and chemically activate gold nanoclusters on MgO. First the MgO surface is functionalized by creation of trapped electrons by exposure to atomic H or to H_2 under UV light or deposition of low amounts of alkali metals on partially hydroxylated surfaces; the second step consists in the self-aggregation of gold clusters deposited from the gas phase. The calculations show that the electron traps act both as nucleation and activation sites. The process can lead to thermally stable gold cluster anions whose catalytic activity is enhanced by the presence of an excess electron, as demonstrated by a catalytic route for the CO oxidation.

3.2 Computational details

MgO (100) surface has been modeled in the framework of the embedded cluster scheme implented in the GUESS code interfaced with Gaussian03 code (see Chapter 2). The quantum-mechanical region (QM) of the cluster is surrounded by about 300 classical ions whose polarizability is described by the shell-model. Cations at the interface between qauntum-mechanical and shell-model regions are modeled by ions (hereafter indicated as Mg^*) on which a semi-local effective pseudopotential (ECP) is located, in order to reproduce the Pauli repulsion and avoid the non-physical polarization of QM interface anions. Region I, QM and SM, is then surrounded by a large array of point charges (PC) in order to correctly reproduce the long-range electrostatic potential. All centers in QM region and Mg* interface atoms

have been fully optimized, whereas only shells – but not cores – have been relaxed in the SM region. The total energy and the electronic structure of the QM cluster are calculated within DFT using the hybrid B3LYP exchange-correlation functional.

The following QM clusters have been used to model regular terrace and morphological defective sites of the MgO surface:

- $Mg_9O_9Mg^*_{17}$ (terrace),
- $Mg_{10}O_{10}Mg^*_{14}$ (edge),
- $Mg_8O_8Mg^*_{12}$ (step),
- $Mg_{10}O_{10}Mg^*_{9}$ (corner),
- $Mg_{17}O_{17}Mg^*_{22}$ (reverse corner).

A larger $Mg_{11}O_{11}Mg^*_{17}$ QM cluster has been used to model a step site for the adsorption of Au_4. The basis sets used are: 6-311+G** on H, 6-31G* on Mg, 6-31G on O. Au has been treated with the lanl2 scalar relativistic effective core potential, which explicitly includes the $5s^2\ 5p^6\ 5d^{10}6s^1$ electrons in the valence. CO and O_2 molecule have the 6-311+G* basis set; with this basis set the O-O distance, 1.21 Å, coincides with the experimental value. The O_2^- anion has an O-O distance of 1.35 Å (exp. 1.34 $\pm$ 0.01 Å).[2]

3.3 Results and discussion

3.3.1 Au atom adsorption on $(H^+)(e^-)$ sites

The interaction of a Au atom, whose valence electronic structure is $5d^{10}6s^1$, with a $(H^+)(e^-)$ center leads to spin coupling and a diamagnetic complex. In the following, the complex is denoted as $(H^+)(Au^-)$:

$$(H^+)(e^-) + Au^0_{ads} \longrightarrow (H^+)(Au^-) \tag{3.1}$$

The high electron affinity of gold, 2.17 eV (theory) and 2.3 eV (exp.),[1] favors the formation of an adsorbed Au^- anion near the surface OH group. The process is very exothermic: the addition of a gas-phase Au atom to the $(H^+)(e^-)$ defect leads to an energy release of 3.5-3.8 eV, depending on the location (edge 3.65 eV; step 3.83 eV; reverse corner 3.67 eV; corner 3.49 eV; see also Figure 3.1).

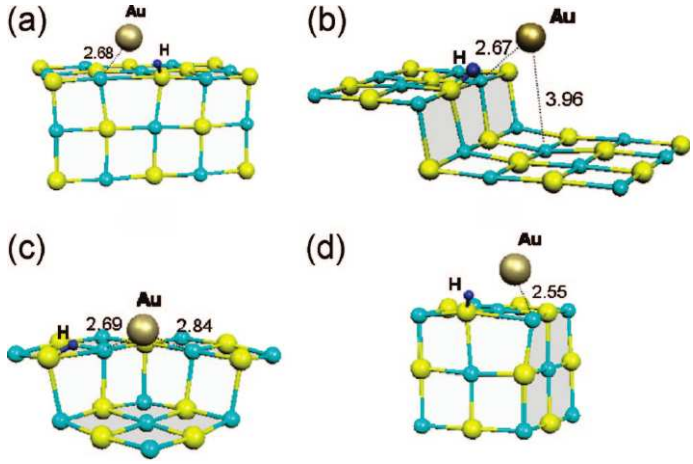

Figure 3.1: Structure of $(H^+)(Au^-)$ surface complexes formed by trapping a diffusing neutral Au atom on a $(H^+)(e^-)$ center: (a) edge; (b) step; (c) reverse corner; (d) corner. Selected distances are given in Å.

However, it is much more likely that Au atoms will thermally diffuse on the surface. In fact, the barrier for diffusion of Au on MgO terraces is estimated to be about 0.2-0.3 eV,[3] which guarantees rapid diffusion above liquid nitrogen temperature. Along their diffusion path the Au atoms can bind to a $(H^+)(e^-)$ site with a large energy gain, of the order of 2.5-3 eV, determined as the difference in stability between a Au adatom bound to the O_{5c} anion of a MgO terrace, 0.82 eV, and that of Au bound to a $(H^+)(e^-)$ center. The process is barrierless: once the diffusing Au atom is within a few lattice parameters from the trapping site, it will be attracted by its deep potential to form the $(H^+)(Au^-)$ surface complex.

On the edge site the Au atom is adsorbed in a bridge position between the Mg_{4c} cation and the OH group, Figure 3.1a, and the corresponding distances are 2.68 and 2.25 Å, respectively.
On the other sites the distances are similar, with a shorter distance from the proton and a longer distance from the closest Mg cation. Only on a corner site is the Au atom almost equidistant from the H and Mg atoms, Figure 3.1d. On a step and on a reverse corner, the Au^- anion can interact also with the Mg_{5c} cation of the basal plane, Figure 3.1b and c.

These results show the ability of $(H^+)(e^-)$ centers to strongly bind gold atoms

and form gold anions. The detachment of Au^- from these sites requires overcoming a substantial energy barrier. The process has been investigated in detail for an edge site:

$$(H^+)(Au^-) \longrightarrow (H^+) \cdots (Au^-)_{ads} \tag{3.2}$$

Reaction 3.2 leads to the formation of a Au^- species well separated from the OH group; on our model Au^- binds preferentially to a Mg_{4c} cation along the edge. In the calculation the anion has been placed about 6.8 Å far from the OH group, and the process has a ΔE = +1.35 eV and an activation barrier of 1.52 eV; therefore, the back reaction occurs with a very small thermal activation, 0.17 eV, and leads again to the very stable $(H^+)(Au^-)$ species. Thus, $(H^+)(e^-)$ centers are strongly anchoring sites for diffusing atoms: once bound to this center, gold will be able to diffuse away only at relatively high temperatures, well above 400 K, as Au^-, not Au^0 (this second process costs in fact 2.5 eV or more).

Another important aspect to be considered is the ability of these centers to act also as nucleation and growth sites. The cluster binding energy, E_b, measures the stability of an adsorbed Au_n cluster with respect to a Au_{n-1} cluster bound to the $(H^+)(e^-)$ center and a neutral Au adatom on a terrace O_{5c} site:

$$E_b = -E[(H^+)(Au_n^-)] + E[(H^+)(Au_{n-1}^-)] + E(Au_1/MgO) - E(MgO) \tag{3.3}$$

Figure 3.2a shows the structure of a gold dimer formed at a $(H^+)(e^-)$ center on a MgO step. Au_2^- acts as a bidentate ligand, with one atom interacting with an oxide anion on the basal plane and the other with a Mg_{4c} cation along the step, at variance from neutral Au_2 which binds to terrace sites with the molecular axis almost perpendicular to the surface.[3] The spin density resides almost entirely on the gold dimer and the Au–Au bond, 2.78 Å, is elongated with respect to neutral Au_2, 2.57 Å, and is similar to gas-phase Au_2^- (2.74 Å). $E_b(Au_2)$ is 0.7 eV, showing the tendency for diffusing Au atoms to bind to the $(H^+)(Au^-)$ complex and form a negatively charged Au dimer.

Diffusion of Au_2 from this site is unfavorable: the $(H^+)(e^-)$ center is a strong anchoring point and nucleation site. In fact, gas-phase Au_2 binds to the $(H^+)(e^-)$ site by 3.38 eV, and to the O_{5c} terrace site by 2.04 eV. This means that the displacement of a gold dimer from the $(H^+)(e^-)$ center is endothermic by 1.3-1.4 eV.

The next step is the addition of a third atom, with formation of a gold trimer. Gas-phase Au_3 has a doublet ground-state and is a Jahn-Teller distorted triangle

with an internal angle of 141° and r(Au-Au) = 2.64 Å; this is also the structure (apart from some distortion) found when neutral Au_3 is deposited on non-functionalized MgO.[4–6] In the presence of the trapped electron, however, the trimer, Figure 3.2b, assumes a much more open structure, (α = 158°) closer to the linear gas-phase Au_3^-. Attempts to start from a different structure, e.g. a triangle with two atoms interacting with the surface and the third one pointing toward the vacuum, failed and resulted in the structure illustrated in the Figure. The ground state of $(H^+)(Au_3^-)$ is diamagnetic, as a result of the addition of a Au atom to the pre-existing $(H^+)(Au_2^-)$ open-shell complex; $E_b(Au_3)$ is extremely large, 1.8 eV, due to the large electron affinity of Au_3, 3.68 eV. The Au–Au distances, 2.60 and 2.72 Å, are close to that of free Au_3^-, 2.65 Å.

The last nanocluster considered is Au_4. On the MgO(100) surface this cluster assumes a slightly distorted rhombic structure with two atoms interacting with the surface and the cluster plane normal to the surface.[6] On a $(H^+)(e^-)$ center, however, the Au_4 cluster is no longer rhombic but is nearly linear, Figure 3.2c, although the gold chain bends to adapt to the step morphology. A T-shaped structure, and the rhombus, Figure 3.2d and 3.2e, are respectively 0.12 and 0.53 eV higher in energy. The Au–Au distances in the chain ranges from 2.66 to 2.73 Å, and the cluster carries a net spin localized mostly on the terminal Au atoms. Notice that a slightly distorted chain or a T-shaped structure is the lowest isomer also for gas-phase Au_4^-, depending on the computational method used.[7,8]
$E_b(Au_4)$ is 0.5 eV, again showing the tendency of diffusing Au atoms to add and aggregate on the supported nanoparticle.

There is ample evidence that gold cluster anions are active species in promoting CO oxidation to CO_2,[9,10] or hydrogen peroxide formation from H_2 and O_2.[8] Both theoretical and experimental studies on gas-phase or oxide-supported gold cluster anions show that a key step in the reaction is the formation of a superoxo species, O_2^-.[11–14] In CO oxidation, this is followed by formation of an OOCO intermediate with no oxygen dissociation.[15,16] This leads to a transition state and then to the release of a CO_2 molecule. The rupture of the O–O bond and simultaneous formation of the O–CO bond is the rate-determining step, and the formation of O_2^- a necessary prerequisite.

The adsorption of O_2 on Au_4^- has thus been considered as a starting point of a catalytic route for the oxidation of CO. O_2 binds to Au_4^- by 0.45 eV in a side-on con-

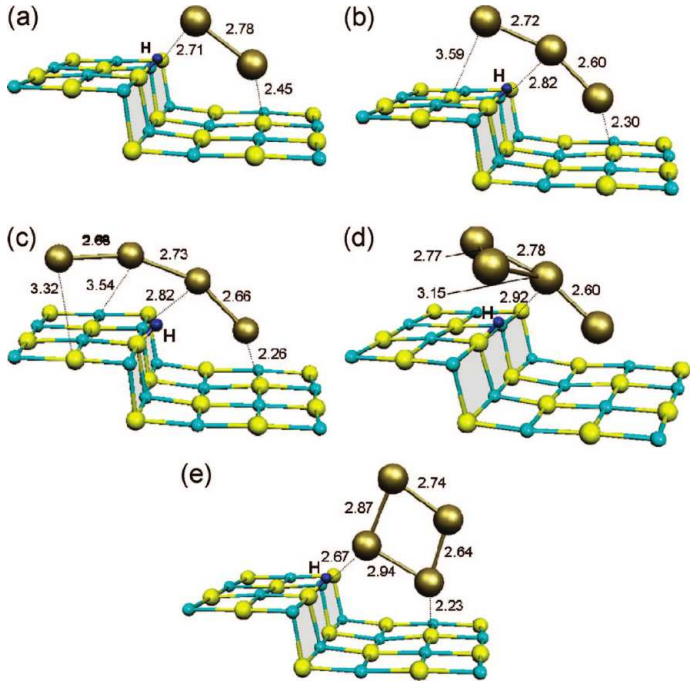

Figure 3.2: Structure of Au dimer (a), trimer (b), and tetramers (c-e) formed on $(H^+)(e^-)$ sites of the MgO surface. Selected distances are given in Å.

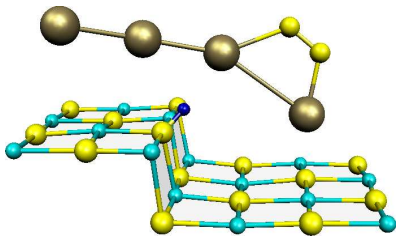

Figure 3.3: Structure of $MgO(H^+)(Au_4/O_2^-)$. Selected distances are given in Å.

figuration, Figure 3.3; a terminal configuration, nearly degenerate with the side-on one, has also been found. The O–O bond activation due to the partial delocalization of the extra electron on the molecule is shown by the elongation of the O–O bond length, 1.31 Å (to be compared with 1.21 Å in the gas-phase O_2 and 1.35 Å in free

O_2^-) and by the analysis of the spin population.

It has been shown that the reaction of CO with activated O_2 can occur following a Langmuir-Hinshelwood (LH) mechanism, dominated by diffusion of CO adsorbed on the Au cluster or at the cluster-oxide interface, or an Eley-Rideal (ER) mechanism where gas-phase CO brought into the vicinity of the superoxo complex reacts spontaneously to form CO_2. In both cases, the activation barrier is low.[17–20]

Our calculations indicate that indeed the following reactions occur according to an ER mechanism on Au_4^-:

$$\mathrm{MgO(H^+)(Au_4/O_2^-) + CO \rightarrow MgO(H^+)(Au_4/OOCO^-) \rightarrow MgO(H^+)(Au_4/O^-) + CO_2} \tag{3.4}$$

$$\mathrm{MgO(H^+)(Au_4/O^-) + CO \rightarrow MgO(H^+)(Au_4/OCO^-) \rightarrow MgO(H^+)(Au_4^-) + CO_2} \tag{3.5}$$

Attempts to identify the same process according to a LH mechanism failed. Our results show that the process is only weakly activated and proceeds via formation of a OOCO intermediate, eq. 3.4.

Reaction 3.4 leads to the formation of $MgO(H^+)(Au_4/O^-)$, Figure 3.4, and CO_2 with an energy gain of 3.2 eV; the barrier for CO_2 desorption is 0.41 eV. A second gas-phase CO molecule readily interacts with $MgO(H^+)(Au_4/O^-)$ to form a OCO intermediate (eq. 3.5) and then CO_2 + $MgO(Au_4^-)$; the process is exothermic by 2.4 eV, and the barrier for CO desorption 0.21 eV only. Therefore, the gold clusters is not poisoned by the adsorbed oxygen and at the end of the cycle $(H^+)(Au_4^-)$ is regenerated.

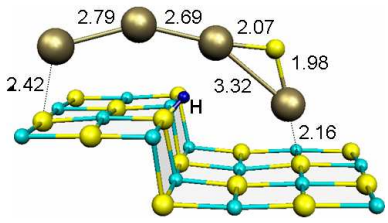

Figure 3.4: Structure of $MgO(H^+)(Au_4/O^-)$. Selected distances are given in Å.

3.4 Conclusions

Making use of both existing experimental evidence and first principles DFT calculations, we suggest that it is possible to prepare thermally stable and chemically active gold nanoclusters on the surface of an ionic oxide like MgO. The preparation should follow a two-step procedure. First, a properly functionalized MgO surface is customed by dropping excess electrons at specific sites. A few well-established routes exist to create electron-rich surfaces, provided that a sufficient number of low-coordinated sites exist.[21] Once the surface electron traps have been generated, low amount of gold can be deposited. The theoretical results indicate that the atoms will diffuse on the surface and get trapped at the $(H^+)(e^-)$ centers, forming thermally stable gold anions, and that nucleation and growth of gold nanocluster anions can easily occur on these sites.

With respect to gold clusters activated on oxygen vacancies, the present method presents three important advantages. First, interaction of a gold cluster with an oxygen vacancy is not always sufficient to guarantee the activation of the O–O bond and the enhanced activity.[22,23] The second, and more important, advantage is that the process which takes place on activated gold clusters at electron traps is in fact catalytic, as it implies the regeneration of the original supported cluster anion at the end of the cycle. This is not granted on oxygen vacencies, where the atomic oxygen formed in the course of the reaction most likely migrates to the interface and fills the vacancy with elimination of the surface defect with a huge gain in energy (8-9 eV), poisoning the catalyst.[24]
The third advantage is that electron traps can be easily produced by chemical methods, at variance with oxygen vacancies which must be produced under severe conditions (electron bombardment, preparation of substoichiometric oxides, high thermal treatment in oxygen-poor atmosphere, etc.).

The results of this chapter have been reported in the following publication:
G. Pacchioni, S. Sicolo, C. Di Valentin, M. Chiesa, E. Giamello, *J. Am. Chem. Soc.* **130** (2008), p. 8690.

Bibliography

[1] *CRC Handbook of Chemistry and Physics*, 88th ed., CRC Press, Boca Raton, 2008.

[2] R. J. Calotta, R. A. Bennet, J. L. Hall, M. W. Siegel, J. Levine, *J. Phys. Rev. A* **6** (1972), p. 631.

[3] A. Del Vitto, G. Pacchioni, F. Delbecq, P. Sautet, *J. Phys. Chem. B* **109** (2005), p. 8040.

[4] G. Barcaro, A. Fortunelli, *J. Chem. Theory Comput.* 1 (2005), p. 972.

[5] L. M. Molina, B. Hammer, *Phys. Rev. B* **69** (2004), p. 155424.

[6] L.M Molina, J. A. Alonso, *J. Phys. Chem. C* **111** (2007), p. 6668.

[7] H. Häkkinen, B. Yoon, U. Landman, X. Li, H.-J. Zhai, L.-S. Wang, *J. Phys. Chem. A* **107** (2003), p. 6168.

[8] F. Wang, D. Zhang, H. Sun, H., Y. Ding, *J. Phys. Chem. C* **111** (2007), p. 11590.

[9] J. Hagen, L. D. Socaciu, M. Elijazyfer, U. Heiz, T. M. Bernhardt, L. Wste, *Phys. Chem. Chem. Phys.* **4** (2002), p. 1707.

[10] W. T. Wallace, R. L. Whetten, *J. Am. Chem. Soc.* **124** (2002), p. 7499.

[11] B. Yoon, H. Häkkinen, U. Landman, *J. Phys. Chem. A* **107** (2003), p. 4066.

[12] B. E. Salisbury, W. T. Wallace Whetten, *Chem. Phys.* **262** (2000), p. 131.

[13] D. Stolcic, M. Fisher, G. Gantefr, Y. D. Kim, Q. Sun, P. Jena, *J. Am. Chem. Soc.* **125** (2003), p. 2848.

[14] G. Mills, M. S. Gordon, H. Metiu, *Chem. Phys. Lett.* **359** (2002), p. 493.

[15] O. Meerson, G. Sitja, C. R. Henry, *Eur. Phys. J. D* **34** (2005), p. 119.

[16] M. Arenz, U. Landman, U. Heiz, *ChemPhysChem* **7** (2006), p. 1871.

[17] L. D. Socaciu, J. Hagen, T. M. Bernhardt, L. Wste, U. Heiz, H. Häkkinen, U. Landman, *J. Am. Chem. Soc.* **125** (2003), p. 10437.

[18] L. M. Molina, B. Hammer, *Phys. Rev. B* **69** (2004), p. 155424.

[19] H. Häkkinen, U. Landman, *J. Am. Chem. Soc.* **123** (2001), p. 9704.

[20] L. M. Molina, B. Hammer, *App. Catal. A* **291** (2005), p. 21.

[21] M. Chiesa, M. C. Paganini, E. Giamello, D. M. Murphy, C. Di Valentin, G. Pacchioni, *Acc. Chem. Res.* **39** (2006), p. 861.

[22] L. M. Molina, B. Hammer, *J. Catal.* **233** (2005), p. 399.

[23] B. Yoon, H. Häkkinen, U. Landman, A. S. Wörz, J.-M. Antonietti, S. Abbet, K. Judai, U. Heiz, *Science* **307** (2005), p. 403.

[24] G. Pacchioni, *ChemPhysChem* **4** (2003), p. 1041.

Chapter 4

Stabilization of Pd_n^- on an electron-rich MgO surface

4.1 Abstract

Density functional theory calculations have been performed on the interaction of Pd atoms and small Pd clusters with an electron-rich MgO surface generated by forming electron traps. By deposition of gas-phase Pd atoms on the properly functionalized MgO surface, one can generate collections of small Pd cluster anions with peculiar chemical properties. The electron traps act as nucleation sites for diffusing Pd atoms and favor the formation of small, thermally stable Pd_n^- clusters. The presence of an extra charge on the metal cluster results in a large vibrational red-shift of adsorbed CO molecules. The present results intend to stimulate experimental work to produce stable metal cluster anions on the surface of an ionic oxide.

4.2 Computational details

MgO (100) surface has been modeled in the framework of the embedded cluster scheme implented in the GUESS code interfaced with Gaussian03 code (see Chapter 2). The quantum-mechanical region (QM) of the cluster is surrounded by about 300 classical ions whose polarizability is described by the shell-model. Cations at the interface between quantum-mechanical and shell-model regions are modeled by ions (hereafter indicated as Mg^*) on which a semi-local effective pseudopotential (ECP) is located, in order to reproduce the Pauli repulsion and avoid the non-physical polarization of QM interface anions. Region I, QM and SM, is then surrounded by a large array of point charges (PC) in order to correctly reproduce the long-range electrostatic potential. All the quantum-mechanically treated atoms, in-

cluding ECPs, have been optimized, whereas only shells – but not cores – have been relaxed in the SM region. The total energy and the electronic structure of the QM cluster are calculated within DFT using the hybrid B3LYP exchange-correlation functional.

The following QM clusters have been used to model regular terrace and morphological defective sites of the MgO surface:

- $Mg_9O_9Mg^*_{17}$ (terrace),
- $Mg_{10}O_{10}Mg^*_{14}$ (edge),
- $Mg_8O_8Mg^*_{12}$ (step),
- $Mg_{10}O_{10}Mg^*_{9}$ (corner),
- $Mg_{17}O_{17}Mg^*_{22}$ (reverse corner).

The basis sets used are: 6-311+G** on H, 6-31G* on Mg, 6-31G on O. Pd has been treated with the lanl2 scalar relativistic effective core potential, which explicitly includes the $4s^2$ $4p^6$ $4d^{10}$ electrons in the valence, together with the lanl2dz basis set augmented with one s function (α = 0.0218) in order to reproduce the electron affinity (EA) of the Pd atom, 0.39 eV to be compared with the experimental value of 0.56 eV.[1] CO molecule has the 6-311+G* basis set; with this basis set the computed CO frequency is 2211 cm^{-1}.

4.3 Results and discussion

4.3.1 Pd atom adsorption on $(H^+)(e^-)$ sites

The four $(H^+)(e^-)$ defect centers where Pd atoms have been adsorbed are shown in Figure 4.1.
Gas-phase Pd atoms bind strongly to $(H^+)(e^-)$ defect centers with binding energies ranging from 2.2 eV to 2.6 eV. Compared to Au atoms (see Chapter 3), Pd atoms are less strongly bound by 1.2-1.3 eV, a difference which reflects the difference in the EAs.[1] The adsorbed Pd atom assumes a position where the shortest distances are from the proton, 2.2-2.5 Å, and from the low-coordinated cation, 2.6-2.7 Å.

In real systems, deposition of Pd occurs through metal vaporization:[2,3] the atoms reach the surface with a thermal energy which allow them to explore large portions

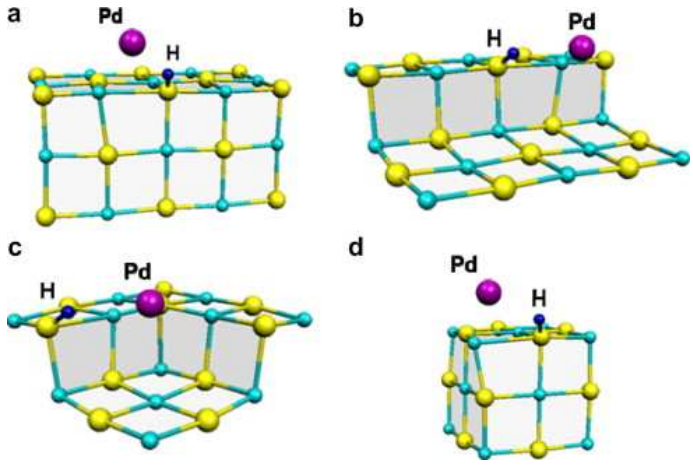

Figure 4.1: Optimal geometry of a Pd atom adsorbed at a $(H^+)(e^-)$ center on a edge (a), step (b), reverse corner (c) and corner (d) sites of the MgO surface.

of the surface before they thermalize and get trapped at a given adsorption site. The Pd atom binds to the regular O sites of the MgO terrace by 1.0 eV (B3LYP result) and diffuses with a computed barrier of about 0.4 eV.

An important quantity to be considered in this context is the cluster binding energy, E_b, which measures the stability of a Pd_n cluster referred to a pre-adsorbed Pd_{n-1} cluster and a neutral Pd adatom bound to a terrace O_{5c} site, as it is assumed that this is the most likely site where Pd atoms are deposited from the gas-phase:

$$E_b = -E[(H^+)(Pd_n^-)] + E[(H^+)(Pd_{n-1}^-)] + E(Pd_1/MgO) - E(MgO) \qquad (4.1)$$

Notice that in typical growth conditions E_b is a key quantity, because cluster growth is dominated by diffusion rather than direct attachment from the gas-phase.[4]
A positive E_b value indicates stability of the cluster against fragmentation. $E_b(Pd_1)$ for an isolated Pd atom ranges between 1.2 eV and 1.6 eV, Table 4.1, which means that once bound to a $(H^+)(e^-)$ center the atom will hardly diffuse away even at relatively high temperatures.

Due to the $4d^{10}5s^0$ configuration of the Pd ground state, its interaction with the $(H^+)(e^-)$ centers leads to a paramagnetic $(H^+)(Pd^-)$ species (doublet ground state), detectable in principle by EPR spectroscopy. The nature of the adsorbed Pd atom has thus been investigated also with the aid of spin density maps, Figure 4.2a,

	$E_a(Pd)^\dagger$, eV	$E_b(Pd)$, eV	r(Pd–Mg), Å	r(Pd–H), Å
Edge	2.27	1.27	2.63	2.15
Step	2.61	1.61	2.62	2.23
Reverse corner	2.35	1.35	2.68	2.37
Corner	2.16	1.16	2.55	2.53

Table 4.1: Adsorption properties of neutral Pd atoms on $(H^+)(e^-)$ defect centers on various sites of MgO (100) surface.
†Computed as $E_a = E[MgO(H^+)(Pd^-)] + E[MgO(H^+)(e^-)] + E(Pd)$.

which show the unpaired electron residing in a 5s orbital of Pd; the population analysis shows that, upon adsorption, the Pd atom has changed its configuration from $4d^{10}5s^0$ to $4d^{10}5s^1$, consistent with the gain of an extra electron.

Stability and diffusion of Pd^- ions on MgO

Pd^- is an intrinsically unstable species when not directly stabilized by a Mg cation. Attempts to identify a diffusion barrier for the movement along the diagonal connecting two Mg_{5c} cations resulted into the loss of the extra electron, which is trapped at low coordinated sites of the MgO surface. This behaviour is consistent with the low EA of the Pd atom.

4.3.2 Pd_n^- clusters in gas-phase and on electron-rich MgO

Pd clusters containing up to five atoms formed by addition of a neutral Pd atom to an existing $(H^+)(Pd_{n-1}^-)$ complex formed at a monoatomic step have been studied. For each cluster size several isomers have been optimized, and the final structures have been compared to gas-phase anion counterparts. In this way, the effect of the extra charge on the geometry of the cluster can be studied, separating it from the effect of the support which also acts to modify the cluster structure.

Pd_2^- The addition of a gas-phase Pd atom to $(H^+)(Pd_1^-)$ leads to an energy gain of 2.14 eV, with E_b = 1.14 eV. Thus, the formation of a dimer is a thermodynamically favorable process also with respect to adsorbed Pd atoms. This is an important conclusion, since it has been shown that the dimerization of late transition metals

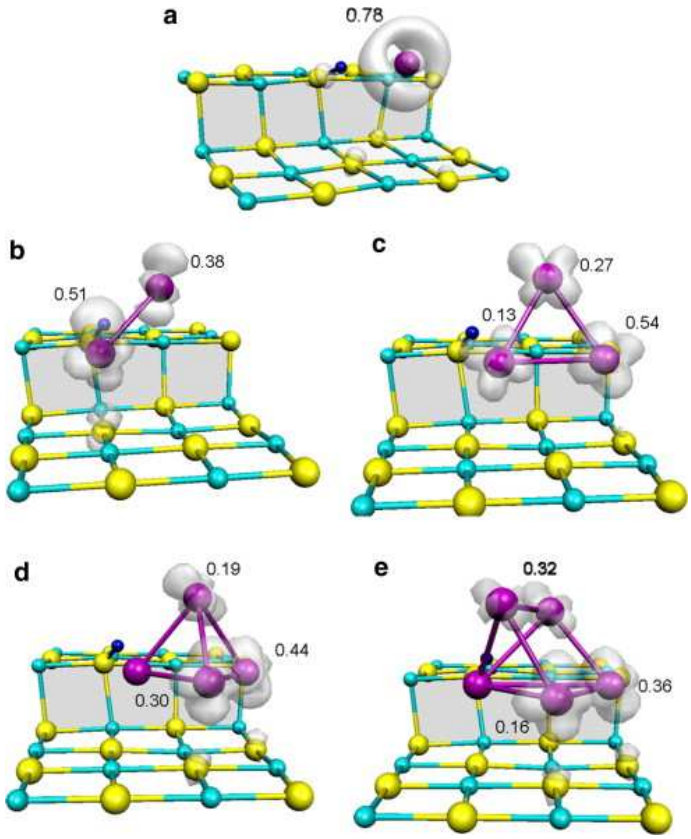

Figure 4.2: Spin density maps of Pd atoms and clusters adsorbed on a $(H^+)(e^-)$ center on a MgO step: (a) Pd_1; (b) Pd_2; (c) Pd_3; (d) Pd_4; and (e) Pd_5. The spin population on each Pd atom is given.

on other common defects like oxygen vacancies of the MgO surface is not favorable[5] or moderately favorable.[6]

The molecule is interacting with the MgO step with one Pd atom close to the proton and to the Mg_{5c} site of the basal plane and the second atom pointing toward a Mg_{4c} ion along the step, Figure 4.3b. The spin is largely residing on the two Pd atoms, Figure 4.2b, with an almost uniform distribution (0.51 and 0.38, respectively). The Pd–Pd distance in supported Pd_2^-, 2.60 Å, is only slightly shorter than that of the gas-phase anion, 2.68 Å.

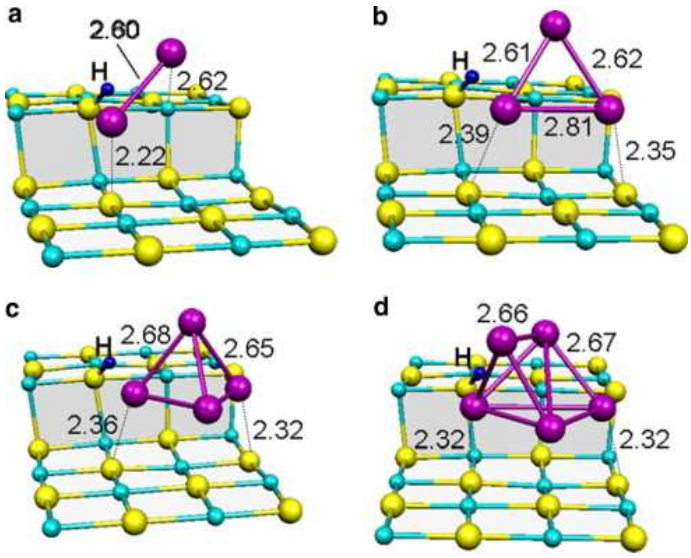

Figure 4.3: Optimal geometry of Pd clusters formed at a $(H^+)(e^-)$ center on a step: (a) Pd_2; (b) Pd_3; (c) Pd_4; (d) Pd_5.

Pd_3^- The addition of a third Pd atom leads to a stable structure with triangular shape, Figure 4.3b; a linear shaped Pd_3 cluster is unstable and spontaneously converts into the triangular structure. The third Pd atom is bound by 2.52 eV, hence E_b is 1.52 eV, again showing the strong tendency of these sites to act as nucleation centers.

The structure is not an equilateral triangle as in the gas-phase (r(Pd–Pd) = 2.61 Å) since the elongation of one of the bonds to 2.81 Å allows two Pd atoms to interact with two Mg_{5c} ions of the lower plane; the third Pd atom is pointing away from the surface and is not interacting with any surface site, forming two bonds of similar length, about 2.6 Å, with the other Pd atoms. Ths geometry closely resembles the one of a neutral Pd_3 cluster deposited on a MgO step.[7] The spin density is mostly localized on the Pd atoms more distant from the OH group, Figure 4.2c.

Pd_4^- The addition of the fourth Pd atom to Pd_3 can result in principle in two different structures, a planar rhombus (two-dimensional growth) or a distorted tetrahedron (three-dimensional growth). Of the two isomers, the distorted tetrahedron (a kind of butterfly structure) is preferred by more than 0.6 eV, Figure 4.3d. Sim-

ilar structures have been found for Pd tetramers on neutral defects of MgO like a divacancy.[7]

The adsorption energy of a gas-phase Pd atom to $(H^+)(Pd_3^-)$ is 2.42 eV and E_b is 1.42 eV, further indicating the favorable cluster growth. As for Pd_3, also in this case the spin is distributed over the three Pd atoms which are not in direct contact with the OH group, Figure 4.2. The Pd–Pd distances are 2.65-2.68 Å for the short bonds and 3.17 Å for the long Pd–Pd distance. For comparison, the average Pd–Pd distances in gas-phase Pd_4^-, a distorted tetrahedron, are 2.70 Å.

Pd_5^- The last cluster considered has been obtained by capping one of the triangular faces of the tetrahedron with a fifth Pd atom, and the resulting geometry can be seen as a distorted trigonal bypyramid, Figure 4.3d.

Also in this case the addition of the fifth Pd atom is exothermic by 1.95 eV, with positive E_b value of 0.95 eV. The spin distribution is shown in Figure 4.2e.

4.3.3 CO adsorption on gas-phase and supported Pd_n^- clusters

CO is often used as a probe molecule to characterize the charge state of a small metal nanoparticle or the nature of an adsorption site.
When adsorbed on a metal, the mechanism of the interaction is described in terms of donation and back donation, where this latter term is responsible for the red-shift of the C–O vibrational frequency.[8] This in turns depends on the coordination of the CO molecule and on the oxidation state of the nanoparticle (oxidized, $\delta+$, or reduced, $\delta-$).

We performed the vibrational analysis of adsorbed CO molecules in order to assign the charge state of the supported Pd nanocluster by means of a direct comparison with the gas-phase neutral and anionic clusters. With this respect, the change in the CO adsorption properties going from free neutral Pd clusters to free Pd cluster anions and to supported Pd cluster anions should provide some trends for the interpretation of the experimental characterization of the nanoclusters. For each cluster, the terminal, bridge and three-fold hollow CO adsorption sites have been checked, Figure 4.4. The results provide useful information and some general trends about the ability of these systems to promote chemical reactions at their surface.

Table 4.2 compares the adsorption properties of CO on gas-phase neutral, gas-phase anion and supported Pd_n clusters (n = 1-5). It is apparent that the strongest

bonds take place between CO and neutral Pd clusters. Here the highest coordinated sites are clearly preferred. CO binds to Pd_1 by 1.8 eV, value which is resembling the one on Pd^-; both are higher than the binding energy on $(H^+)(Pd^-)$ by about 0.4 eV. On Pd_2 the bridge site is highly preferred over the terminal bond by more than 1 eV. On Pd_3, Pd_4 and Pd_5 the three-fold hollow site is the most stable, with binding energies ranging between 2.2 eV and 2.9 eV.

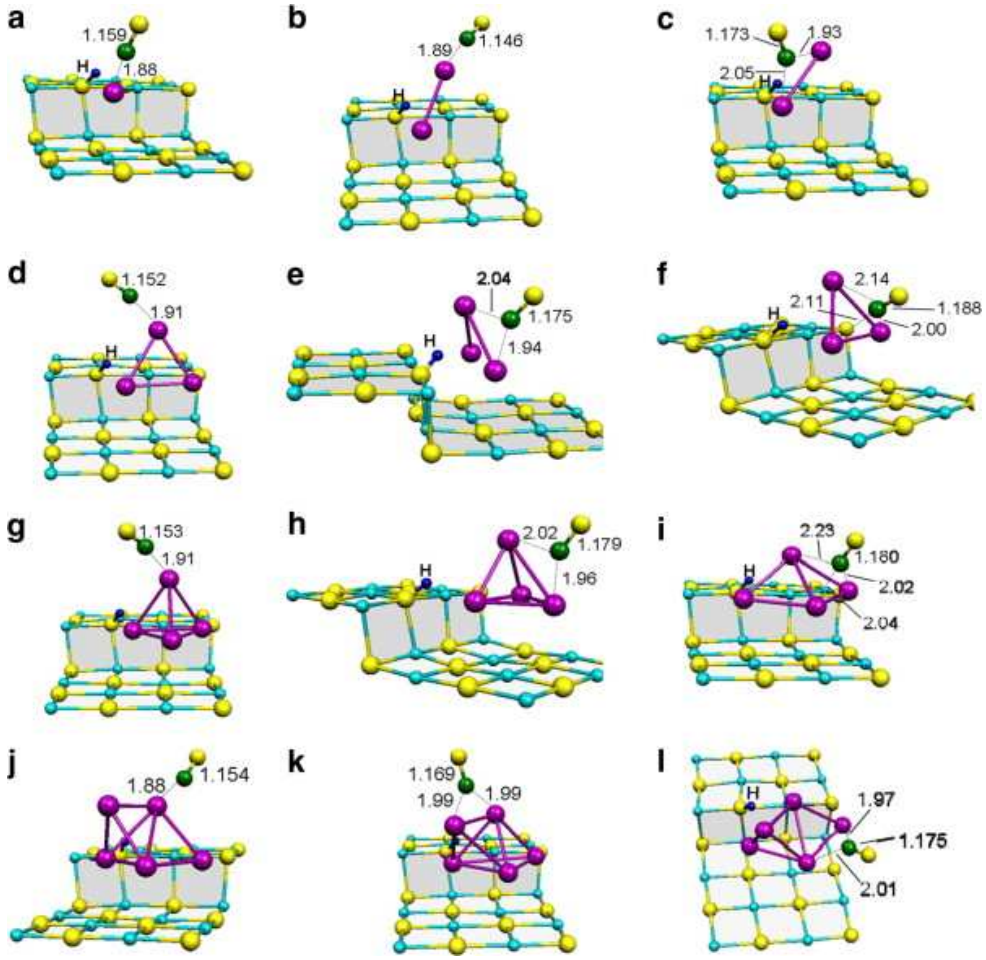

Figure 4.4: Optimal geometry of Pd clusters formed at a $(H^+)(e^-)$ center on a step: (a) Pd_2; (b) Pd_3; (c) Pd_4; (d) Pd_5.

n	CO site		Pd_n	Pd_n^-	$(H^+)(Pd_n^-)$
1	μ^1	D_e eV	1.79	1.87	1.37
		ω_e(C–O) cm^{-1}	2111	1981	1991
2	μ^1	D_e eV	1.67	2.42	1.36
		ω_e(C–O) cm^{-1}	2088	1982	2049
	μ^2	D_e eV	1.67	2.42	1.36
		ω_e(C–O) cm^{-1}	2088	1982	2049
3	μ^1	D_e eV	1.57	1.64	1.11
		ω_e(C–O) cm^{-1}	2109	1992	2019
	μ^2	D_e eV	/	1.43	1.31
		ω_e(C–O) cm^{-1}	/	1845	1866
	μ^3	D_e eV	2.85	1.42	1.54
		ω_e(C–O) cm^{-1}	1819	1724	1778
4	μ^1	D_e eV	1.46	2.01	1.10
		ω_e(C–O) cm^{-1}	2106	1981	2011
	μ^2	D_e eV	/	1.48	1.57
		ω_e(C–O) cm^{-1}	/	1853	1847
	μ^3	D_e eV	2.64	1.49	1.57
		ω_e(C–O) cm^{-1}	1776	1737	1819
5	μ^1	D_e eV	1.24	1.77	1.49
		ω_e(C–O) cm^{-1}	2084	1984	2017
	μ^2	D_e eV	/	1.30	1.13
		ω_e(C–O) cm^{-1}	/	1846	1917
	μ^3	D_e eV	2.12	1.65	1.65[†]
		ω_e(C–O) cm^{-1}	1766	1712	1859[†]

Table 4.2: Properties of CO adsorbed on terminal, bridge, or hollow sites of gas-phase Pd_n and Pd_n^- clusters and of MgO supported $(H^+)(Pd_n^-)$ clusters.
D_e = dissociation energy, ω_e = harmonic vibrational frequency.
[†]The geometry is between bridge and hollow.

The preference for high coordinated sites is no longer present on gas-phase Pd_n^- anions and is much less pronounced on the MgO supported $(H^+)(Pd_n^-)$ clusters. On gas-phase Pd_2^- the only stable isomer is the one where CO binds to the apical position; on the supported clusters two isomers exist, bridge and terminal, the bridge one being preferred over the terminal by 0.4 eV. Also on free and supported Pd_3^- there is no clear preference for a specific bonding site, with energy differences of at most 0.4 eV and often smaller. On free Pd_4^- and Pd_5^- there is a tendency for CO to bind preferentially on-top of a Pd atom, while on the corresponding supported units the most stable site is bridge. Here too, however, the energy differences are relatively small compared to the neutral clusters. In general, the smaller binding of CO to the negatively charged clusters compared to the neutral ones can be explained with a stronger Pauli repulsion:[9] an excess electron results in a more diffuse electron density that the CO molecule has to penetrate in order to efficiently overlap its $2\pi^*$ orbitals with the rather contracted 4d orbitals of Pd. This results in a net negative contribution to the bond strength which is not present on the neutral units.

The most important property, from an experimental point of view, providing indications on the charge state of the cluster is however the C–O vibrational frequency. In addition, it must be taken into account that the frequency depends either on the surrounding charge and on the coordination of the CO molecule (Tab. 4.2).

For the neutral Pd clusters the adsorption in an apical position gives a rather uniform frequency of 2100 $\pm$ 15 cm^{-1}; on a bridge site (stable only for Pd_2) this decreases to 1939 cm^{-1} and on three-fold hollow sites the frequency drops to about 1770-1800 cm^{-1}.

The effect of adding an extra electron to the cluster consists in a red shift of all the frequencies, which is especially apparent for CO adsorbed on terminal sites. On the Pd_n^- clusters the frequency is always about 1980 cm^{-1}, with a red-shift of about 120 cm^{-1} compared to CO adsorbed on the same site of Pd_n; on MgO-supported $(H^+)(Pd_n^-)$ clusters the red-shift is less pronounced, and the frequency for terminal CO ranges between 1991 and 2049 $cm-1$. This can be easily rationalized with the fact that the cluster anion is sitting near an adsorbed proton and some Mg ions of the surface, so that the valence electrons of the Pd cluster are polarized towards these sites and less available for back-bonding to CO.

The same effect is found when CO is bound to bridge or hollow sites: on bridge sites of Pd_n^- clusters the CO frequency is about 1850 cm^{-1}, whereas it ranges from

1847 to 1917 cm^{-1} for supported $(H^+)(Pd_n^-)$; for the three-hollow sites the C–O frequency can be as low as 1712 cm^{-1} for free Pd_n^- clusters, but never below 1778 cm^{-1} on supported clusters. Notice also that on $MgO(H^+)(Pd_n^-)$ clusters the distinction between hollow and bridge sites is often ambiguous: due to the special conformation of the supported cluster and of the surface, sometimes the CO molecule is formally in a bridge site but forming a long bond with a third Pd atom, assuming coordination which is intermediate between bridge and hollow. Also for this reason the identification of the structure of the supported Pd cluster by means of IR spectroscopy of adsorbed CO is hard if not impossible. On the other hand, the experimental identification of higly red shifted frequencies would clearly indicate the formation of Pd cluster anions.

The results reported show quite unambiguously that the extra charge is localized on the Pd unit also for clusters formed at $(H^+)(e^-)$ defect centers, since the properties of these systems are closer to those of the gas-phase Pd_n^- anions than of the neutral counterparts.

4.4 Conclusions

Electron-rich surfaces offer new opportunities for the deposition of metal atoms from the gas-phase and nucleation of small clusters with enhanced chemical activity.[10] In this context, $(H^+)(e^-)$ centers act on one side as anchoring sites for metal clusters thus preventing their diffusion and coalescence; on the other hand, the excess electron delocalizes over the cluster forming a supported cluster anion. In principle, these charged clusters can be more efficient in chemical reactions and can provide a way towards a new class of model catalysts.[11]

This theoretical study only provided some trends and predictions that need to be confirmed by means of experiments, and this study is indeed meant to stimulate specific experimental interest in the system.

The results of this chapter have been reported in the following publication:
S. Sicolo, G. Pacchioni, *Surf. Sci.* **602** (2008), p. 2801.

Bibliography

[1] *CRC Handbook of Chemistry and Physics*, 88th ed., CRC Press, Boca Raton, 2008.

[2] C. Henry, *Surf. Sci. Rep.* **31** (1998), p. 231.

[3] H.-J. Freund, *Surf. Sci.* **500** (2002), p. 271.

[4] G. Haas, A. Menck, H. Brune, J. V. Barth, J. A. Venables, K. Kern, *Phys. Rev. B* **61** (2000), p. 11105.

[5] A. Bogicevic, D. R. Jennison, *Surf. Sci.* **437** (1999), p. L741.

[6] L. Giordano, C. Di Valentin, J. Goniakovski, G. Pacchioni, *Phys. Rev. Lett.* **92** (2004), p. 096105.

[7] L. Giordano, G. Pacchioni, *Surf. Sci.* **575** (2005), p. 197.

[8] G. Blyholder, *J. Phys. Chem.* **68** (1964), p. 2772.

[9] P. S. Bagus, K. Hermann, C. W. J. Bauschlicher, *J. Chem. Phys.* **80** (1984), p. 4378

[10] G. Pacchioni, S. Sicolo, C. Di Valentin, M. Chiesa, E. Giamello, *J. Am. Chem. Soc.* **130** (2008), p. 8690.

[11] S. Abbet, A. Sanchez, U. Heiz, W.D. Schneider, A.M. Ferrari, G. Pacchioni, N. Rösch, *J. Am. Chem. Soc.* **122** (2000), p. 3453.

Part II

Charging by means of tunneling through thin films

Chapter 5

Adsorption of late transition metal atoms on MgO ultrathin films

5.1 Abstract

The adsorption properties of Ni, Pd, Pt, Cu, Ag, and Au atoms on MgO ultrathin films deposited on Mo(100) or Ag(100) substrates are determined from first principle DFT calculations and compared with the corresponding adsorption characteristics on the bare MgO(100) surface. The three supports clearly exhibit different behaviors. On MgO/Mo(100) thin films a more or less pronounced charge transfer can be observed from the metal/oxide interface to the adatoms. This has dramatic consequences on the adsorption properties – such as the preferred adsorption sites, the bond strength and the magnetic state of the adatoms – which differ significantly from what found for the same atoms on the bare MgO(100) surface. MgO/Ag(100) films have an intermediate behavior between that of MgO/Mo(100) thin films and of the non-functionalized MgO(100) surface: the charge transfer is found only for Au and, to a smaller extent, for Pt atoms. All other atoms keep essentially their atom-like properties. The reasons for the different behavior are rationalized in terms of global properties of the metal/oxide interface and in particular of its work function.

5.2 Computational details

The calculations are based on density functional theory at the level of the generalized gradient approximation (PW91 exchange-correlation functional) implemented in the VASP program (see Chapter 2) which uses a plane wave basis set with a cutoff of 400 eV and a projector augmented wave method (PAW) for the treatment of core electrons. The MgO(100) single crystal surface has been modeled by a three-layers

slab; MgO ultrathin films have been represented by two-layers deposited either on three Ag(100) layers or four Mo(100) layers. In order to allow for a perfect interface, the MgO lattice parameter has been adapted to that of the underlying metal, which means a compression of 2% for the case of Ag(100) and an expansion of 5% for the case of Mo(100). In all systems the bottom layer has been kept frozen during geometry optimization. For the calculations we used a 3×3 supercell and the atoms within the supercell have been relaxed until a 0.01 eV/Å convergence threshold was reached for atomic forces. Brillouin-zone sampling has been performed on a 4×4×1 k-points mesh according to MonkhorstPack integration scheme. The properties of the metals have been analyzed considering three high-symmetry adsorption sites, O-top, Mg-top and hollow, and performing optimizations with symmetry constraints. Spin polarized calculations have been performed to account for the presence of unpaired electrons in the valence shell of the TM atoms.

As a measure of the spin polarization in the cell we report the difference between spin up and spin down populations, $n_\uparrow$ - $n_\downarrow$, whose interpretation requires some caution. In fact, several contributions – amongst which the presence of a metal substrate in combination with the use of a smearing parameter and the formation of metal induced gap states which penetrate into the oxide layer and hybridize with the metal atomic states – contribute to the significant deviation from integer numbers that are expected for spin populations, leading to misleading considerations in apparent contradiction with other properties. The critical interpretation of the spin populations has been indeed the most demanding task of this work.

5.3 Results and discussion

5.3.1 Adsorption on bare MgO (100)

The adsorption of metal atoms on the bare MgO surface has been described in several studies.[1–4] Here we discuss this system only in order to analyze the changes which originate when a TM atom is adsorbed on a MgO ultrathin film. To this end we have monitored the local adsorption properties (adsorption energy and geometry, magnetization, Bader charge, Table 5.1).

Cu, Ag, Au The valence configuration of Cu, Ag, and Au atoms is $nd^{10}(n+1)s^1$. The presence of a filled d shell and a singly occupied s orbital prevents the atoms

from easily changing their electronic configuration due to the interaction with the substrate. This is shown by the values of the magnetization, $n_\uparrow$ - $n_\downarrow$ = 1.0 e^-, Table 5.1. For the case of gold, this bonding nature has been confirmed experimentally.[5] The relatively weak bonding found for Cu, Ag, and Au is the consequence of the presence of a diffused singly occupied valence (n+1)s orbital and the difficult s-d hybridization. The O-top adsorption site is always preferred to the Mg-top one, which in fact is not even a local minimum. Also hollow sites are local minima and represent transition states in the diffusion process from an O-top site to the next one.[6] The trend in bond strength is Au > Cu > Ag. Ag behaves somewhat differently from Cu and Au also in terms of the bond distance which is longer than for the other two members of the triad, Table 5.1. These differences may be related to the large energy separation between the Ag 4d and 5s levels compared to the d-s separation in Cu and Au which results in very different $s^1d^{10} \rightarrow s^2d^9$ transition energies.[1] The smaller s-d hybridization and consequently the small mixing with the oxygen orbitals is the reason for the weaker bonding of Ag compared to Cu and Au.

TM	site	E_{ad} eV	r(M-X) Å	$n_\uparrow$ - $n_\downarrow$	Bader charge
Cu	O-top	0.95	1.97	1.00	-0.12
	Mg-top	0.25	2.74	1.00	-0.06
Ag	O-top	0.42	2.41	1.00	-0.13
	Mg-top	0.20	2.90	1.00	-0.05
Au	O-top	0.89	2.28	1.00	-0.30
	Mg-top	0.44	2.72	1.00	-0.21
Ni	O-top	1.77	1.79	0.00	-0.15
	Mg-top	0.28	2.77	2.00	-0.03
Pd	O-top	1.44	2.07	0.00	-0.21
	Mg-top	0.52	2.57	0.00	-0.11
Pt	O-top	2.46	1.97	0.00	-0.37
	Mg-top	0.55	2.66	1.90	-0.23

Table 5.1: Adsorption properties of TM on the MgO(100) surface.

Ni, Pd, Pt The interaction of Ni, Pd, and Pt atoms with MgO is considerably more complex than that of the coinage metal atoms, because of the interplay between the d^{10}, the d^9s^1 and, at least for Ni, the d^8s^2 configurations of the atoms. The O-top site is always preferred compared to the Mg-top one, Table 5.1. The trend in bond strength is Pt $>$ Ni $>$ Pd, and shows the same behavior along the group observed for the coinage metal atoms. The low-spin coupling of the metal open-shell electrons seems to be preferred when the bonding is with the surface oxygen. However, for atoms like Ni there is a near degeneracy of magnetic and non-magnetic states as discussed in the literature.[1,7] On the Mg sites, where the bonding is much weaker, the values of the magnetization are closer to those of the free atoms (triplet states). The Bader charge analysis performed on all metal atoms shows non-zero values, due to the mixing of metal and oxide states. These charges are indicative of the formation of a covalent polar bond, and do not reflect the occurrence of a significant charge transfer.[1,2] Larger values of the Bader charges (0.37 e^-) are found in correspondence of stronger bonds (e.g. Pt, Table 5.1).

5.3.2 Adsorption on MgO/Mo(100)

In this section we analyze the behavior of TM atoms adsorbed on a 2ML MgO film deposited on Mo(100). The MgO/Mo(100) interface exhibits a smaller work function compared to the MgO/Ag(100) one, 2.08 eV vs. 3.01 eV, with the present computational setup. In this respect, this support is expected to show larger deviations from the adsorption properties of the bare MgO surface. We start the discussion from the coinage metal atoms.

Cu, Ag, Au On MgO/Mo(100), the three metals experience much stronger bonds than on bare MgO, Table 5.2: the binding energies increase by about a factor two for Ag and Au, while a less pronounced change is found for Cu. The other major difference is that O-top is no longer the most stable adsorption site: the hollow site, where the metal atom interacts with two cations, becomes preferred. The order of stability is hollow $>$ Mg-top $>$ O-top, although the three sites are always nearly isoenergetic within 0.1-0.3 eV. This indicates a rather flat potential energy surface for the adsorption of Cu, Ag and Au atoms on MgO/Mo(100). Besides the adsorption energies, also the other properties (adsorption geometry, Bader charges, magnetization) are nearly the same on the three adsorption sites, reflecting a lack of bond directionality

that is typical of electrostatic interactions and therefore represents a first indication of a strong change in the nature of the surface chemical bond compared to MgO. As it has been discussed already for Au atoms on MgO/Mo(100),[8] a charge transfer from the metal/oxide interface to the adsorbed atom can occur for some adsorbates. This is reflected primarily by the fact that the ground state is non-spin polarized, by the value of the Bader charge on the adatom which is close to 1 e^-, by the DOS curves which show that the (n+1)s level falls below the Fermi level, and by the local structural distortions in response to the presence of a negative adsorbate. In the following we analyze these properties for the three atoms of the series.

TM	site	E_{ad} eV	r(M-X) Å	$n_\uparrow$ - $n_\downarrow$	Bader charge
Cu	O-top	1.29	2.49	0.17	-0.62
	hollow	1.42	2.77 (Mg)	0.00	-0.67
	Mg-top	1.35	2.55	0.00	-0.66
Ag	O-top	1.10	2.76	0.00	-0.63
	hollow	1.23	2.92 (Mg)	0.00	-0.67
	Mg-top	1.17	2.69	0.00	-0.64
Au	O-top	2.15	2.75	0.00	-0.82
	hollow	2.42	2.79 (Mg)	0.00	-0.82
	Mg-top	2.32	2.58	0.00	-0.79
Ni	O-top	2.17	1.80	0.30	-0.34
	hollow	1.76	1.92 (O)	0.08	-0.20
	Mg-top	1.22	2.63	1.15	-0.56
Pd	O-top	1.82	2.14	0.47	-0.52
	hollow	1.41	2.79 (Mg)	0.00	-0.48
	Mg-top	1.09	2.53	0.78	-0.59
Pt	O-top	3.26	2.22	1.04	-0.95
	hollow	2.73	2.60 (Mg)	0.74	-1.07
	Mg-top	2.22	2.51	1.00	-0.95

Table 5.2: Adsorption properties of TM on the MgO/Mo(100) surface. For the hollow sites the closest atom to which r(M-X) is referred is given in the parentheses.

The DOS curves computed for the Cu atom adsorbed on the hollow site, Figure 5.1 (E_{ad} = 1.42 eV, followed by Mg-top, E_{ad} = 1.35 eV and O-top, E_{ad} = 1.29 eV, Table

5.2) show that the metal atom is no longer magnetic as in the gas-phase. Its formal configuration is closed shell $3d^{10}4s^2$ since both α and β components of the 4s level are filled and well below the Fermi level. Notice that the 4s states are in the same energy region of the 3d states, Figure 5.1. The absence of spin polarization and the fact that the 4s level falls below E_F is indicative of the occurrence of a charge transfer to the Cu atom despite its moderate electron affinity, 1.23 eV.[9] The occurrence of a charge transfer is confirmed by the relatively high values of the Bader charge (0.6–0.7 e^-), independent of the adsorption site. Upon Cu adsorption the surface Mg cations and O anions experience a rumpling of about 0.2 Å toward (or away from) the Cu atom, respectively. This is the most prominent contribution to the surface relaxation due to the presence of charged species. It can be considered as a kind of polaronic distortion which contributes to stabilize the extra charge on the Cu atom. The occurrence of this polaronic distortion is an important proof of the presence of a charged adatom.[10]

The Ag case is similar to that of Cu, and indeed Ag has a similar electron affinity, 1.30 eV.[9] The hollow site is slightly preferred over the on-top sites (1.23 eV vs. 1.17 eV and 1.10 eV for Mg-top and O-top, respectively, Table 5.2). The Bader charges and the magnetization values point towards a negatively charged Ag atom. As found already for the bare MgO surface, however, the bonding of the Ag atom to the MgO/Mo(001) film is weaker than for Cu and the distance from the surface is longer. The other relevant difference is in the electronic structure: the 5s level is below E_F but the Ag 4d levels are much deeper in energy compared to the Cu 3d states, Figure 5.1. Thus, the separation between the d and s states, almost absent in the case of Cu, is rather large for Ag. This may result in a smaller s-d hybridization and can explain the observed weaker adsorption. The results obtained on Ag/MgO/Mo(100) using the PAW method are similar to those reported in a previous study[8] based on ultra-soft pseudopotentials. In that work, however, we also considered the dependence of the adsorption properties on the number of MgO layers and we found that the tendency of Ag atoms to trap charge decreases by increasing the thickness of the oxide film.

The last case considered is that, widely discussed, of Au,[8,11] and the present results therefore do not add to what is known already about this system. The atom is charged, as indicated by the high value of the Bader charge (0.8 e^-), and the extent of the charge transfer is similar on every adsorption site. The Au 6s level is well below

E_F, consistent with the high electron affinity of this atom, 2.30 eV.[9] Not surprisingly, also the adsorption energies are the largest in the group of the coinage metals, being about 2.2-2.4 eV, with the hollow adsorption site being slightly preferred, Table 5.2. The observed surface rumpling subsequent to adsorption is substantial, leading to displacements of the surface anions (inward) or of the surface cations (outward) of the order of 0.2-0.3 Å.

To summarize, all three coinage metal atoms exhibit completely different adsorption properties on the bare MgO surface and on MgO/Mo(001) 2L films. In particular, while on the bare oxide the only stable adsorption sites are the O anions, on the thin films the atoms bind in a similar way to O anions, Mg cations, and hollow sites. The other important difference is that the bonding to the surface is much stronger on the thin films than on the bare oxide despite the fact that the surface-adatom distance has considerably increased, Table 5.2. All these results, which would be difficult to interpret on the basis of a classical interaction mode, are the consequence of the net charge transfer from the metal/oxide interface to the adatom.

Ni, Pd, Pt We have seen above that the bonding of Ni, Pd and Pt with the MgO surface is dominated by the strong mixing of TM d orbitals with the 2p orbitals of the surface oxygens which leads to strong, directional covalent-polar bonds.[1,2] Much weaker bonds are found with the surface cations where the interaction is more of electrostatic (polarization) nature. As a general trend, all three atoms are more strongly bound on MgO/Mo(100) films than on the bare MgO surface, confirming the trend observed for Cu, Ag and Au. At variance with the coinage metals, however, the net preference for O-top sites is maintained, and the potential energy surface is more corrugated than in the Cu, Ag and Au cases.

On bare MgO the magnetic moment of the Ni atom is quenched and the ground state is non spin polarized, Table 5.1.[7] This is true also on MgO/Mo(100). The adsorption of Ni on a surface anion results in a high binding energy (2.17 eV, 0.4 eV larger than on bare MgO) and a similar bond length (1.80 Å versus 1.79 Å); the Bader charge (0.34 e^-) together with the value of the magnetization (0.30), the shape of the DOS curves and a small inward displacement of the O atom (-0.09 Å) suggest the occurrence of a small charge transfer. For comparison, the Bader charge on bare MgO is 0.15 e^-. Thus, the interaction is not the same as for the coinage metals, and we have no evidence of a net charge transfer. The DOS curves, Figure 5.1, show the

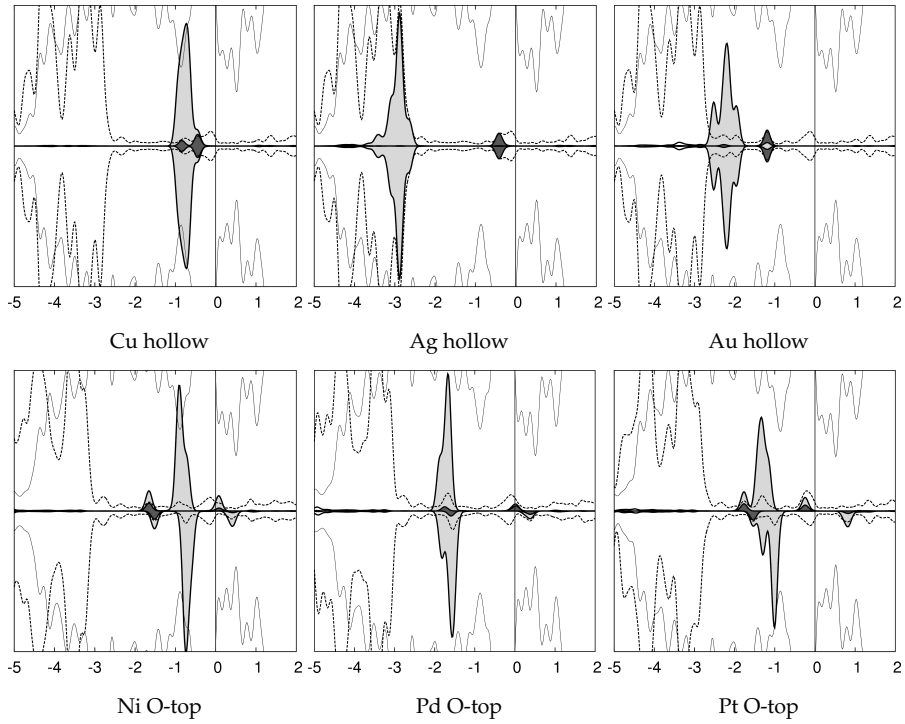

Figure 5.1: DOS curves of Cu, Ag, Au, Ni, Pd, and Pt atoms on MgO/Mo(100) thin films.

absence of magnetization and the presence of filled Ni 4s and partly filled 3d states (configuration $3d^8 4s^2$-like). The fact that the atom cannot be classified as a full anion is due to the substantial mixing with the O 2p states and the covalent nature of the interaction.

Pd, with its $4d^{10}$ configuration, exhibits the lowest electron affinity (0.56 eV) amongst the considered metal atoms.[9]

As for Ni, the adsorption of Pd on the MgO/Mo(100) thin film results in a small charge transfer as inferred by the DOS curves reported for the most stable O-top adsorption site. One component of the 5s state is crossed by the Fermi level, hence partly occupied. This is not the case of Pd adsorption on the bare MgO surface (DOS not shown), where empty 5s orbital is well above E_F.

Also the Bader charge increases compared to the bare MgO case by 0.3/0.4 e^- depending on the adsorption site, see Table 5.1 and Table 5.2. The occurrence of a

small charge transfer is consistent with the displacements of the surface ions, about 0.1 Å outwards (Mg-top) or inwards (O-top). The O-top site is about 0.4 eV more stable than the hollow site and 0.7 eV more stable than the Mg-top site. Therefore, Pd largely keeps its atomic nature and is only partly charged. It should be mentioned that the tendency of Pd to trap charge decreases rapidly by increasing the film thickness, so that on 3L or thicker films the atoms can be considered as essentially neutral.[13]

After Au, Pt has the highest electron affinity (2.13 eV),[9] and is thus expected to exhibit a net charging. This is in fact what emerges from the Bader analysis, which attributes almost a full electron to the adatom on every adsorption site, Table 5.2. Pt exhibits a much stronger bonding with the surface anions, with an adsorption energy of 3.26 eV which is 0.8 eV higher than on the bare MgO surface. There is a considerable displacement of the oxygen atom (0.28 Å) which is consistent with the presence of a full anion. This is also clear from the DOS curves, Figure 5.1, and the net magnetization. The DOS curves suggest for Pt a $4d^9 5s^2$-like electronic configuration which explains the magnetization $n_\uparrow$ - $n_\downarrow$ of 1.04 e^-, Table 5.2.
The hollow site is about 0.5 eV less stable than the O-top one, but the bonding presents the same features, with a net charge transfer and a magnetic ground state. Also the surface relaxation of the Mg cations toward the Pt atom and of the surface anions away from it (0.31 Å and 0.14 Å, respectively) is indicative of the negative nature of the adsorbate. This is more or less the situation found for the Mg-top site: a net charge transfer occurs towards the Pt atom which becomes negatively charged. However, the interaction with Mg cation is about 1 eV weaker than with the O anion. Clearly, covalent mixing largely contributes to the surface chemical bond and determines the preferred adsorption site.

5.4 Adsorption on MgO/Ag(100)

Cu, Ag, Au On MgO/Ag(100), Cu atoms bind on O-top sites with an adsorption energy, 0.93 eV, nearly identical to that found on bare MgO (0.95 eV) and with the same Cu–O distance, Table 5.3.
Also the Bader charge is virtually the same as on bare MgO, and the magnetization is high (0.56), sign that the atom has kept its atomic-like structure with no charge transfer (see also the discussion of the magnetic moments in Sec. 5.2). Compared

to MgO/Mo(100), there is a decrease of 0.36 eV of the adsorption energy. These results, together with the negligible rumpling of the surface anion, are indicative of the fact that no charge transfer has occurred, as on bare MgO. The DOS analysis is also consistent with this conclusion, showing that the β component of the 4s orbital is above the Fermi level, Figure 5.2. The hollow and Mg-sites are 0.30 eV less stable than the O-top one but the bonding is stronger than on the same site of bare MgO, and the Bader charge is larger (0.5-0.6 e^-). Together with the smaller value of the magnetization and the displacements of the underlying anions and cations (-0.15 Å and +0.20 Å away from and towards the metal atom, respectively; hollow site), these data are indicative of a partial charging of the Cu atom on hollow and Mg-top sites. Clearly, the presence of the Mg cation favors the charge transfer to Cu which is not possible on the bare MgO surface, thus resulting in a stronger bond. Of course, since the hollow and Mg-top sites are not the most stable ones, this result is purely hypothetical but it opens interesting questions related to the surface diffusion of the Cu atoms on MgO/Ag(100) since the atoms are expected to change character from neutral to ionic as they move from site to site over the surface.

For Ag, the three adsorption sites are isoenergetic, within 20 meV, Table 5.3. Also here, as for Cu, the nature of the interaction is completely different for the O-top and for the hollow and Mg-top adsorption sites. When sitting on the surface anion, Ag is involved in a covalent bond with a moderately low polar character as inferred by the Bader charge (0.3 e^-) and by the non-zero value of the magnetization (0.4); on the bare MgO surface the Bader charge is 0.13 e^- and the magnetization is close to one, Table 5.3. This is rather different from the MgO/Mo(100) case where the Bader charge, 0.6 e^-, and the non-magnetic ground state are clearly indicative of a charge transfer. The occurrence of a partial charge transfer is more evident on the Mg-top and hollow sites where the Bader charge is 0.45 e^- and the magnetization between 0.2 and 0.3, Table 5.3. Notice that on MgO/Ag(100) the Ag atoms are expected to have a very high mobility (low diffusion barriers) even at very low temperatures.

Gold is a different and well known case[8,11,14] and, somehow, simpler: a charge transfer occurs on all sites and leads to the formation of a full anion. As such, adsorbed Au atoms are accompanied by all typical effects associated to charge transfer: zero magnetization, strong lattice distortion at the adsorption site, large Bader charge, Table 5.3. The hollow site is the preferred one, but small energy differences of 0.1-0.2 eV separate this site from the other sites. The bonding is stronger than on

bare MgO(100) but weaker than on MgO/Mo(100). The DOS curves of Ag and Au atoms adsorbed on the hollow sites of the MgO/Ag(100) films are shown in Figure 5.2.

TM	site	E_{ad} eV	r(M-X) Å	$n_\uparrow$ - $n_\downarrow$	Bader charge
Cu	O-top	0.93	1.97	0.56	-0.11
	hollow	0.65	2.82 (Mg)	0.00	-0.58
	Mg-top	0.62	2.61	0.28	-0.52
Ag	O-top	0.50	2.69	0.39	-0.31
	hollow	0.50	3.03 (Mg)	0.19	-0.45
	Mg-top	0.48	2.81	0.27	-0.44
Au	O-top	1.47	2.81	0.00	-0.81
	hollow	1.64	2.79 (Mg)	0.00	-0.83
	Mg-top	1.54	2.57	0.00	-0.79
Ni	O-top	1.68	1.80	-0.06	-0.16
	hollow	1.29	1.94 (O)	0.88	+0.38
	Mg-top	0.65	2.71	1.35	-0.44
Pd	O-top	1.41	2.09	0.00	-0.24
	hollow	0.96	2.58 (Mg)	0.00	-0.21
	Mg-top	0.59	2.60	0.00	-0.23
Pt	O-top	2.45	2.03	0.00	-0.50
	hollow	1.76	2.67 (Mg)	0.84	-0.95
	Mg-top	1.51	2.57	1.00	-0.77

Table 5.3: Adsorption properties of TM on the MgO/Ag(100) surface. For the hollow sites the closest atom to which r(M-X) is referred is given in the parentheses.

Ni, Pd, Pt The adsorption of Ni on the anionic sites of MgO/Ag(100) ultrathin films resembles that on bare MgO. The Ni-O distance for O-top adsorption (preferred) is 1.80 Å as on MgO(100), and the adsorption energy is slightly lower, 1.68 eV versus 1.77 eV, Table 5.3. Thus, the bond is weaker than on MgO/Mo where the adsorption energy on the O-top site is 2.17 eV. These results already suggest a substantial similarity of the bonding in MgO(100) and MgO/Ag(100).
The interaction on the O-top site is covalent, and leads to a complete quenching of

the atomic magnetic moment, Table 5.3. This is clearly shown also by the DOS plots which suggest the formation of a Ni atom in a formal $3d^8 4s^2$ state, Figure 5.2. The covalent nature of the interaction is confirmed by the low value of the Bader charge, 0.16 e^-, the same found on bare MgO. Thus, the adsorption of a Ni atom on a thin MgO/Ag(100) film or on the bare oxide does not present significant differences.
Some changes are found for the other, less stable, adsorption sites. First of all, in the hollow site the Ni atom induces a strong outward relaxation of the two O ions below it, Table 5.3; these atoms interact with the Ni atom and partly oxidize it, as shown by the positive value of the Bader charge and by the DOS plots (not shown). The charge depletion is consistent also with the value of the magnetization and the average atomic configuration which is close to $3d^8 4s^1$.
The last site, Mg-top, has a weak adsorption energy and a long distance and gives rise to a partial charge transfer to the Ni atom (Bader charge: 0.44 e^-); as usual, there is a distortion of the surface with the Mg cation displaced outward by 0.27 Å.
To summarize, the nature of the interaction of a Ni atom with the MgO/Ag(100) films is very dependent on the adsorption site, although the covalent bond with the oxide anions clearly dominates, as on MgO(100).
Also for Pd the O-top site is the global minimum on the potential energy surface. On this site the adsorption properties are nearly identical to those found on bare MgO(100): bond length (2.09 Å vs. 2.07 Å), bond strength (1.41 eV vs. 1.44 eV), Bader charge on Pd (0.24 e^- vs. 0.21 e^-) and magnetization (null) are the same, indicating no effect due to the film thickness.
The main feature of the DOS curves, Figure 5.2, which can be compared with those obtained on MgO/Mo(100) films, Figure 5.1, is the presence of empty orbitals above the Fermi level which confirm that no charging has occurred. Things are not much different if one forces the Pd atom to be in hollow or Mg-top positions. No charging is found, but the bonding is much weaker.

The last case considered is that of Pt. The O-top site is much more stable than the Mg-top and hollow ones, Table 5.3. As for Pd, the adsorption characteristics on the O-top site of the MgO/Ag(100) films are very similar to those of the bare MgO surface. The only difference is a slightly enhanced Bader charge, 0.50 e^- vs. 0.37 e^-, which however does not result in a stronger adsorption energy (2.45 eV on the thin film, 2.46 eV on MgO(100)). In both cases the magnetization of the free atom is quenched, as shown also by the DOS curves, Figure 5.3. Therefore, Pt atoms

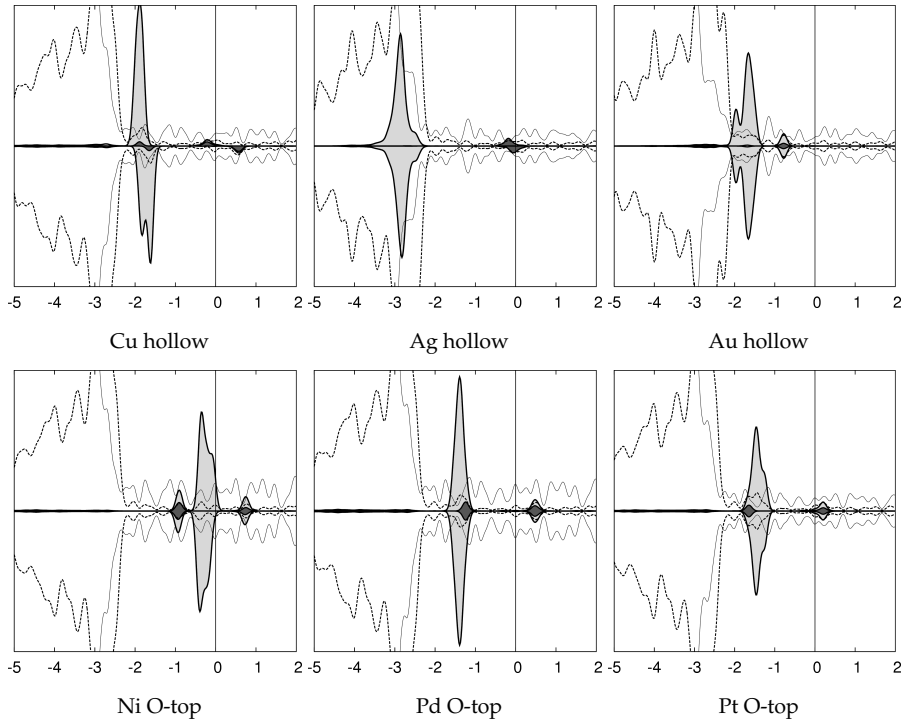

Figure 5.2: DOS curves of Cu, Ag, Au, Ni, Pd, and Pt atoms on MgO/Ag(100) thin films.

adsorbed on MgO/Ag(100) have a very different nature than the same atoms deposited on the MgO/Mo(100) films where a full anion is formed. Only when the Pt atom is placed on a hollow or Mg-top site a net charge transfer is found, as shown by the large value of the Bader charge and by the magnetization close to one, Table 5.3. However, these two sites are considerably less stable than the O-top case and are therefore much less relevant for the discussion.

Concluding this section, we have strong evidence that the adsorption properties of MgO/Ag(100) thin films are very different from the MgO/Mo(100) counterparts. The reasons for these differences will be discussed in the next concluding section.

5.5 Conclusions

The results presented in the previous sections clearly that the deposition of TM atoms on three different forms of the MgO surface result in quite different adsorption properties and bonding mechanism. On the bare MgO(100) surface Ni, Pd, Pt, Cu, Ag and Au atoms are bound by covalent bonds with the oxide anions of the surface. The polar character of the bond results in small formal negative charges on the metal atoms. The coinage metals keep essentially their atomic character; this is true also for the Ni, Pd, Pt triad except that a magnetic quenching is found for Ni and Pt as a consequence of the interaction with the substrate. The bonding with the surface Mg cations of MgO(100) has a totally different origin, mainly polarization, and is much weaker so that it never competes with the adsorption on O-top sites.

The 2L MgO/Mo(100) films provide a totally different picture. The TM atoms adsorbed on these films become full anions (Cu, Ag, Au, Pt) or exhibit a partial anionic character (Ni, Pd) by effect of a charge transfer from the metal/oxide interface. Thus, this is not restricted to the atoms with large electron affinity like Au and Pt, but is found also for atoms with smaller EA like Cu. The occurrence of charge transfer is inferred by the change in adsorption properties with respect to the non-functionalized MgO surface. There is no longer a specific preferred adsorption site, since the three sites, O-top, Mg-top and hollow, exhibit similar binding energies with a general preference for the hollow site; the surface gives rise to a pronounced relaxation in response to the presence of the ionic adsorbate; the magnetic moment changes drastically so that open shell atoms like the coinage metals become diamagnetic by effect of trapping an extra electron.

The case of MgO/Ag(100) films is somehow in between. A charge transfer is observed only for the atoms with the highest electron affinity, Au and Pt, but not for the other TM atoms. However, the different atomic properties of Au and Pt also result in significant differences in the bonding mechanism of the two species. Whereas Au exhibits non-directional bondings, with a slight preference for the hollow sites, typical of charged adsorbates, Pt definitely prefers the bonding to oxide anions of the MgO/Ag(100) films and shows only a partial charge transfer. A net charge transfer is observed for Pt on Mg-top or hollow sites, but this is not sufficient to compensate for the loss of direct covalent bond and these sites are less stable. This behavior is even more pronounced for the other atoms: on MgO/Ag(100) they prefer to bind to the oxide anions with similar characteristics as on the bare MgO(100) surface while

a charge transfer is found for the Mg-top or hollow sites but, again, these sites are nont competitive in terms of stability.

These results show that the nature of the adatoms can be tuned by varying the substrate,thanks to four major contributions that can lead to the stabilization of anions on the surface: (1) the possibility for the oxide substrate to distort and generate a small polaron that stabilizes the adsorbed charged species; (2) the electron affinity of the adatom; (3) the work function of the metal/oxide interface; (4) the penetration of the metal wave function through the oxide layers and the hybridization of these states with those of the supported species. These two latter terms in particular differentiate the behavior of MgO/Mo(100) with respect to MgO/Ag(100) films. As it has been extensively studied,[15–17] the ionic MgO layer has the effect to reduce the work function of the two metals by means of an electrostatic compressive effect. Since the computed interface distance in MgO/Mo(100) is much shorter than the MgO/Ag(100) one, the compressive effect is more efficient in the case of the MgO/Mo interface and this leads to a more pronounced reduction of the metal work function. Eventually, the work function for the MgO/Mo(100) interface is about 2 eV, whereas it is 3 eV on MgO/Ag(100) films. Furthermore, the shorter interface distance in MgO/Mo(001) also favors the penetration of the metal induced gap states and their interaction with the adsorbed atoms. This can explain the different bond strengths for atoms with similar charge (see e.g. Au on MgO/Ag and on MgO/Mo). Thus, the relatively large differences in adsorption properties found for the two interfaces can be referred to these basic properties. Of course, this conclusion is valid as long as the predicted difference in work function is real and not an artifact of the calculations.[18]

Recent accurate measurements of work function values of MgO/Ag(100) and MgO/Mo(100) thin films have been reported using different experimental techniques. Combining a Kelvin probe microscope, a field emission experiment and a scanning tunneling spectroscopy measurements, Heyde *et al.*[19] have been able to measure a work function change for MgO/Ag(100) thin films compared to Ag(100) of 1.2-1.3 eV, in excellent agreement with the theoretical predictions ($\Delta\Phi$ = 1.22 eV). In a different study based on photoemission spectroscopy, Bernhardt *et al.* have performed similar measurements for 2-3 layers of MgO deposited on Mo(100) and found a work function change of about 1.3 eV,[20] much smaller than the one predicted by the calculations ($\Delta\Phi$ = 1.82 eV).

Specific work is planned to account for the observed differences, and at the moment only some hypotheses can be formulated. In our calculations the MgO 2L film is contracted by 2% in case of Ag(100) and expanded by 5% in the case of Mo(100) in order to allow an epitaxial growth of the oxide on the metal. Experimentally, in the low coverage regime MgO actually grows with a contracted lattice parameter in order to match the Ag(100) substrate.[21] Conversely, in the case of Mo(100), due to the larger and expansive mismatch, MgO films between 1 and 7 layers forman ordered network of interfacial misfit dislocations with a periodicity of 60 Å.[22] The use of a 5% expanded unit cell in the case of Mo(100) could result in a more reactive oxide film,[23] in a stronger adhesion and in a shorter interface distance. This could give as a final result a non-realistic reduction of the work function. Work is in progress to create larger unit cells which can accommodate the MgO film without introducing the strain associated to the lattice expansion. However, preliminary results show that even the release of the strain in the film does not chenge the large work function change computed for this system. In real systems the strain is released by formation of line defects and grain boundaries. To what extent these defects affect macroscopic properties like the work function is still under investigation.

The results of this chapter have been reported in the following publication:
S. Sicolo, L. Giordano, G. Pacchioni, *J. Phys. Chem C* **113** (2009), p. 16694.

Bibliography

[1] I. Yudanov, G. Pacchioni, K. Neyman, N. Rösch, *J. Phys. Chem.* **101** (1997), p. 2786.

[2] K. Neyman, C. Inntam, V. A. Nasluzov, R. Kosarev, N. Rösch, *Appl. Phys. A* **78** (2004), p. 823.

[3] S. Fernandez, A. Markovits, F. Fuster, C. J. Minot, *Phys. Chem. C* **111** (2007), p. 6781.

[4] G. Barcaro, A. Fortunelli, *J. Chem. Theory Comput.* **1** (2005), p. 972.

[5] M. Yulikov, M. Sterrer, M. Heyde, H.-P. Rust, T. Risse, H.-J. Freund, G. Pacchioni, A. Scagnelli, *Phys. Rev. Lett.* **96** (2006), p. 146804.

[6] A. Del Vitto, G. Pacchioni, F. Delbecq, P. Sautet, *J.Phys. Chem. B* **109** (2005), p. 8040.

[7] A. Markovits, M. K. Skalli, C. Minot, G. Pacchioni, N. Lopez, F. Illas, *J. Chem. Phys.* **115** (2001), p. 8172.

[8] Pacchioni, G.; Giordano, L.; Baistrocchi, M. Phys. Rev. Lett. 2005, 94, 226104.

[9] *CRC Handbook of Chemistry and Physics*, 55th ed., edited by R. C. Weast (CRC Press, Cleveland, OH, 1974).

[10] L. Giordano, U. Martinez Pozzoni, S. Sicolo, G. Pacchioni, *J. Chem. Phys.* **127** (2007), p. 144713.

[11] K. Honkala, H. Hakkinen, *J. Phys. Chem. C* **111** (2007), p. 4319.

[12] K. Neyman, C. Inntam, V. A. Nasluzov, R. Kosarev, N. Rösch, *Appl. Phys. A* **78** (2004), p. 823.i

[13] L. Giordano, M. Baistrocchi, G. Pacchioni, *Phys. Rev. B* **72** (2005), p. 115403.

[14] M. Sterrer, T. Risse, U. Martinez Pozzoni, L. Giordano, M. Heyde, H.-P. Rust, G. Pacchioni, H.-J. Freund, *Phys. Rev. Lett.* **98** (2007), p. 096107.

[15] L. Giordano, F. Cinquini, G. Pacchioni, *Phys. Rev. B* **73** (2006), p. 045414.

[16] S. Prada, U. Martinez Pozzoni, G. Pacchioni, *Phys. Rev. B* **78** (2008), p. 235423.

[17] J. Goniakovski, C. Noguera, *Interf. Sci.* **12** (2004), p. 93.

[18] L. Giordano, A. Del Vitto, G. Pacchioni, *J. Chem. Phys.* **124** (2006), p. 034701.

[19] T. König, G. H. Simon, M. Heyde, H.-J. Freund, *J. Phys. Chem. C* (2009), p. 10264.

[20] M. E. Vaida, T. Gleitsmann, R. Tchitnga, T. M. Bernhardt, *J. Phys. Chem. C* **113** (2009), p. 10264.

[21] P. Luches, S. D. DAddato, S. Valeri, E. Groppo, C. Prestipino, C. Lamberti, F. Boscherini, *Phys. Rev. B* **69** (2004), p. 045412.

[22] S. Benedetti, P. Torelli, S. Valeri, H. M. Benia, N. Nilius, G. Renaud, *Phys. Rev. B* **78** (2008), p. 195411.

[23] G. Pacchioni, J. M. Ricart, F. Illas, *J. Am. Chem. Soc.* **116** (1994), p. 10152.

Chapter 6

Observable consequences of formation of Au anions on ultrathin oxide films

6.1 Abstract

As seen in the previous chapter, negatively charged gold atoms form spontaneously from neutral Au atoms deposited on ultrathin MgO films. The charge state of adsorbate is a subtle property to be proven experimentally, and also theoretically the discrimination between neutral and charged adsorbed species is not straightforward. In this work we perform an accurate analysis of the observable consequences of the formation of Au anions on an oxide surface. To this end we consider the following properties: spin distribution, density of states, Bader charges, substrate relaxation, simulated scanning tunneling microscopy images, work function changes, CO vibrational frequency, electric field effects and core level shifts. Most of these properties are accessible experimentally, at least in principle. Taken individually, these properties do not necessarily provide conclusive evidence about the charged nature of the adsorbate, but taken together in a wider picture they offer a complete and unambiguous characterization of the formation of Au anions.

6.2 Computational details

The calculations are based on density functional theory at the level of the generalized gradient approximation (PW91 exchange-correlation functional). The method is implemented in the VASP program (see Chapter 2) which uses a plane wave basis set, a projector augmented wave method (PAW) for the treatment of core electrons and a kinetic energy cutoff of 400 eV.

The atoms within the supercell are relaxed until the atomic forces are less than

0.01 eV/Å. The Ag(100) substrate has been modeled by four metal layers (three for the study of the effect of an electric field, Sec. 6.3.7) which reproduce well the corresponding metal band structure. A two-layer (2L) MgO film has been deposited on the metal substrate. The MgO(100) single crystal surface has been represented by a three-layer MgO slab. The Ag lattice constant (a = 4.16 Å) is 2% smaller than the MgO one (a = 4.25 Å), therefore the MgO layers are slightly contracted with respect to their bulk distance when supported on the Ag substrate. During geometry optimization of the MgO/metal interface, all atoms in the MgO film and in the two surface nearest Ag layers were relaxed while the remaining two metal layers were frozen at bulk positions. On the MgO(100) surface the optimization is restricted to the two outermost layers of the slab. For the calculations we used 3×3 and 4×4 supercells containing 9 Ag and 18 Mg+O or 16 Ag and 32 Mg+O atoms per layer, respectively.

Spin polarized calculations have been performed to account for the presence of an unpaired electron in the valence shell of Au atoms.

Brillouin-zone integrations have been performed on a grid of $4\times4\times1$ (3×3 cell) and $2\times2\times1$ (4×4 cell) Monkhorst-Pack points. The calculations in the presence of an external electric field and for CO adsorption have been performed at Γ point.

The work function of Ag(100) and MgO(2L)/Ag(100) surfaces and interfaces has been defined as the energy of the vacuum level (determined as the self-consistent potential in the vacuum) with respect to the Fermi level of the metal or of the metal/oxide interface.

6.3 Results and discussion

In the following we discuss a series of evidences of the occurrence of a charge transfer in Au/MgO/Ag(100) films when certain conditions are met. We will compare these results with those obtained for Au atoms which are clearly in their atomic neutral state: this can be obtained either by depositing Au atoms on unsupported MgO slabs resembling the bulk oxide surface or on MgO/Ag(100) thin films where we forced the system to converge to the neutral state of the atom (see below).

6.3.1 Spin properties

Neutral Au has a $5d^{10}6s^1$ valence configuration: in the absence of charge transfer, a net spin density of ≈1 is also expected for adatoms. This is, indeed, the situation found for Au atoms deposited on the terrace sites of the MgO(100) surface.[1] Electron paramagnetic resonance (EPR) spectra have been obtained for Au atoms on ≈20 layer MgO films on Mo(100), providing a clear and unambiguous evidence for the presence of a residual spin density on the adsorbed Au atom. Furthermore, it has been possible to measure the hyperfine coupling constants of the deposited Au with the 17O nuclides of the MgO substrate, showing that the Au atoms sit on top of the oxide anions of the surface, as predicted theoretically.[2] A spin density of about 1 e^- is computed for Au_1/MgO(100) as the difference between spin up and spin down for the entire system and the corresponding hyperfine coupling constants have been determined using cluster models, Figure 6.1. The EPR properties of supported Au atoms differ from those of free Au atoms because of polarization effects due to the Pauli repulsion of the 6s valence level with the MgO surface; the shifts are not due to the occurrence of a net charge transfer.[1,3] These studies have proven unambiguously that Au atoms on the surface of MgO(100) are basically neutral, being the charge transfer from the oxide anion to Au of 0.2 e^- at most.

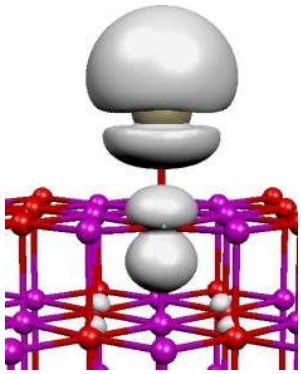

Figure 6.1: Spin density contour plot for a Au atom adsorbed on top of an oxide anion on the MgO(100) surface.

When Au atoms are adsorbed on two to three layer MgO films on Mo(100) or Ag(100) metal single crystals, a nonmagnetic solution has been found. This result has to be carefully checked in order to guarantee that the absence of spin polar-

ization is not due to the smearing parameter used to generate the density of states (DOS) plots. Once the absence of net magnetic moment is confirmed, there are only three possible explanations of the spin quenching: *(a)* a charge transfer has occurred from the Au atom to the substrate, forming Au^+; *(b)* a charge transfer has occurred from the substrate to the Au atom, forming Au^-; *(c)* a covalent bonding has formed by coupling an unpaired electron on the substrate with the singly occupied 6s level of Au. Mechanism *(c)* can be discarded since the number of paramagnetic defects on the MgO surface is below the detection limit of EPR.[4,5] This leaves space only for hypotheses *(a)* and *(b)*, occurrence of charge transfer.

The fact that for $Au_1/MgO/Ag(100)$ the calculation converges to a nonmagnetic solution is sufficient to conclude that a charge transfer has occurred, but it does not provide information about the direction of this charge transfer.

6.3.2 Density of states

A clear indication of the nature of the charge transfer is provided by the DOS curves. When Au is deposited on the MgO(100) surface, the two α and β components of the 6s level shows an uneven occupation, reflecting the atom-like nature of the supported species, Figure 6.2a.
When Au is adsorbed on MgO/Ag(100) or MgO/Mo(100) films, the distinction between empty and filled states is determined by the Fermi level of the metal substrate.[6,7] Notice that this is not the same as the Fermi level of the pure metal, since the presence of the oxide film can produce deep changes in the metal work function (see below).

In Figure 6.2b are shown the DOS curves of a Au atom adsorbed on MgO/Ag. It is apparent that both the α and β components of the Au 6s level are occupied, both being below the Fermi level. Thus, one electron has been transferred from the MgO/Ag(100) substrate to the 6s valence level, which becomes doubly occupied, accounting for the absence of spin polarization in the ground state of the system. This could be interpreted as the formation of a Au^- species with valence configuration $5d^{10}6s^2$. However, it should be noted that the 5d states are partly hybridized with the O 2p states. In semicovalent oxides (e.g., TiO_2) this could lead to a charge flow from the filled 5d levels to the partly filled O 2p states, thus reducing the net charge on Au, $Au^{\delta-}$, with $\delta \leq 1$. This situation is rather unlikely on MgO due to the highly ionic nature of the oxide and to the presence of fully reduced O_2^- anions.

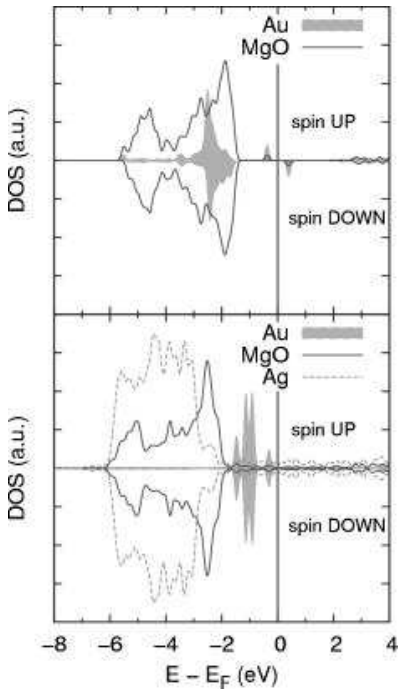

Figure 6.2: Spin density contour plot for a Au atom adsorbed on top of an oxide anion on the MgO(100) surface.

On this basis, one can conclude that the DOS curves provide clear, although purely theoretical, evidence of the formation of a gold anions. This result is independent of the site where the Au atom is sitting: total energy calculations have shown that the adsorption on top of O, on top of Mg or in the fourfold hollow sites of ultrathin MgO films is equally preferred within one-tenth of an eV and that the charge transfer occurs at any site. Notice that on thick MgO films, where charge transfer does not occur, adsorption on top of O is definitely preferred.[1,6]

6.3.3 Bader charges

The asymmetric distribution of electrons in chemical bonds results in partial charges on the atoms. Despite its usefulness, the concept of atomic charge is somewhat arbitrary, because it depends on the criterion used to discriminate between one atom and its neighbours in a molecule or a solid. It is not surprising that this problem

has been a challenge for quantum chemists for decades. One of the most popular approaches, based on the Mulliken population analysis,[8] leads sometimes to unphysical results due to the equal division of the off-diagonal terms of the overlap population between two centers.

A completely different approach has been followed by Richard Bader in his theory of atoms in molecules,[9] based on the definition of an atom in a complex system (molecule or solid) in terms of the topology of the electron density, as a region in the real space bounded by surfaces through which there is a zero flux in the gradient vector field of the electron density. This provides a mathematical definition for a given basin where to integrate the charge.

Using this method, we have determined the charges for a Au atom adsorbed on MgO(100) and on a MgO/Ag(100) film. On MgO(100) the Au atom carries a small negative charge of 0.2 e^-, which is due to the mixing of the Au's 6s and 6p states with the 2p orbitals of the surface anions: being MgO an ionic solid, its oxygen atoms are almost full anions and can only donate charge (basic character).

For Au adsorbed on MgO(2L)/Ag(100) films we have considered two adsorption sites: on top of Mg and the fourfold hollow site. For both situations the values of the Bader charge (0.77 e^- and 0.79 e^- respectively) are consistent with the prefesence of a full anion, moreover confirming the considerations drawn on the basis of the DOS analysis. This result alone clearly shows the very different nature of atomic gold deposited on the bare MgO surface or on an ultrathin film.

A less elegant way to determine the atomic charges of deposited Au atoms is to plot the total electron density of the system on a plane parallel to the surface as function of the z coordinate, Figure 6.3.
In this way one can identify the minimum of the density profile between the surface and the adatom layer, and integrate the charge around the adatom from this minimum point to large z values where the electron density vanishes, Figure 6.3. With this approach we found 11.58 electrons associated with the Au adatom, corresponding to a net charge of 0.58 e^-, a bit smaller than that obtained with the Bader analysis. This method, although less accurate than the Bader analysis, is yet much more reliable than another technique used time to time in the literature and based on the determination of charge density difference maps. In our system, this procedure would consist in determining the following quantity:

$$\Delta\rho = \rho[\mathrm{Au/MgO/Ag(100)}] - \rho(\mathrm{Au}) - \rho[\mathrm{MgO/Ag(100)}] \tag{6.1}$$

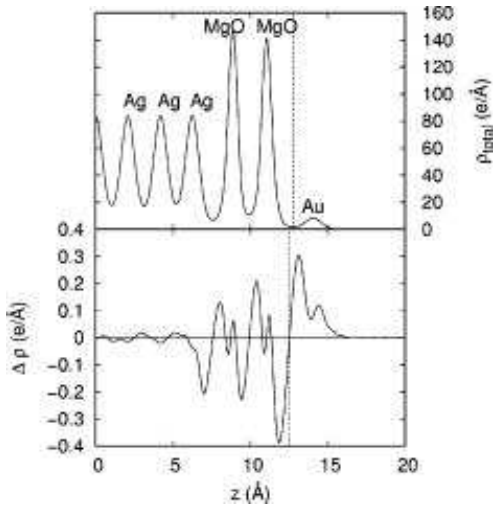

Figure 6.3: Profile of the laterally integrated total charge density ρ (top) and of the charge density difference $\Delta\rho$ (bottom) as a function of z (plotted along the line which goes through the Au adatom). The vertical dotted line indicates the point used to integrate the charge around the Au adatom (see text)

a charge accumulation is indeed found around the Au adatom, consistent with the fact that electrons flow from the substrate to the adsorbate, but a quantitative estimate of the amount of charge transferred, however, is less straightforward. Integrating the charge around Au, taking the plane where $\Delta\rho = 0$ as separation from the MgO/Ag(100) substrate, we obtain a net charge on Au of 0.38 e^-, i.e., one-half of the more realistic Bader charge. This is due to the rather arbitrary choice of subtracting noninteracting fragments from a bound system.

6.3.4 Polaronic distortion

The formation of a charged species inside or on the surface of an insulator is conceptually similar to the creation of an electron trap in the material. Very often, the formation of charge traps in insulators is accompanied by a substantial polaronic distortion of the lattice, which helps in stabilizing the state occupied by cahrged species. In many respects the formation of a negatively charged Au atom on the surface of MgO resembles this situation.

A case where this phenomenon has been clearly observed is that of Au atoms on ultrathin NaCl films on Cu(111). Using the tip of a scanning tunneling microscope (STM), Repp *et al.*[10] have been able to selectively charge Au atoms and transform them into Au^- anions. DFT calculations have shown that the formation of the Au^- anion induces a strong relaxation of the substrate which is essential to stabilize the charged state and which is released once the electron is detached from the Au atom. In particular, the Cl^- anion underneath the Au adatom moves downward by 0.6 Å and the surrounding Na^+ cations move 0.6 Å upward.

This phenomenon is also observed when Au is deposited on MgO/Ag(100) two-layer films. Upon adsorption on a Mg-top site, the Mg cation where Au is bound relaxes outward by 0.44 Å and the O anion underneath relaxes downward by 0.2 Å; the other oxide anions in the top layer around the adsorption site relax inward by 0.10 Å, Figure 6.4. This polaronic relaxation contributes by 0.8 eV to the stability of the surface complex (computed with respect to the unrelaxed surface) and is an essential contribution for the stabilization of the charged state.

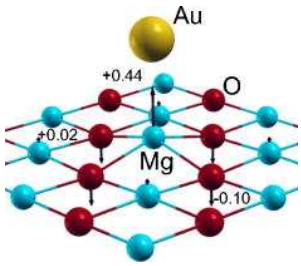

Figure 6.4: Schematic representation of the polaronic distortion due to the formation of a Au anion on MgO/Ag(100) films.

To further illustrate this point, a constrained calculation on the same system has been performed, preventing the MgO substrate from relaxation. In this case no charge transfer is found. The ground state is spin polarized (spin polarization on Au is 0.60 e^-, computed as the difference between spin up and spin down populations for the entire system) with the 6s level of Au only singly occupied, Figure 6.5. Also the Bader analysis assigns to this atom a charge of 0.36 e^- only, consistent with the presence of a basically neutral Au atom. The occurrence of a strong spontaneous distortion of the substrate in response to the adsorption of Au is a strong indication of the occurrence of a charge transfer. Although difficult to measure, this distortion

represents an observable property accessible in principle to experiment.

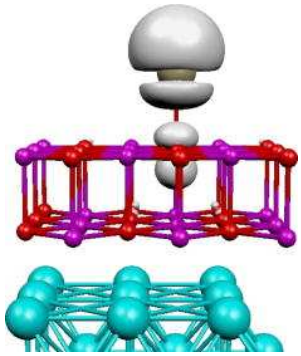

Figure 6.5: Spin density contour plot for a Au atom adsorbed on the MgO/Ag(100) surface in the absence of substrate relaxation. In this case the charge transfer does not occur and the Au adatom remains essentially neutral.

6.3.5 STM images

In the aforementioned paper by Repp et al.,[10] the most direct proof of the formation of a negatively charged gold atom by injection of one electron from the STM tip is provided by the very different appearance of the STM images of Au^0 and Au^- species. In particular, while neutral gold appears as a big bright spot, charged gold has a different profile with an about 0.5 Å smaller protrusion and a bright central region surrounded by a dark depression. The profile of the image exhibits a sombrero effect which seems to be typical of negatively charged atoms on conducting substrates. The same effect has also been observed very recently for Ag^- adatoms formed on ultrathin NaCl films.[11] The origin of this sombrero shape of the STM image is not entirely clear. A possible explanation is that the depression arises from two related effects: the transfer of electrons from metal free-electron states into more localized states of an electronegative adsorbate and the subsequent screening of this transferred charge by the conduction electrons.[12]

Recently, Sterrer *et al.* have been able to deposit isolated Au atoms at very low temperature on ultrathin MgO/Ag(100) films.[13] The STM images, taken at 4 K and a bias of +0.5 V, clearly show isolated Au atoms which exhibit the same sombrero shape found by Repp et al. in their experiment. Simulated STM images can be

obtained from DFT calculations using the Tersoff-Hamann approach.[14] As described in the previous paragraph, by freezing the coordinates of the substrate we've been able to converge on a solution where the charge transfer does not occur and the Au atom is neutral, procedure which allows a direct comparison of the simulated STM images of neutral and charged Au atoms on the same substrate, MgO/Ag(100). As can be seen in Figure 6.6, the two images are quite different and, for the Au^- case, in perfect agreement with the experiments of Sterrer *et al.* This provides a strong and direct proof of the charged nature of the supported Au atom.

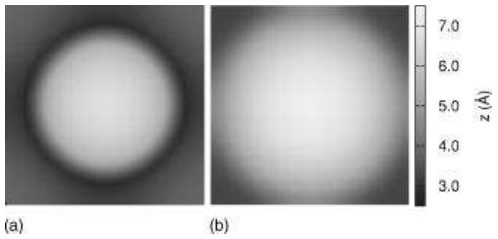

Figure 6.6: (a) Simulated STM image of Au^- formed on MgO/Ag(100); (b) simulated STM image of a Au^0 atom formed on MgO/Ag(100). The z = 0 reference plane is that of the MgO surface. The dimension of the images is 9 Å $\times$9 Å.

6.3.6 Work function change

The formation of an overlayer of charged species adsorbed on a metal surface has direct consequences on the work function Φ of the system. The classical picture proposed by Kingdom and Langmuir[15] and by Gurney[16] is that Φ increases for a negative adsorbate on a metal since an image charge forms into the bulk metal giving rise to a dipole layer which the emitted electron must pass through.[17] On the MgO(2L)/Ag(100) film the computed work function is 2.92 eV, i.e., about 1 eV smaller than on pure Ag(100) because of polarization-compression effects.[18,19] Once Au atoms are deposited on these ultrathin films, Φ becomes 5.29, 4.76, and 4.48 eV, respectively, for Au adsorption on top of Mg, in the hollow sites and on top of O. Thus, there is an increase in work function by 1.5-2.3 eV induced by adsorbed Au, according to the expectation of Gurney's model for a negative adsorbate. The work function change, $\Delta\Phi$, is clearly dependent on the adsorption site: $\Delta\Phi$ = 2.37 eV for Au^- on top of Mg is much larger than for adsorption on top of O ($\Delta\Phi$ = 1.56 eV).

The reason is a larger charge separation, hence a larger surface dipole, in the case of the Au^{-}–Mg^{2+} adsorption. The change in work function is a direct proof of the formation of an ionic adsorbate and is in principle accessible to experiment. Of course, the magnitude of $\Delta\Phi$ depends on the concentration of the adsorbed species: with a 3×3 supercell (on-top Mg adsorption) $\Delta\Phi$ is 2.37 eV; when the larger 4×4 supercell is used $\Delta\Phi$ decreases to 1.48 eV.

6.3.7 Electric field effects

An interesting method to check the presence of a strong asymmetry in the charge distribution of a chemical bond, hence of a large dipole moment, is the response of this dipole to an external uniform electric field. In the limiting case of a neutral adsorbate and absence of surface dipole, the electric field will only induce a polarization of the electron density. In the case of an ionic adsorbate on a conducting substrate, a net dipole results from the formation of an image charge and a strong interaction with the external electric field is expected. These concepts have been developed in the pioneering work of Bagus and co-workers and applied to the study of the ionic nature of atomic adsorbates on metal surfaces.[20–23]

In the presence of a charged adsorbate, large changes in the equilibrium geometry can be induced by an external electric field. Consider a uniform electric field F directed normal to the surface in the z direction. The first-order perturbation theory (FOPT) energy is

$$\mathrm{E_{FOPT}(F) = E_{tot}(F = 0) - \mu(F = 0) \cdot F} \tag{6.2}$$

where μ(F = 0) is the field-free surface dipole. Clearly, a large dipole gives rise to a significant change in potential energy curve, hence in the equilibrium distance. What we have determined is the response of the system to the presence of the field, including electron polarization effects. The applied fields are in the range of $\pm$0.5 V/Å (5×10^7 V/cm). For comparison, in semiconductors fields of the order of 10^6 V/cm can be maintained, while fields within the double layer at the electrode-electrolyte interface can reach 10^7 V/cm. Exposed cations in zeolite cavities create fields of 10^8 V/cm (1 V/Å). The upper limit of electric field strength that can be maintained over microscopic distances before field emission or field evaporation take place is of the order of $\approx$6 V/Å; this is also the field experienced by valence electrons in atoms and molecules. The sign of F is such that $F < 0$ attracts electrons from the adsorbate toward the surface.

We first applied a uniform electric field to Au atoms adsorbed on the MgO(100) surface (on top of O adsorption). Here the changes in geometry going from F = 0 to F = $\pm$0.5 V/Å are small. For F = -0.5 the Au–O distance increases by 0.02 Å, Table 6.1.

Adsorption site	distances, Å	F = -0.5 V/Å	F = 0	F = +0.5 V/Å
MgO(100)				
O-top	$r_{Au-O}, \Delta r$	2.299, +0.029	2.270	2.246, -0.024
	Δz_O	-0.028	0.0	+0.050
MgO(2L)/Ag(100)				
Mg-top	$r_{Au-Mg}, \Delta r$	2.542, -0.052	2.594	2.688, +0.094
	Δz_{Mg}	0.028	0.0	-0.023
hollow	$r_{Au-Mg}, \Delta r$	2.744, -0.066	2.810	2.929, +0.119
	Δz_{Au}	-0.021	0.0	+0.059

Table 6.1: Changes in Au adsorption geometry on MgO(100) and MgO(2L)/Ag(100) as a function of external electric field.

This, however, is not due to a displacement of the Au atom but more to the oxide anion that moves downward. Changing the sign of the field, the oxide anion is pushed outside the surface by 0.05 Å; also the Au atom moves slightly outward by 0.03 Å, as a response to the displacement of the oxygen atom, and the Au–O distance decreases by 0.02 Å only. Thus, the oxide anion of MgO feels the external field much more than the Au adatom, consistently with the basically neutral nature of the adsorbate.

Things are different for MgO ultrathin films. The external electric field has been applied to Au/MgO(2L)/Ag(100) for two cases: Au adsorbed on top of a Mg ion and Au adsorbed in the four fold hollow site, Table 6.1. The most pronounced effect is found when Au is on top of Mg. For F = 0, r(Mg–Au) is 2.594 Å; in a field F = -0.5 V the distance reduces to 2.542 Å (Δr = -0.052 Å) because the Au atom, negatively charged, is pushed toward the surface. At the same time the Mg cation moves to a slightly higher position, from 0.452 to 0.480 Å above the surface plane. Notice that the polaronic distortion (Sec. 6.3.4) is not removed by the application of the electric field. A field with opposite sign, F = +0.5 V, has an even larger effect: the Au atom moves outward and since there is no repulsion with the surface in this case, r(Au–Mg) increases to 2.688 Å, with Δr = 0.094 Å. The Mg cation moves downward, but

only by 0.023 Å, Table 6.1.

Similar displacements, although smaller in magnitude, have been found for Au adsorbed on a fourfold hollow site. Here the largest changes are in the shortest Mg–Au distances which ranges between 2.744 Å (F = -0.5 V/Å), 2.810 Å (F = 0 V/Å) and 2.927 Å (F = +0.5 V/Å). All these shifts are consistent with the presence of a negative Au adsorbate on MgO(2L)/Ag(100).

6.3.8 CO vibrational frequency

CO is largely used as a probe molecule to identify the charge state of a surface site, of a metal atom in a complex or on a surface, of a nanoparticle. In particular, the vibrational frequency of the C–O stretching mode is very sensitive to changes in the electron density of the atoms where the molecule is bound. According to the classical Blyholder model,[24] an increased electron density results in a larger backdonation of charge into the antibonding $2\pi^*$ molecular orbital (MO) of CO and in a considerable redshift of its frequency. For CO on metal surfaces it is well known that the CO frequency (2143 cm^{-1} in the gas phase) is shifted to 1950–2140 cm^{-1} when CO is adsorbed on top, to 1800–2000 cm^{-1} for CO on bridge sites and to 1700–1900 cm^{-1} for three-hollow sites.[25]

A large body of data exists for CO adsorbed on Au particles on oxides, and, depending on the nature of the support and on the size of the particles, the frequency ranges between 2000 and 2170 cm^{-1}.[26–29] Signals below 2090 cm^{-1} are assigned to negatively charged Au nanoclusters nucleated at defect sites, whereas values between 2140 and 2100 cm^{-1} are typical of neutral Au clusters. Values higher than 2140 cm^{-1} have been assigned to oxidized gold particles. In this scenario, CO adsorption can represent a powerful tool to distinguish between Au^0 and Au^- atoms formed on MgO. However, the assignment of the charge state based on the vibrational analysis is non-trivial, and the vibrational shifts of CO adsorbed on Au adatoms, either neutral or anionic, provide some elements of surprise.

Let's consider the vibrational properties of a CO molecule adsorbed on the system Au/MgO/Ag(100). The calculations have been performed for Au atoms adsorbed in the fourfold hollow sites of the MgO film. Here all aforementioned evidences hint at the presence of Au^- species. The presence of a doubly occupied 6s level has a first consequence on the strength of the Au–CO bond, which is very weak due to the strong Pauli repulsion between the diffuse 6s orbital and the CO

5σ lone pair. The 5d shell of Au is also full, and there are no simple mechanisms to reduce this repulsion by changing the atomic configuration as it happens with transition metal atoms in d^9s^1 or d^8s^2 configuration, which switch to a d^{10} configuration upon CO adsorption.[30] The result is that the Au–CO distance on MgO/Ag(100) is rather long, 2.23 Å, and the interaction energy is 0.21 eV only. The CO molecule is tilted with respect to the surface normal in order to allow a better overlap of the Au 6s-5d(z^2) hybrid orbital with the CO 2π* MO (the Au–C–O internal angle is 124°, Figure 6.7).

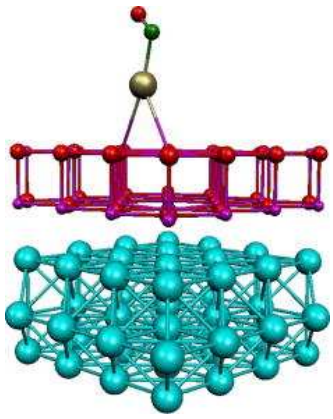

Figure 6.7: Structure of the Au^-–CO complex formed on MgO/Ag(100).

This overlap also results in a substantial charge transfer from Au^- to CO, hence in a large redshift of the CO frequency which becomes 1943 cm^{-1}, i.e., 186 cm^{-1}, lower than in the gas phase (2129 cm^{-1}, is the computed frequency for free CO). This is a strong indication of the negatively charged nature of supported Au. There are no experimental data available for Au^-–CO gas-phase complexes. However, negatively charged Au clusters have been produced in the gas phase and the vibrational frequency of adsorbed CO has been measured using IR multiple photon dissociation spectroscopy.[31]

The smallest cluster produced, Au_3^-–CO shows a CO frequency of 1995 cm^{-1}, with a redshift of 148 cm^{-1}; for larger clusters the redshift is reduced because the charge is delocalized over several Au atoms (e.g., Au_8^-–CO has a CO frequency of 2045 cm^{-1}). Thus, the value calculated here for a supported Au^-–CO complex, 1943

cm^{-1}, is coherent with a negative charge localized on a single Au atom.

The effect of an external electric field (F = $\pm$0.5 V/Å) on the same system has also been considered. The shifts with respect to the field-free case, F = 0, are large: $\Delta\omega$ = -72 cm^{-1} and +96 cm^{-1}, for positive and negative field respectively, Table 6.2.

	Free CO		CO/Au/MgO/Ag	
	ω	$\Delta\omega$	ω	$\Delta\omega$
F = -0.5 V/Å	2158	+29	2039	+96
F = +0.5 V/Å	2103	-26	1871	-72
dω/dF (cm^{-1} Å/V)	110		336	

Table 6.2: Field induced vibrational shifts in cm^{-1} for free CO and for CO adsorbed on Au_1/MgO/Ag(100).

These shifts are in accord with the occurrence of a charge transfer from Au^- to CO: a positive field moves electrons toward the adsorbate, increases the backdonation, and leads to a strongly redshifted CO frequency, 1871 cm^{-1}. A negative field, which moves the electrons toward the surface, reduces the backbonding and results in a higher frequency of 2039 cm^{-1}, still redshifted compared to free CO (2129 cm^{-1}). The computed vibrational shifts induced by the field correspond to a tuning rate, dω/dF, of 336 cm^{-1} Å/V; for comparison, experimental measurements in electrochemical cells for CO on Pd(111)[32] and Pt(111)[33] electrodes give dω/dF values of $\approx$150 and $\approx$200 cm^{-1} Å/V. Therefore, we can conclude that a CO molecule bound to Au/MgO/Ag(100) feels a higher electron density than the one experienced on transition metal surfaces.

At this point a comparison between the vibrational frequencies of Au^-–CO and Au^0–CO complexes formed on the surface of MgO is needed. Based on the previous considerations, the expectation is to find a high frequency for CO adsorbed on neutral Au, about 2100 cm^{-1}; however, things are quite different and a novel and unexpected phenomenon occurs. This has been described in detail in other studies,[34,35] and here we provide only a brief account to compare the results with those of Au^-–CO. The adsorption of CO on neutral Au atoms deposited on the MgO(100) surface induces a net electron transfer from the singly occupied Au 6s level to the CO $2\pi^*$ MO. This net charge transfer is driven by the reduction of the Pauli repulsion, and the CO molecule can approach much more closely the gold atom, resulting

in a stronger interaction (D_e = 0.81 eV according to PW91 plane wave calculations) and in a shorter Au–CO distance, 1.99 Å. The Au–C–O tilt angle, 137°, is slightly larger than for Au^-. The net electron transfer into the $2\pi^*$ MO, well documented by the spin density analysis, has dramatic consequences on the CO frequency which becomes 1848 cm^{-1}, with a red shift of 281 cm^{-1}. The computed frequency is very close to that measured experimentally at low temperature for the same system, 1852 cm^{-1}, providing strong support to the theoretical analysis.

It has been proposed that this is a special case of *final state effect*: before CO adsorption the Au atom is in a neutral state, as clearly shown by EPR measurements,[1] but CO adsorption induces a strong chemical modification and a net electron transfer into the $2\pi^*$ antibonding orbital. The consequence is a paradox: the frequency of Au^0–CO formed on MgO, 1848 cm^{-1}, is more redshifted than the frequency of Au^-–CO formed on the same surface, 1943 cm^{-1}. However, there is no contradiction in this result. In fact, in Au^0–CO a whole electron is transferred into the $2\pi^*$ MO, formally resulting in a Au^+–CO^- complex. In Au^-–CO the CO molecule cannot get sufficiently close to the Au atom because of the Pauli repulsion so that the overlap is smaller and the charge transfer from Au into the $2\pi^*$ MO of CO is only partial.

The vibrational frequency of adsorbed CO still represents a valid tool to learn about the nature of the supported atoms or clusters, but a correct analysis of the response requires a sound theoretical interpretation.

6.3.9 Core level shifts

X-ray photoemission spectroscopy (XPS) is a powerful technique to study the oxidized or reduced nature of a supported metal particle and some examples have been reported for the specific case of Au nanoparticles on oxide substrates.[36,37] The interpretation of these spectra is not always straightforward as the final core level shift is the result of several contributions, often of opposite sign.[38–40] The simplest and most immediate interpretation of a core level binding energy (CLBE) shift is that a decrease corresponds to a reduced species, since extra electronic charge results in a stronger Coulomb potential which acts to destabilize the core levels of the system.

In this work, the CLBEs of the 4f levels of supported gold atoms in neutral and negative charge states have been determined. To this end we have used the densities obtained for Au^0/MgO/Ag(100) (no relaxation) and Au^-/MgO/Ag(100) (pola-

ronic relaxation), see Sec. 6.3.4. The Kohn-Sham eigenvalues, -ε_i, have been considered as a measure of the CLBEs of supported gold: in this way final state effects are not included, but since we are interested in trends and not in absolute values, the approximation of considering initial state effects is justified and provides an internally consistent measure of the core level shift.

The ionization of the 4f level costs 78.0 eV in Au^0/MgO/Ag(100) and 76.1 eV in Au^-/MgO/Ag(100): the reduction of the CLBE of 1.9 eV is a very large shift in XPS measurements, which is consistent with the presence of a negative charge on the Au adatom and further reinforces the analysis obtained with other methods. This shift is in principle accessible experimentally, although, as for other measurements, several factors can contribute to hamper the experimental signal; amongst these, we mention the very low concentration of deposited atoms and the possible interference of gold-substrate interactions, cohalescence of atoms to give larger particles, etc.

6.4 Conclusions

The characterization of the charged state of supported species is a non-trivial issue. In this work we have compared several properties of neutral and anionic Au atoms deposited on regular and functionalized MgO(100) surfaces. Using a variety of properties, some of them directly related to measurable quantities, we have been able to show that the two species give rise to very characteristic and distinct behaviours. Even if a single evidence may not be sufficient to assign the charge of gold atoms, the combination of a number of properties provides a convincing proof of the nature of the adsorbate. We believe that the methods and measurements described above do not apply exclusively to the case of Au atoms on MgO surface, but provide a general framework to identify ionic adsorbates on surfaces.

The results of this chapter have been reported in the following publication:
L. Giordano, U. Martinez, S. Sicolo, G. Pacchioni, *J. Chem. Phys.* **127** (2007), p. 144713.

Bibliography

[1] M. Yulikov, M. Sterrer, M. Heyde, H. P. Rust, T. Risse, H.-J. Freund, G. Pacchioni, A. Scagnelli, *Phys. Rev. Lett.* **96** (2006), p. 146804.

[2] A. Del Vitto, G. Pacchioni, F. Delbecq, P. Sautet, *J. Phys. Chem. B* **109** (2005), p. 8040.

[3] M. Chiesa, E. Giamello, C. Di Valentin, G. Pacchioni, Z. Sojka, S. Van Doorsiaer, *J. Am. Chem. Soc.* **127** (2005), p. 16935.

[4] M. Sterrer, F. Fishbach, T. Risse, H.-J. Freund, *Phys. Rev. Lett.* **94** (2005), p. 186101.

[5] M. Sterrer, M. Heyde, M. Novicki, N. Nilius, T. Risse, H.-P. Rust, G. Pacchioni, H.-J. Freund, *J. Phys. Chem. B* **110** (2006), p. 46.

[6] G. Pacchioni, L. Giordano, M. Baistrocchi, *Phys. Rev. Lett.* **94** (2005), p. 226104 (2005).

[7] L. Giordano, G. Pacchioni, *Phys. Chem. Chem. Phys.* **8** (2006), p. 3335.

[8] R. J. Mulliken, *J. Chem. Phys.* **23** (1955), p. 1833.

[9] R. F. W. Bader, *Atoms in Molecules: A Quantum Theory* (Clarendon, New York, 1994).

[10] J. Repp, G. Meyer, F. E. Olsson, M. Persson, *Science* **305** (2004), p. 493.

[11] F. E. Olsson, S. Paavilainen, M. Persson, J. Repp, G. Meyer, *Phys. Rev. Lett.* **98** (2007), p. 176803.

[12] F. E. Olsson, M. Persson, N. Lorente, L. J. Lauhon, W. Ho, *J. Phys. Chem. B* **106** (2002), p. 8161.

[13] M. Sterrer, T. Risse, U. Martinez Pozzoni, L. Giordano, M. Heyde, H.-P. Rust, G. Pacchioni, H.-J. Freund, *Phys. Rev. Lett.* **98** (2007), p. 096107.

[14] J. Tersoff, D. R. Hamann, *Phys. Rev. B* **31** (1985), p. 805.

[15] K. H. Kingdom, I. Langmuir, *Phys. Rev.* **21** (1923), p. 380.

[16] R. W. Gurney, *Phys. Rev.* **47** (1935), p. 479.

[17] A. Zangwill, *Physics at Surfaces* (Cambridge University Press, Cambridge, 1988).

[18] J. Goniakowski, C. Noguera, *Interface Sci.* **12** (2004), p. 93.

[19] L. Giordano, F. Cinquini, G. Pacchioni, *Phys. Rev. B* **73** (2005), 045414.

[20] L. G. M. Pettersson, P. S. Bagus, *Phys. Rev. Lett.* **56** (1986), p. 500.

[21] P. S. Bagus, G. Pacchioni, M. R. Philpott, *J. Chem. Phys.* **90** (1989), p. 4287.

[22] P. S. Bagus, G. Pacchioni, *Electrochim. Acta* **36** (1991), p. 1669.

[23] G. Pacchioni, P. S. Bagus, *Surf. Sci.* **286** (1993), p. 317.

[24] G. Blyholder, *J. Phys. Chem.* **68** (1964), p. 2772.

[25] N. Sheppard, T. T. Nguyen, in *Advances in Infrared and Raman Spectroscopy*, edited by R. E. Hester and R. J. H. Clark (Heyden, London, 1978), Vol. 5, p. 67 and references therein.

[26] F. Boccuzzi, A. Chiorino, M. Manzoli, D. Andreeva, T. Tabakova, *J. Catal.* **188** (1999), p. 176.

[27] B. Yoon, H. Häkkinen, U. Landman, A. S. Wrz, J. M. Antonietti, S. Abbet, K. Judai, U. Heiz, *Science* **307** (2005), p. 403.

[28] A. S. Wrz, U. Heiz, F. Cinquini, G. Pacchioni, *J. Phys. Chem. B* **109** (2005), p. 18418.

[29] R. Meyer, C. Lemire, S. K. Shaikhutdinov, H. Freund, *Gold Bull.* **37** (2005), p. 72.

[30] G. Pacchioni, N. Rsch, *Acc. Chem. Res.* **28** (1995), p. 390.

[31] A. Fielicke, G. van Helden, G. Meijer, B. Simard, D. M. Rayner, *J. Phys. Chem. B* **109** (2005), p. 23935.

[32] S. Zou, R. Gomez, M. J. Weaver, *J. Electroanal. Chem.* **474** (1999), p. 155.

[33] A. Rodes, R. Gomez, J. M. Feliu, M. J. Weaver, *Langmuir* **16** (2000), p. 811.

[34] M. Sterrer, M. Yulikov, T. Risse, H.-J. Freund, J. Carrasco, F. Illas, C. Di Valentin, L. Giordano, G. Pacchioni, *Angew. Chem., Int. Ed.* **45** (2006), p. 2633.

[35] L. Giordano, J. Carrasco, C. Di Valentin, F. Illas, G. Pacchioni, *J. Chem. Phys.* **124** (2006), p. 174709.

[36] J. Radnik, C. Mohr, P. Claus, *Phys. Chem. Chem. Phys.* **5** (2003), p. 172.

[37] A. Zwijnenburg, A. Goossens, W. G. Sloof, M. W. J. Craj, A. M. van der Kraan, L. J. De Jongh, M. Makkee, J. Moulijn, *J. Phys. Chem. B* **106** (2002), p. 9853.

[38] P. S. Bagus and G. Pacchioni, *Phys. Rev. B* **48** (1993), p. 15262.

[39] S. Lizzit, A. Baraldi, A. Grosso, K. Reuter, M. V. Ganduglia-Pirovano, C. Stampfl, M. Scheffler, M. Stichler, C. Keller, W. Wurth, D. Menzel, *Phys. Rev. B* **64** (2001), p. 205419.

[40] P. S. Bagus, F. Illas, G. Pacchioni, F. Parmigiani, *J. Electron Spectrosc. Relat. Phenom.* **100** (1999), p. 215.

Chapter 7

CO adsorption on 1-, 2-, 3-dimensional Au clusters supported on ultrathin films

7.1 Abstract

The adsorption properties of CO molecules adsorbed on free and MgO supported Au clusters have been investigated by means of a first principles density functional theory (DFT) approach. CO does not bind to the high-coordinated Au atoms of one- or two-dimensional (1D or 2D) gold clusters or islands but only to the low-coordinated atoms at the periphery of these structures. A red-shift of about 50-60 cm^{-1} is found in ω(CO) for gold clusters deposited on MgO/Ag(001) thin films compared to the same clusters deposited on bare MgO(001) or to the neutral gas-phase counterparts. This shift, due to the occurrence of a charge transfer from the metal support to the deposited gold cluster, is found only for small 1D or 2D clusters or, for 3D clusters, when the CO molecule is bound at the MgO/Au interface. On 3D gold clusters, CO adsorbs on the top layers with binding energies and vibrational frequencies typical of neutral supported gold particles. This shows that the charging effect observed on ultrathin MgO films is largely restricted to the gold layer at the interface with the oxide support, supporting the perimetral model originally proposed by Masatake Haruta.

7.2 Computational details

The calculations are based on density functional theory at the level of the generalized gradient approximation (PW91 exchange-correlation functional). The method is implemented in the VASP program (see Chapter 2) which uses a plane wave basis set, a projector augmented wave method (PAW) for the treatment of core electrons

with a kinetic energy cutoff of 400 eV. The Ag(001) substrate has been modeled by three metal layers, which reproduce well the corresponding metal band structure. A two-layer (2 L) MgO film has been deposited on the metal substrate. Also, the MgO(001) single crystal surface has been represented by a two-layers MgO slab; it has been shown both theoretically and experimentally that the properties of the MgO(001) surface are reasonably converged with two oxide layers.[1,2] For the calculations, 4×5 or 5×5 supercells have been used. Unless differently specified, all atoms in the Au adsorbate, MgO film and in the two surface nearest Ag layers were relaxed while the remaining metal layers has been frozen at bulk positions. On the bare MgO(001) surface, the optimization is restricted to the top layer of the film. The atoms within the supercell have been relaxed until the atomic forces were converged within 0.01 eV/Å. Spin-polarized calculations have been performed for open shell structures; Brillouin-zone integrations have been performed at Γ point. The gas-phase clusters have been calculated in a cubic unit cell (l = 16 Å); for anionic clusters, a homogeneous background charge is added, compensating the extra-electron.

7.3 Results and discussion

7.3.1 Au gas-phase clusters

The properties of CO adsorbed on small Au_n clusters (n = 2-6) in various charge states (+1, 0, -1), has been studied previously using the same DFT functional adopted in this work (PW91).[3] It has been found that CO binds to neutral and anionic gold clusters by about 1 eV (PW91 functional).[88] More delicate is the issue of the CO stretching frequency which for the gas-phase anions can be considerably lower than for the neutral units due to the enhanced back-donation.[3–5] In general, however, the extent of the back-donation from the metal to CO is overestimated by DFT methods because of the low position of the empty $2\pi^*$ MO levels of CO:[6,7] this leads to overestimated red-shifts of the vibrational frequency of adsorbed CO.

To calibrate the accuracy of our frequencies, we have determined ω(CO) for CO adsorbed on gas-phase Au_3^-, a relatively simple system for which accurate measurements of the C–O stretching frequency have been reported using the Free Electron Laser for Infrared eXperiments (FELIX).[8] The structure obtained subsequent to geometry optimization is the same reported based on ion mobility measurements and

DFT calculations:[9] Au_3CO^- is bent with a linear Au-Au-Au unit and a tilted CO molecule, Figure 7.1a; the bonding of CO is 0.95 eV and the computed CO frequency 1932 cm^{-1}, to be compared with the experimental value, 1995 cm^{-1}.

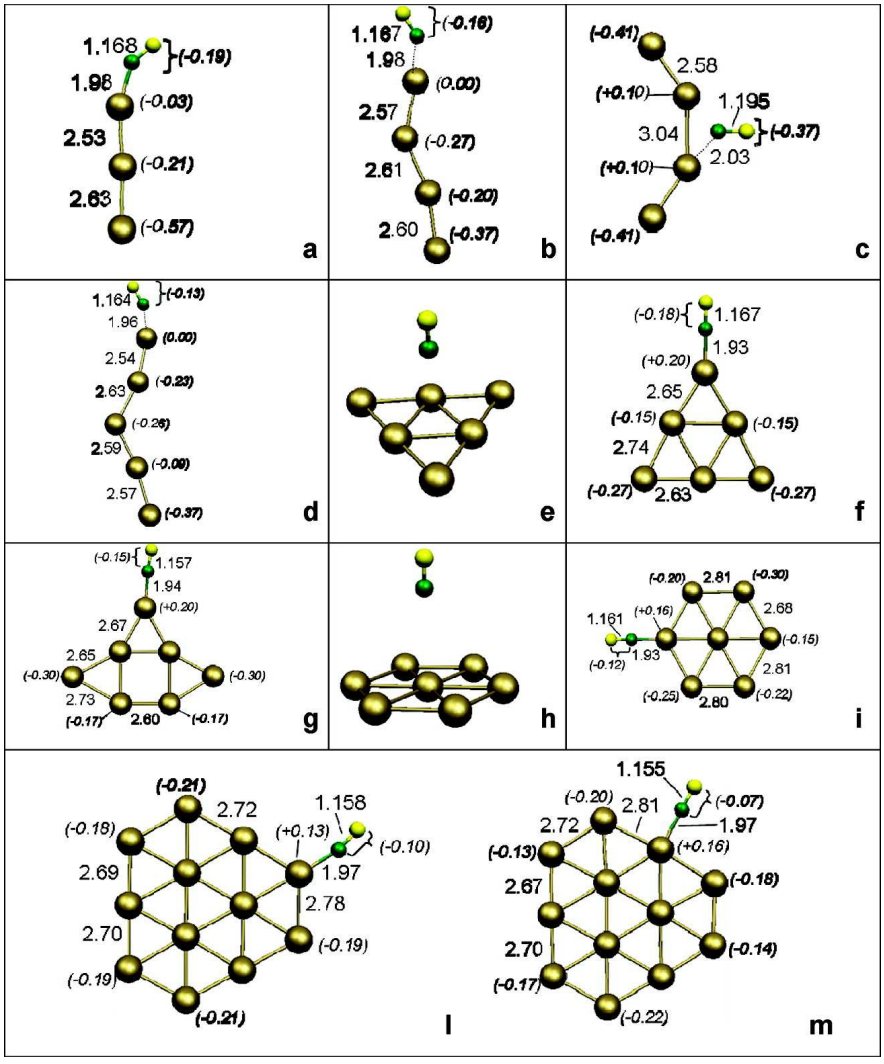

Figure 7.1: Optimal structures of gas-phase Au_nCO^- 1D and 2D clusters. Selected distances (in Å) are given, together with computed Bader charges (in parentheses) for some of the atoms. On the configuration shown in figures *e* and *h* the CO molecule is unbound.

In order to bring the computed data into agreement with the experiment, a scaling factor f = 1995/1932 = 1.0326 has been applied to Au_3^- and to all gold clusters considered in this work, regardless of the charge and size of the cluster, Table 7.1. The reliability of this scaling procedure is proved by the accord between our computed values – both absolute frequencies and relative shifts – and experimental measures for clusters of different dimensionalities and charge states.[10] In the following, only scaled frequencies are discussed.

The other gas-phase Au clusters considered besides Au_3^- are the 1D Au_4^- and Au_5^- chain structures similar to those found on MgO/Ag(001),[11] the 2D Au_6^-, Au_7^-, and Au_{12}^- structures, Figure 7.1; finally, we considered a three-layered 3D Au_{22}^- cluster, Figure 7.2. Of course, other isomers are possible, often with similar total energies, but nevertheless the considered clusters represent local minima on the potential energy surface. To these clusters, we added a single CO molecule in various positions.

For Au_4CO^- two structures have been found: adsorption either on a terminal or a bridge position, Figure 7.1b and Figure 7.1c respectively. The adsorption on the bridge position is more favorable (D_e = 1.32 eV vs. 1.05 eV, Table 7.1) but the CO molecule leads to a considerable distortion of the central Au–Au bonds and is basically bound to two weakly interacting Au dimers (r(Au-Au) = 3.04 Å). We will see that this isomer has no counterpart on the surface, since the breaking of the central Au–Au bond is hindered by the interaction with the substrate. In the other isomer, Figure 7.1b, CO is bound by 1.05 eV, slightly tilted, and the Au chain is partly distorted. Not surprisingly, the scaled vibrational frequencies of the two isomers reflect the different CO coordination: 1833 cm^{-1} for bridge bonded CO and 1993 cm^{-1} for terminal CO. This latter frequency is nearly the same found for Au_3CO^-, 1995 cm^{-1}.

CO adsorption on Au_5^- leads to a considerable distortion of the gold chain with loss of linearity, Figure 7.1d. Also in this case, the CO molecule is tilted with respect to the closest Au–Au bond, but the vibrational frequency, 2036 cm^{-1}, is higher than for the smaller cluster anions.

In the attempt to understand this difference, we have considered the Bader charges on the individual atoms of the gold–CO clusters, see Figure 7.1. On all structures considered, the atom which is directly bound to CO is neutral, and the negative charge is distributed on the Au atoms far from CO. This result is due to the Pauli

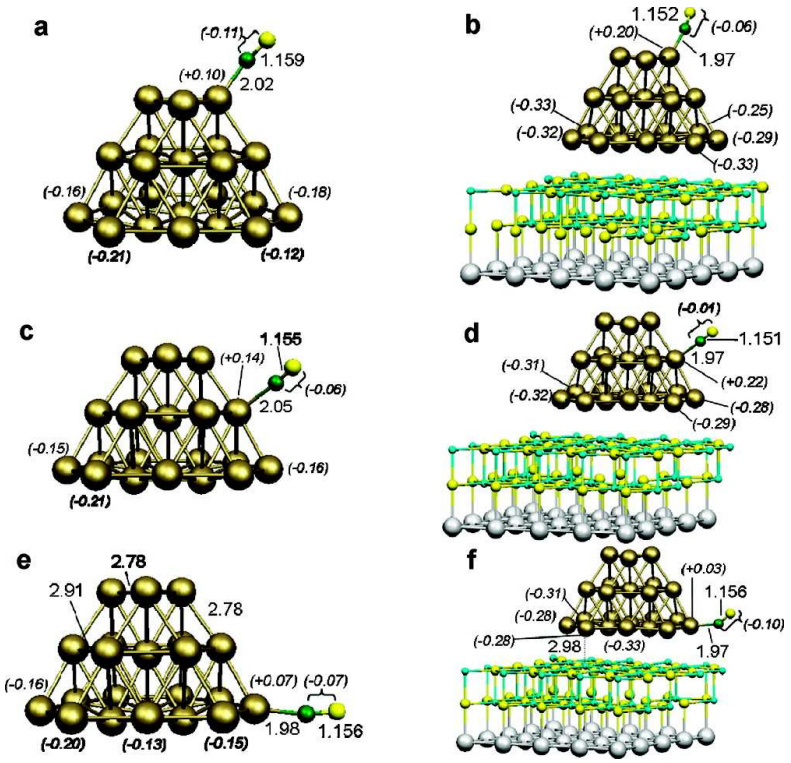

Figure 7.2: Optimal structures of a CO molecule adsorbed on gas-phase $Au_{22}CO^-$ 3D cluster and on a Au_{22} cluster deposited on a MgO/Ag(100) two-layers film. (a,b) CO adsorbed on top layer; (c,d) CO adsorbed on central layer; (e,f) CO adsorbed on bottom (interface) layer. Selected distances (in Å) are given, together with computed Bader charges (in parentheses) for some of the atoms.

repulsion between the filled CO orbitals, and in particular the 5σ MO, and the metal electrons. Furthermore, the back-donation from the metal to the CO 2π* MO reduces the charge density on the atom where CO is bound. The charge distribution is similar in Au_3CO^-, Au_4CO^- and Au_5CO^-, so that this is not the reason for the different vibrational frequencies. We suggest that on the longer Au_5 chain the extra electron is more efficiently delocalized and thus less available to reinforce the back-donation.

On the 2D Au_6^- cluster two different CO orientations have been considered: vertical and coplanar. In the vertical orientation, CO is placed above a three-hollow site, Figure 7.1e, and is unbound (or very weakly bound if we take into account

dispersion forces which are not properly included in DFT), whereas a stable isomer has been found when CO is bound on-top of an apical Au atom, Figure 7.1f. In this configuration, the Au_6CO^- complex is bound by 1.16 eV and the CO frequency is 2025 cm^{-1}, Table 7.1, in line with what reported by Wu *et al.*[5] Notice that there is another possible coplanar adsorption site, with the CO molecule bound to an edge site of the cluster. However, recent work performed by Zhai *et al.* clearly shows that the apex site is preferred.[12]

The same picture emerges from the analysis of Au_7CO^-. We have considered two Au_7^- isomers: one more stable, Figure 7.1g, and one more symmetric (a centered hexagon, Figure 7.1, parts h and i) but which is 0.76 eV higher in energy. On the most stable isomer CO is bound to a Au_{2c} atom with D_e = 1.10 eV and a CO frequency of 2089 cm^{-1}. On the second isomer, CO has been adsorbed normal to the Au_7 cluster plane directly on-top of the central Au atom or coplanar and on-top of one of the peripheral Au atoms, Figure 7.1. In the normal orientation CO is unbound, while in the coplanar isomer the bonding is 1.34 eV (this larger bonding is probably due to the lower stability of the hexagonal Au_7 cluster). The corresponding CO frequency is 2068 cm^{-1}, Table 7.1.

The next gas-phase gold cluster analyzed is $Au_{12}CO^-$, Figure 7.1l and m. Also in this case, a CO molecule with the molecular axis normal to the cluster plane desorbs (not shown). Stable isomers have been found only when CO is coplanar and bound to the apical Au_{3c} or edge Au_{4c} atoms. The bond is stronger on the less coordinated Au_{3c} atom, 0.95 eV, but on the Au_{4c} atom is only 0.1 eV lower, Table 7.1. This suggests an easy scrambling of the CO molecule around the cluster border, with a fluxional behavior at finite temperatures. The corresponding vibrational frequencies are 2064 cm^{-1} (Au_{3c}) and 2091 cm^{-1} (Au_{4c}), respectively. Also for the planar isomers, we observe the same effect found on the gold chains: the atom where CO is bound is neutral or even positively charged and the extra electron present on the cluster is delocalized over several atoms at the cluster periphery, far from CO.

It is interesting to compare the results obtained on the Au_{12} cluster anion with those obtained on a neutral Au_{12} cluster. The optimized structure of $Au_{12}CO$ is similar to that of the anion and the Au–Au distances differ at most by 0.01 Å. CO binds to neutral Au_{12} in a similar way as for the anionic counterpart, Figure 7.1l; the CO binding energy, 1.06 eV, is 0.1 eV larger because of the reduced Pauli repulsion on the neutral cluster. The CO frequency, 2141 cm^{-1}, is 77 cm^{-1} higher than in Au_{12}^-

(2064 cm^{-1}) due to the reduced back-donation, Table 7.1.

These results show that CO has no tendency to bind to the internal, high coordinated atoms of 2D gold cluster anions; stable complexes are formed only when CO is bound on-top of a low-coordinated Au atom. This is in line with previous theoretical studies[5] but also with experiments performed on the gas-phase clusters.[8] The binding energy for the on-top sites of the most stable isomers ranges between 0.9 and 1.2 eV, and the vibrational frequency ranges from 1993 cm^{-1} for Au_4^- to 2089 cm^{-1} for Au_7^-, with intermediate values for other cluster sizes. This shows a significant spread of nearly 100 cm^{-1} of the computed frequencies for free gold cluster anions as a function of the cluster size and shape, Table 7.1.

The last cluster considered is Au_{22}^-, which contains 12, 7, and 3 Au atoms in the bottom, central, and top layers, respectively, Figure 7.2. The adsorption of CO has been modeled optimizing the geometry of the CO molecule only, while keeping the Au cluster position frozen; this procedure has been necessary since, upon adsorption of CO, the Au cluster experiences severe reconstruction, thus losing the structural features that make it interesting in this study. The optimal geometrical parameters and the Bader charges are shown in Figure 7.2. The binding energies are 0.80 eV (bottom layer), 0.48 eV (central layer), and 0.67 eV (top layer), Table 7.1, and the CO stretching frequency is between 2043 and 2075 cm^{-1}, rather typical for negatively charged gold clusters and consistent with what found for the smaller aggregates.

Also in this case, we compared the results of Au_{22}^- to those obtained on the neutral form. The neutral unit has been fully optimized, then the structure has been frozen and only the position of adsorbed CO has been optimized, in analogy to the procedure followed for the anionic form. The binding energies are 0.87, 0.52, and 0.75 eV for bottom, central and top layers, respectively, i.e., slightly higher than on the corresponding anion. However, the CO stretching frequencies are considerably higher, ranging from 2098 cm^{-1} (top layer) to 2114 cm^{-1} (bottom layer), Table 7.1.

From these results it is possible to conclude that the red-shift due to the extra charge is 50-60 cm^{-1}, depending on the adsorption site, on gold nanoparticles, while larger or smaller shifts can be found on subnanometer gold clusters containing only a few atoms. This is due to the subtle interplay between various contributions to the CO ω shift, like electrostatic interactions, coordination, Pauli repulsion and charge transfer.[4]

7.3.2 Supported Au clusters

STM images of very small Au_n clusters formed on 2-3 MgO layers on Ag(001) show that Au_3 is a flat-lying chain which, according to first principle calculations, carries one extra electron.[11] The structure of the supported cluster is therefore very similar to that of the gas-phase cluster anion, Au_3^-, and differs substantially from the neutral counterpart, which assumes a triangular shape both in the gas-phase and when supported on bare MgO(001).[13]

The Au_3 cluster is bound to MgO/Ag(001) by 3.0 eV, i.e., 1 eV per gold atom. CO is bound on Au_3/MgO/Ag(001) by 0.99 eV, an energy which is very similar to that computed for CO on the free cluster anion, Table 7.1. The structure is also similar, with the CO molecule tilted with respect to the MgO surface normal by 56° (α(AuCO) = 161°), Figure 7.3a. The vibrational frequency is 2096 cm^{-1}, i.e., about 100 cm^{-1} higher than for the free gas-phase anion, Table 7.1. This result can be explained by the fact that, on the supported cluster, the extra charge is mostly localized at the interface, thus is less available for back-donation than in the free cluster. Yet, the frequency is slightly red-shifted with respect to neutral gold clusters.

The structure of Au_4 deposited on MgO/Ag(001) is shown in Figure 7.3b. The nearly linear chain is the most stable isomer, while in gas-phase, a zigzag chain and a T-shaped Au_4^- structures are very close in energy.[5] The chain structure of Au_4 on MgO/Ag(001) differs from what reported for MgO ultrathin films deposited on Mo(001), where it was found that the most stable isomer has a T-shape.[14] The two structures are actually similar in energy, but on MgO/Ag(001) films the chain is preferred as shown by STM images. The adhesion energy of the cluster, computed with respect to neutral Au_4, is 3.71 eV, i.e., nearly 1 eV per Au atom. The Bader analysis and the DOS curves (not shown) show that the cluster is negatively charged and that nearly two electrons have been transferred to the cluster (see Bader charges, Figure 7.3b).[11]

On this cluster, CO has been adsorbed in a bridge position at the center of the chain but no bonding is found for this adsorption geometry: the fact that the Au cluster strongly adheres to the MgO film does not allow shape modification as in the gas-phase. Also, attempts to bind CO on-top of one of the atoms along the chain results in CO desorption. A stable isomer is found only when CO is bound at the end of the chain, Figure 7.3b. Here, the CO molecule interacts mainly with the terminal Au atom and weakly with the MgO(001) substrate, being more or less

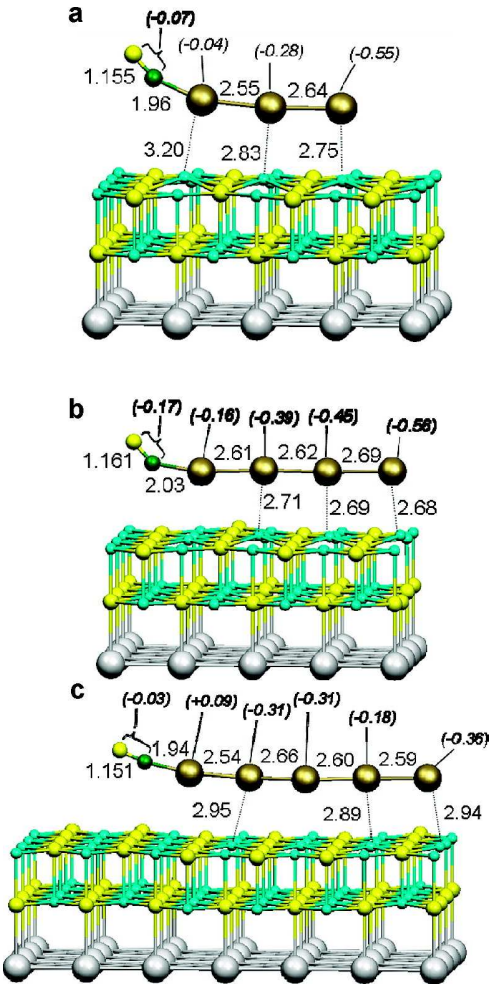

Figure 7.3: Optimal structure of a CO molecule adsorbed on Au_3, Au_4 and Au_5 chain clusters deposited on a MgO/Ag(100) two-layers film. Selected distances (in Å) are given, together with computed Bader charges (in parentheses) for some of the atoms.

above a hollow position on the MgO lattice. The CO molecule is tilted, forming a Au–C–O angle of 141° (59° with respect to the surface normal). The bonding of CO to the cluster is rather weak, 0.49 eV, which indicates that desorption could occur for lower temperatures than for most of the other clusters (see below). This weak bonding can be attributed to the fact that formally two electrons have been

transferred from the Ag substrate to the supported cluster, thus resulting in a larger Pauli repulsion. The CO vibrational frequency, 2028 cm^{-1}, is 35 cm^{-1} larger than for the gas-phase complex (1993 cm^{-1}); the blue shift can be ascribed to the interaction with the MgO substrate.

On Au_5/MgO/Ag(001) CO is bound to a distorted Au chain structure similar to that found in the gas-phase and the CO molecule forms a Au–C–O angle of 168° and a tilt angle of 66° with respect to the surface normal, Figure 7.3c. The CO binding energy is 0.90 eV, and the vibrational frequency, 2093 cm^{-1}, is very similar to CO–Au_3/MgO/Ag(001)but blue-shifted by about 30 cm^{-1} with respect to the gas-phase counterpart, see Table 7.1. Also for the supported chain structures we observe the asymmetric distribution of charge on the cluster, with the Au atom bound to CO being slightly positively charged, the other atoms of the chain carrying a negative charge, Figure 7.3c.

We now consider Au_{12} on MgO/Ag(001). A flat Au_{12} cluster has been placed above the MgO surface and the structure fully optimized. The geometry remains similar to that of the gas-phase Au_{12}^-, Figure 7.4, with average interface distances of about 2.9 Å. The adhesion energy of the cluster, computed with respect to neutral Au_{12}, is 4.13 eV, i.e., only about 0.35 eV per Au atom. This is consistent with other studies of the deposition of Au clusters on MgO thin films, which show a decreasing adhesion energy per atom as a function of the cluster size.[15] The Bader analysis shows a net charge of 2.9 e^- associated to this cluster. However, only part of this charge is due to electron tunneling through the oxide thin film, the rest being due to the interaction with the MgO substrate: indeed, a calculation on a 2D Au_{12} cluster on the bare MgO(001) surface, Figure 7.5 , shows a Bader charge of 0.82 e^- (0.07 e^-/atom). This charge is due to the interaction with the oxide anions, and has nothing to do with electron transfer from the metal substrate as in Au_{12}/MgO/Ag(001). Notice that the 2D Au_{12} cluster is bound to MgO(001) by 1.62 eV, corresponding to 0.13 eV/atom only: this clearly indicates the importance of the charge transfer across the film to increase the adhesion of the Au cluster to the oxide surface.[15] By subtracting the charge of Au_{12}/MgO(001) from that of Au_{12}/MgO/Ag(001) one obtains a net charge transfer due to the metal substrate of 2.06 e^- (0.17 e^-/atom). As for the gas-phase clusters, CO does not bind to the Au_{12} cluster plane. Based on these results and on the results for gas-phase $Au_{12}CO^-$, only one isomer has been considered for the supported cluster. In this structure, the CO molecule is bound

to a Au_{3c} atom at the cluster border, Figure 7.4. The bonding, 0.72 eV, is slightly weaker than on gas-phase Au_{12}^- (0.95 eV). The CO molecule is tilted forming an angle of 45° with the MgO surface plane (Au–C–O angle 158°). The CO stretching frequency for this adsorption mode is 2051 cm^{-1}, in line with that computed for the most stable $Au_{12}CO^-$ isomer, 2064 cm^{-1}. The similarity of the CO adsorption properties on Au_{12}/MgO/Ag(001) and Au_{12}^- reflects the accumulation of charge on the supported cluster, a specific property of the thin film.

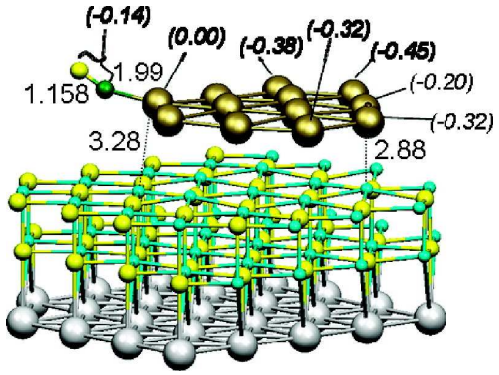

Figure 7.4: Optimal structure of a CO molecule adsorbed on a Au_{12} cluster deposited on a MgO/Ag(100) two-layers film. Selected distances (in Å) are given, together with computed Bader charges (in parentheses) for some of the atoms.

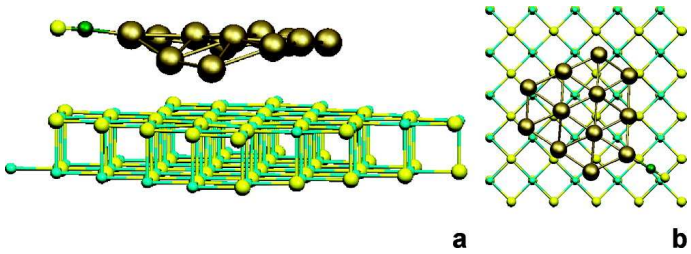

Figure 7.5: Optimal structure of a CO molecule adsorbed on a Au_{12} cluster deposited on a MgO(001) surface. (a) Side view; (b) top view.

This is further corroborated by the results for CO adsorption on Au_{12} deposited on the bare MgO(001) surface, Table 7.1 and Figure 7.5. We notice that the isomer considered has been obtained starting from the geometry found on MgO/Ag and

is a local minimum in the potential energy surface. The CO binding, 0.87 eV, is slightly reduced, the CO molecule is almost parallel to the surface (Au–C–O angle of 175°), and the CO frequency, 2126 cm^{-1}, is blue-shifted by +75 cm^{-1} compared to Au_{12}/MgO/Ag(001). These results indicate that the nature of Au_{12} deposited on MgO(001) is essentially the same as free Au_{12}; the small differences can be ascribed to the tiny charge transfer from the oxide anions to the gold particle. At the same time, the nature of Au_{12} deposited on MgO(001) and on MgO/Ag(001) films is totally different, for the reasons previously discussed.

The last case considered is Au_{22} supported on MgO/Ag(001) films and on bare MgO(001), Figure 7.2. Here, the cluster with or without CO has been relaxed with no constraints, but the interaction with the substrate does not change the topology of the cluster which maintains the initial structure. The Bader analysis indicates a charge of 2.38 e^- for Au_{22} on MgO/Ag(001); since on bare MgO there is a negative charge of 1.12 e^-, this means that a net increase in the charge of the cluster of about 1.2 e^- occurs on the MgO film. It is interesting to compare the adsorption properties of Au_{22}/MgO/Ag(100) with those of the gas-phase Au_{22} cluster anion, Table 7.1. In both cases, we can distinguish three CO adsorption sites, on the top, center and bottom layers of the cluster. The CO adsorption energies are larger for supported Au_{22} than for the gas-phase anion: 0.65 eV in average on Au_{22}, 0.83 eV in average on Au_{22}/MgO/Ag(100), Table 7.1. The C–O vibrational frequency is more red-shifted on Au_{22}^- than on the supported counterpart, Table 7.1. On the gas-phase, the frequencies range from 2043 cm^{-1} for CO adsorbed on the top layer to 2075 cm^{-1} for CO bound to the bottom layer; on the supported cluster, the frequency of CO adsorbed on the top layer is 2125 cm^{-1}; this is in the range of frequencies calculated for neutral gold clusters, Table 7.1, and actually higher than that computed for the same site of neutral Au_{22} (2098 cm^{-1}). The frequency of CO adsorbed on the central layer of Au_{22}/MgO/Ag(001) is also typical of neutral gold clusters, 2116 cm^{-1}, Table 7.1. This shows that when CO is adsorbed on the upper layers of a 3D gold cluster the interaction with the oxide substrate is largely screened, and the effect of charging is absent. This is not the case when CO is bound to the bottom layer of the cluster, at the interface with the MgO film. Here, the bond strength is similar as for the top layer, 0.86 eV, but the C–O stretching frequency, 2085 cm^{-1}, is about 40 cm^{-1} lower and comparable to that computed for the same site of Au_{22}^-, 2075 cm^{-1}, Table 7.1. The CO molecule is tilted, and forms an angle of 51° with respect to the MgO sur-

face normal, so that also in this case the intensity of the corresponding mode should be reduced.

Finally, we have considered the properties of Au_{22} on bare MgO(001). Here, the results are reported only for CO adsorbed on the top and bottom layers of the cluster: when the interaction involves atoms of the central layer, in fact, the cluster rearranges and changes the topology considerably. The fact that this does not occur on MgO/Ag(001) films is an indication that the extra charge provides additional stability to the gold cluster cage. On the top layer CO is bound by 1.15 eV and exhibits the same vibrational frequency (2125 cm^{-1}) of CO adsorbed on the outer layer of Au_{22} supported on MgO/Ag(001) films, Table 7.1. On the bottom layer, CO has similar adsorption properties as on the MgO film but the CO frequency is 20 cm^{-1} higher, 2105 cm^{-1}, consistent with the neutral nature of the gold nanoparticle.

These results lead to the conclusion that the accumulation of extra electronic charge from the metal support to the cluster by tunneling through the thin oxide films occurs at the interface and affects mainly the atoms of the cluster at direct contact with the support. in accordo col modello perimetrale This latter conclusion has been reported previously for gold clusters on bare MgO supports but here the chemical difference is definitely more pronounced.[16,17] The difference between bare MgO and thin MgO films is that in the first case the role of the interface is to provide a geometrical arrangement that allows the adsorbed molecule to interact simultaneously with the metal particle and with the atoms of the support; in the case of the thin oxide film, in addition to this effect, the chemical nature of the bottom layer of the metal particle is modified by the charge accumulation. Indeed, it has been suggested that 2D gold clusters deposited on MgO thin films are chemically more active in the oxidation of CO to CO_2.[18]

	site	D_e eV	r(Au–C) Å	r(C–O) Å	ω(CO)^{scaled} cm^{-1}
gas-phase clusters					
Au_3^-	Au_{1c}	0.95	1.98	1.168	1995
Au_4^-	Au_{1c}	1.05	1.98	1.167	1993
	bridge	1.32	2.03	1.195	1833
Au_5^-	Au_{1c}	1.45	1.96	1.164	2036
Au_6^-	Au_{2c}	1.16	1.93	1.167	2025
Au_7^-	Au_{2c}	1.10	1.94	1.157	2089
Au_7^-	Au_{3c}	1.34	1.93	1.161	2068
Au_{12}^-	Au_{3c}	0.95	1.97	1.158	2064
	Au_{4c}	0.85	1.97	1.155	2091
Au_{12}	Au_{3c}	1.06	1.96	1.150	2141
Au_{22}^-	top	0.67	2.02	1.159	2043
	center	0.48	2.05	1.155	2067
	bottom	0.80	1.98	1.156	2075
Au_{22}	top	0.75	2.00	1.153	2098
	center	0.52	2.05	1.151	2110
	bottom	0.87	1.98	1.151	2114
supported clusters					
Au_3^-/MgO/Ag	Au_{1c}	0.99	1.96	1.155	2096
Au_4^-/MgO/Ag	Au_{1c}	0.49	2.06	1.161	2028
Au_5^-/MgO/Ag	Au_{1c}	0.90	1.94	1.151	2093
Au_{12}/MgO/Ag	Au_{3c}	0.72	1.99	1.158	2051
Au_{12}/MgO	Au_{3c}	0.87	1.96	1.151	2126
Au_{22}/MgO/Ag	top	0.89	1.97	1.152	2125
	center	0.74	1.97	1.151	2116
	bottom	0.86	1.97	1.156	2085
Au_{22}/MgO	top	1.15	1.96	1.152	2125
	bottom	0.81	1.99	1.152	2105

Table 7.1: Properties of CO adsorbed on free and supported Au clusters; a scaling factor of 1.0326 has been applied to all computed frequencies (see text).

7.4 Conclusions

From the results presented in the previous Sections, one can draw the following conclusions. CO does not bind to the high-coordinated Au atoms of 1D and 2D gold clusters or islands but only to the low-coordinated atoms at the periphery of these structures. This holds for both the gas-phase and supported clusters. For large 2D islands, this means that only a minority of the gold atoms are available to bind CO.

On the free clusters, the CO molecule is coplanar with the Au atoms of the 2D structures; on the supported clusters, the molecule forms a tilt angle of about 40°–50° with the surface normalr; this means that the intensity of the corresponding vibrational mode will be reduced since the component of the dipole change parallel to the surface will be canceled by surface dipole selection rules.

In the gas-phase, the bonding of CO to the Au clusters is strong, nearly 1 eV, and varies only moderately with the charge (0 or -1). On Au clusters supported on MgO/Ag(001) thin films, the CO molecule is slightly less bound, 0.7–0.9 eV. Only on Au_4/MgO/Ag(001) we compute a much lower bond, 0.5 eV, due to the fact that on this cluster, two extra charges are transferred from the substrate, resulting in a larger Pauli repulsion and weaker bonding. These binding energies are overestimated because of the use of the PW91 functional. Estimating an overbinding of PW91 of 50%, the expected real binding energies for most clusters should be about 0.5–0.6 eV. Using a Redhead equation and a frequency factor ν = 1013 s^{-1}, a binding energy of 0.5–0.6 eV corresponds to a desorption temperature of about 200–250 K in a thermal programmed desorption (TPD) experiment.

The vibrational frequency of CO adsorbed to a Au cluster has been scaled taking as a reference the Au_3CO^- gas-phase complex, for which a clear experimental value exists. With this scaling, we found that the frequency of CO adsorbed on neutral Au_{22} is 2100–2120 cm^{-1}; on negatively charged free clusters the CO frequency ranges between 1993 cm^{-1} (Au_4^-) and 2089 cm^{-1} (Au_7^-) with a large spread of values, depending on the cluster size, shape and on the adsorption site. For the same cluster and adsorption site, the red-shift due to the extra charge is about 50–60 cm^{-1}. These values are consistent with those reported in the literature for neutral and negatively charged gold clusters due to the interaction with defects. A red-shift of about 50–60 cm^{-1} (or less) is found also for gold clusters deposited on MgO/Ag(001) thin films compared to the same clusters deposited on bare MgO(001) or to neutral gas-phase clusters. This shift confirms the occurrence of a charge transfer from the metal

support to the deposited gold cluster. However, the shift is found only for small 1D or 2D clusters or, for 3D clusters, when the CO molecule is bound at the MgO/Au interface. On 3D gold clusters, CO adsorbs on the top layers with binding energies and vibrational frequencies rather typical of neutral gold clusters on MgO. This shows that the charging effect is largely restricted to the gold layer at the interface with the oxide support.

On the basis of all these considerations, we conclude that it may be difficult to measure the vibrational frequencies of CO adsorbed onto an ensemble of charged Au nanoclusters deposited on oxide ultrathin films. Three main effects will hamper their observation in an infrared experiment: (1) only a small fraction of the total Au atoms are binding sites for CO on these 1D and 2D clusters; (2) in case the particle size distribution is not a δ function, the oscillator strength of the CO stretching vibrations will be spread over approximately 100 cm^{-1}. This weakens the intensity of individual lines small and hence renders experimental limitations such as background stability a crucial issue; and (3) the tilted orientation of CO adsorbed at the cluster-surface boundary reduces the intensity of the IR vibration because of the surface selection rule.

The results of this chapter have been reported in the following publication:
S. Sicolo, L. Giordano, G. Pacchioni, *J. Phys. Chem. C* **113** (2009), p. 10256.

Bibliography

[1] G. Pacchioni, L. Giordano, M. Baistrocchi, *Phys. Rev. Lett.* **94** (2005), p. 226104.

[2] S. Schintke, S. Messerli, M. Pivetta, F. Patthey, L. Libioulle, M. Stengel, A. De Vita, W.-D. Schneider, *Phys. Rev. Lett.* **87** (2001), p. 276801.i

[3] X. Wu, L. Senapati, S. K. Nayak, A. Selloni, M. Hajaligol, *J. Chem. Phys.* **117** (2002), p. 4010.

[4] P. S. Bagus, G. Pacchioni, *J. Phys.: Conf. Ser.* (2008), p. 117012003.

[5] M. Sterrer, M. Yulikov, T. Risse, H.-J. Freund, J. Carrasco, F. Illas, C. Di Valentin, L. Giordano, G. Pacchioni, *Angew. Chem., Int. Ed.* (2006), **45**, p. 2633.

[6] Y. Wang, S. De Gironcoli, N. S. Hush, J. R. Reimers, *J. Am. Chem. Soc.* **129** (2007), p. 10402.

[7] G. Kresse, A. Gil, P. Sautet, *Phys. Rev. B* (2003), p. 68073401.

[8] A. Fielicke, G. Von Helden, G. Mejer, B. Simard, D. M. Rayner, *J. Phys. Chem. B* **109** (2005), p. 23935.

[9] F. Furche, R. Alrichs, P. Weis, C. Jacob, S. Gilb, T. Bierweiler, M. M. Kappes, *J. Chem. Phys.* **117** (2002), p. 6982.

[10] M. Sterrer, M. Yulikov, E. Fishbach, M. Heyde, H.-P. Rust, G. Pacchioni, T. Risse, H.-J. Freund, *Angew. Chem., Int. Ed.* **45** (2006), p. 2630.

[11] V. Simic-Milosevic, M. Heyde, X. Lin, T. Knig, H.-P. Rust, M. Sterrer, T. Risse, N. Nilius, H.-J. Freund, L. Giordano, G. Pacchioni, *Phys. Rev. B* **78** (2008), p. 235429.

[12] H.-J. Zhai, L.-L. Pan, B. Dai, B. Kiran, J. Li, L.-S. Wang, *J. Phys. Chem. C* **112** (2008), p. 11920.

[13] L. M. Molina, J. A. Alonso, *J. Phys. Chem. C* **111** (2007), p. 6668.

[14] P. Frondelius, H. Häkkinen, K. Honkala, *Phys. Rev. B* (2007), p. 76073406.

[15] D. Ricci, A. Bongiorno, G. Pacchioni, U. Landman, *Phys. Rev. Lett.* (2006), p. 97036106.

[16] L. M. Molina, B. Hammer, *Phys. Rev. Lett.* **90** (2003), p. 206102.

[17] L. M. Molina, B. Hammer, *Phys. Rev. B* **69** (2004), p. 155424.

[18] C. Zhang, B. Yoon, U. Landman, *J. Am. Chem. Soc.* **129** (2007), p. 2228.

Chapter 8

Formation of AuPt bimetallic clusters on MgO/Ag(100) ultrathin films

8.1 Abstract

Bimetallic clusters and surfaces often exhibit superior properties (chemical, optical, magnetic, ...) which are not the same of the constituent elements. In the context of metal clusters activation on oxide thin films, we investigate the opportunity to design new systems by exploiting the characteristics of two different metals. The guiding lines for the synthesis of such systems bases on the evidence that Pt binds much more strongly than other metals to MgO thin films, whereas charging phenomena seem to be triggered by the adsorption of Au (see Chapter 5). We will show that, due to the stronger Pt-oxide bonds, it is possible in principle to design systems where the nucleation and growth is is determined by the presence of adsorbed Pt atoms acting as anchoring sites, whereas spontaneous charging is guaranteed by the presence of the Au atoms. Making use of plane waves gradient corrected density functional theory (DFT), we have determined the preferred structures and analyzed the final charge state of the supported cluster.

8.2 Computational details

We have performed spin polarized DFT calculations at the level of the generalized gradient approximation (PW91 exchange-correlation functional) as implemented in the VASP program, which uses a plane wave basis set and a projector augmented wave method (PAW) for the treatment of core electrons (see Chapter 2). MgO ultrathin films have been represented by two MgO layers deposited on three Ag(100) layers, the bottom one being frozen in order to account for the behaviour of the

bulk. In order to allow for a perfect interface, the MgO lattice parameter has been adapted to that of the underlying metal, which means a compression of 2% for the case of Ag(100). For the calculations we used 3×3, 3×5 (for the linear trimers) and 4×5 (for the pentamer) supercells and the atoms within the supercell have been relaxed until a 0.01 eV/Å convergence threshold was reached for atomic forces. Brillouin-zone sampling has been performed on a 4×4×1 k-points mesh according to MonkhorstPack integration scheme. The properties of the PtAu clusters have been analyzed by considering different isomers, performing optimizations without symmetry constraints.

8.3 Results and discussion

We define the adsorption energy, $\mathrm{E_a}$, of a cluster $\mathrm{Pt}_m\mathrm{Au}_n$ on the MgO/Ag(100) surface as:

$$\mathrm{E_a} = -\mathrm{E(Pt_mAu_n/MgO/Ag)} + \mathrm{E(Pt_mAu_n)} + \mathrm{E(MgO/Ag)} \tag{8.1}$$

Thus, a positive $\mathrm{E_a}$ indicates a bound state for the atom or the cluster compared to the gas-phase.

In order to evaluate the spontaneity of the nucleation of gold clusters at an adsorbed Pt site, we calculate the cluster binding energy, $\mathrm{E_b}$, which measures the stability of a supported PtAu_n cluster with respect to a pre-existing adsorbed PtAu_{n-1} unit and a Au atom diffusing on the MgO film:

$$\mathrm{E_b} = -\mathrm{E(PtAu_n/MgO/Ag)} + \mathrm{E(PtAu_{n-1}/MgO/Ag)} + \mathrm{E(Au_1/MgO/Ag)} - \mathrm{E(MgO/Ag)} \tag{8.2}$$

In typical growth conditions $\mathrm{E_b}$, which must be a positive number according to the notation of the latter equation, is the critical quantity since cluster formation is dominated by diffusion of adsorbed atoms and not by direct attachment from the gas-phase.

8.3.1 Au and Pt atoms on MgO/Ag(100)

The adsorption properties of Au and Pt atoms on MgO ultrathin films have been discussed at length in previous works (see also Chapter 5).[1–3] A charge transfer occurs when Au is adsorbed on all sites of the MgO film, Mg-top, O-top and 4-fold hollow. The hollow site is the preferred one, but small energy differences of

0.1-0.2 eV separate this from the other sites. This suggests that the diffusion of Au atoms on the MgO/Ag(100) films occurs with energy barriers of about 0.2 eV at most and possibly even smaller. Thus, Au atoms deposited on the films will rapidly diffuse even at temperatures as low as about 100 K and will be trapped only at more strongly binding sites like point or extended defects (step edges, vacancies, etc.). It is only at very low temperatures (< 10 K) that the Au atoms can be stabilized on the flat terraces of the MgO films.[3]

The situation is quite different in the case of Pt. The anionic sites of MgO bind Pt atoms much stronger than the Mg and hollow ones and more than any other studied metal by about 1 eV (see Chapter 5). The hollow site thus represents the preferred site for diffusion, but the energy is about 0.7 eV higher than on the O-top site, which can be taken as an estimate of the real diffusion barrier. Such a barrier suggests that the diffusion process for Pt atoms on MgO/Ag(100) films is much more difficult than for Au. Assuming a simple activated diffusion with a typical exponential prefactor of 10^{-11}, a barrier of 0.7 eV corresponds to a diffusion temperature of about 300 K. There is also another reason why the Pt diffusion can be much more difficult than for Au. On the surface of a MgO thin film, Au atoms turn into anions because of the interaction with basically all the available sites of the surface, so that there is no change in the character of the adsorbate during the diffusion process. Instead, Pt forms a covalent polar bond with O sites, with only a partial charge transfer, whereas it carries a net charge close to 1 e^- when sitting on the hollow sites. This means that a charge rearrangement must take place during the diffusion process. More important, the charge transfer is accompanied by a significant lattice distortion (polaronic distortion) which may further reduce the mobility of the adsorbed Pt atoms. This makes the Pt atoms excellent candidates to act as nucleation sites for the growth of PtAu bimetallic clusters.

8.3.2 PtAu dimers on MgO/Ag(100)

Gas-phase AuPt has a doublet ground state with a singly occupied Pt $5d_{z^2}$ orbital; the molecule is strongly bound, 2.58 eV, and is characterized by a bond distance of 2.48 Å. These values are similar to those reported in the literature.[4,5] We have considered several possible orientations of the PtAu molecule on the MgO/Ag(100) film. In some of these structures the molecule lies flat on the surface, with the Pt atom bound to a surface oxygen and the Au atom either close to Mg or O sites; in

other configurations the molecule is upstanding, normal or bent with respect to the surface plane.

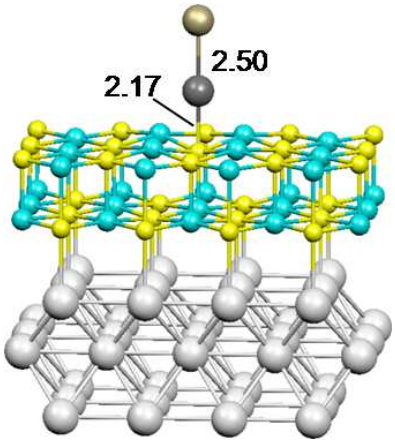

Figure 8.1: Side view of a PtAu dimer adsorbed on-top of an O^{2-} ion of a two-layers MgO film deposited over the Ag(100) surface. Pt is directly bond to the MgO film. Selected distances are given in Å.

In these cases both Pt or Au atoms sitting either O-top or Mg-top have been considered. However, the only stable minima are those where the molecule is standing perpendicular to the surface with one metal atom directly bound on top of O, Figure 8.1. Not surprisingly, the Pt-down isomer is 1.27 eV more stable than the Au-down one (E_a = 2.79 eV, Table 1). All other geometry optimizations led to one of these two minima. The formation of the PtAu most stable dimer is accompanied by E_b = 1.28 eV (Table 8.1), indicating that a diffusing Au atom will stick to the preadsorbed Pt forming a very stable species.

In both isomers the PtAu dimer changes the spin state from doublet to singlet by effect of the transfer of one electron from the MgO/Ag interface, with formation of a negatively charged $PtAu^-$ unit. This is consistent with a Bader charge that, for the ground state structure, is 1.07 e^-, with a larger portion of the extra electron on Pt (0.74 e^-) and the rest on Au (0.33 e^-), Table 1. Notice that the occurrence of a charge transfer has almost no effect on the Pt–Au distance which becomes 2.50 Å. This can be explained with the extra electron being largely localized on a non-bonding Pt atomic orbital, with little effect on the Pt–Au bond strength.

The large energy difference between the two isomers, Pt-down or Au-down, reflects the binding properties of the isolated Pt and Au atoms and shows the clear preference for having Pt directly in contact with the MgO film. The Au atoms can then bind to Pt which acts as a seed for the cluster growth. Also experimentally, the procedure consists in depositing Au after the deposition of Pt atoms in order to create anchoring sites for the nucleation of gold: in a recent study, Au, Pt, and Au–Pt clusters were grown on TiO_2(110) at room temperature and studied by scanning tunneling microscopy. For the same metal coverages, the deposition of pure Pt resulted in smaller clusters and higher cluster densities compared to pure Au, because of the greater mobility of Au on the surface. For the deposition of 0.024 ML of Pt followed by 0.072 ML of Au, bimetallic clusters were formed from the nucleation of Au at existing Pt clusters, whereas the reverse order of deposition resulted in pure Pt clusters and pure Au clusters coexisting on the surface. The presence of Pt in the bimetallic Pt–Au clusters inhibits sintering, and the average size of the clusters after annealing decreases with increasing Pt composition.[6]

8.3.3 $PtAu_2$ and Pt_2Au clusters on MgO/Ag(100)

In this section we consider the structure of bimetallic PtAu trimers. The lowest gas-phase isomer of $PtAu_2$ is a triangle with Pt–Au distances of 2.55 Å and Au–Au distance of 2.79 Å, Figure 8.2a The binding energy per atom, D_e, is 1.65 eV. This structure is definitely more stable than the linear isomer reported by Song *et al.* as the ground state of $PtAu_2$. In this latter structure Pt is between two Au atoms. According to our calculations this structure is not even a minimum, and, if computed with a geometrical constraint, it is less stable by 0.30 eV (D_e = 1.65 vs. 1.35 eV).

On the MgO surface we have considered initial $PtAu_2$ geometries where one Pt atom is on-top of O^{2-} ion. The most stable isomer, E_a = 2.30 eV (Table 8.1), has the same triangular shape found in gas-phase, with one of the Au atoms pointing toward a Mg^{2+} cation of the surface and the other Au atom on-top of the Pt, Figure 8.3a, defining the plane of the cluster which is therefore perpendicular to the surface. The cluster is charged, as shown by the Bader charge, 0.81 e^-, and by the spin population, 0.72: having the gas-phase $PtAu_2$ a singlet ground state, the Bader charge and the spin population are both null. The negative charge on the cluster explains the favorable attractive interaction between one Au atom and the surface cation. Starting the geometry optimization from a triangular unit parallel to the

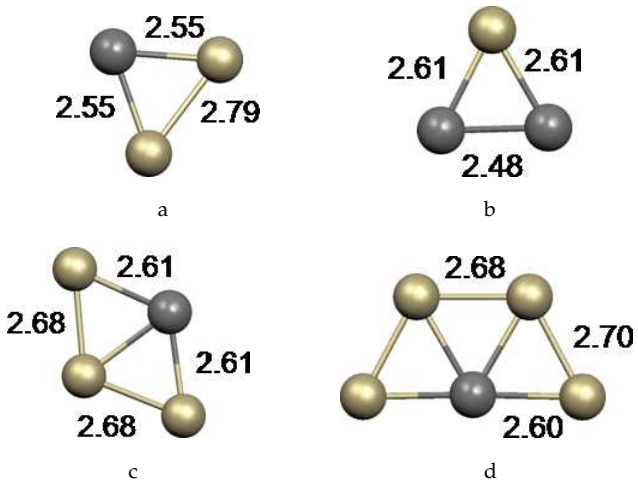

Figure 8.2: Optimized structures of the most stable Pt_nAu_m gas-phase isomers. Selected distances are given in Å.

surface results in the same standing cluster described above. Another minimum is found when the optimization starts from a linear Au-Pt-Au cluster (the two Au atoms are oriented towards the surface O ions, Figure 8.3b). This isomer is only a local minimum, E_a = 2.07 eV, but it is also charged, carrying 1.43 e^-, and has a spin population close to 1. The attachment of a second Au atom to an existing PtAu dimer exhibits a cluster binding energy E_b which is only 0.24 eV for the most stable isomer, slightly higher than the barrier for Au diffusion on the surface. This means that at moderate temperatures there is a finite possibility that the Au atoms will detach from the adsorbed $PtAu_2$ complex and further diffuse on the surface.

The other trimer considered is Pt_2Au, Figure 8.3c. In the gas-phase this cluster is triangular with Pt–Au distances of 2.61 Å and a Pt–Pt distance of 2.48 Å, Figure 8.2. The binding energy per atom is 1.98 eV. On the MgO film the cluster is preferentially bound with the two Pt atoms sitting near two O^{2-} ions of the surface and the Au atom in bridge position over the Pt atoms forming a perfect isosceles triangle. The metal-metal bond distances are 2.60 Å, and a short Pt–O interface bond, 2.12 Å, is formed. The cluster plane is normal to the surface.

There are two possible orientations for this cluster, one aligned along the (110) direction and one along the (100) direction, Figure 8.3c and d. In this latter case, in fact, the Pt–Pt distance, 2.60 Å, is closer to the O–O one, 2.98 Å, than in the (100)

orientation where the distance between the O^{2-} ions, separated by a Mg^{2+} cation, is of 4.16 Å. This leads to a considerable strain in the cluster and an elongated Pt-Pt distance of 2.67 Å, with partial loss of stability. The two structures are bound by 3.17 eV and 3.01 eV, respectively, with respect to gas-phase Pt_2Au. Attempts to optimize triangular clusters parallel to the MgO surface failed as the structure goes back to those described above. We have also considered a linear structure where a Au atom

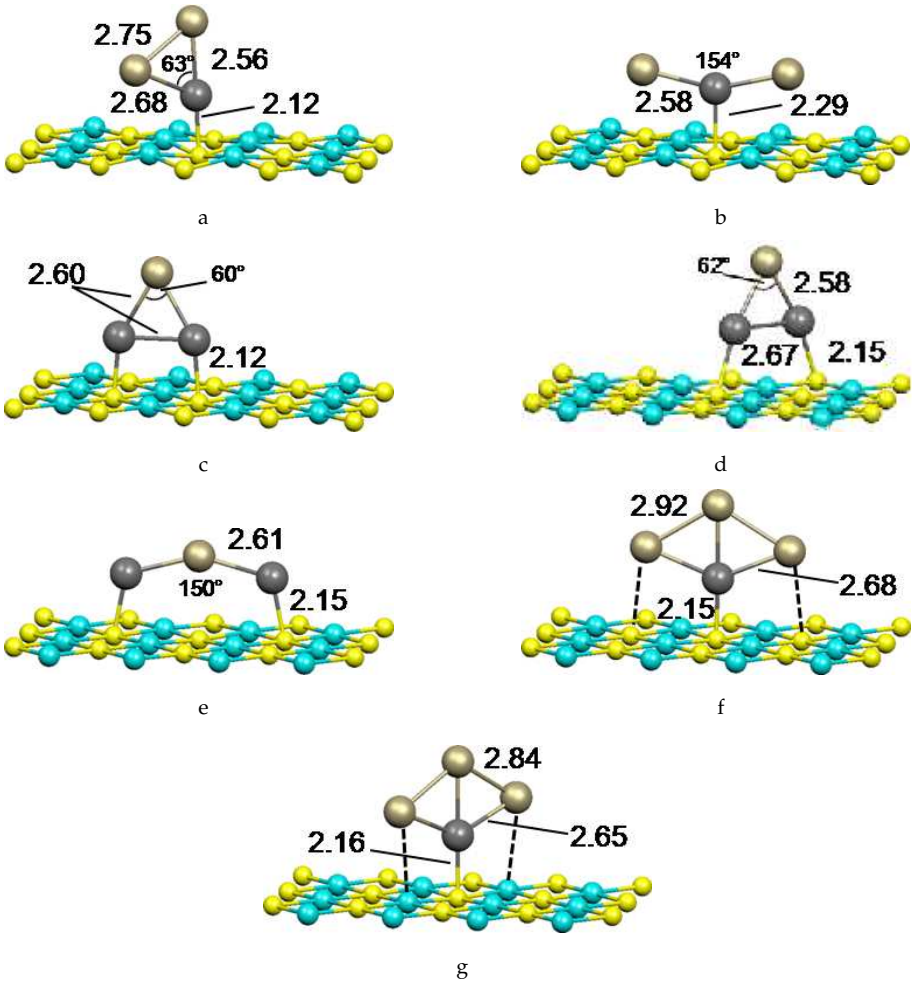

Figure 8.3: Optimized structures of the most stable Pt_nAu_m isomers adsorbed on MgO/Ag(100) films. Only the top MgO layer is shown for clarity. Selected distances are given in Å.

is between two Pt atoms, Figure 8.3e. In this case, however, the loss of Pt–Pt bonding introduces a penalty which is not compensated by the formation of two Pt–O bonds and the structure is about 1 eV less stable than the triangular units.

All Pt_2Au trimers considered show the occurrence of a charge transfer and the formation of a negatively charged species, as shown by the value of the Bader charge, 0.81 e^- for the triangle and 1.34 e^- for the chain-like structure, Table 8.1. The two structures are spin polarized with nearly one unpaired electron.

These results show the preference to form Pt–O bonds rather than Au–O bonds, already found for the isolated atoms (see Chapter 5). Taking into account the informations underlying the synthesis of supported Au–Pt bimetallic clusters[6] also confirmed by our theoretical calculations, we chose to focus the work only on Pt_1Au_n clusters anchored to the surface by means of a Pt–O bond, reproducing the experimental conditions which rely on the role of Pt as nucleation site for diffusing Au atoms.

8.3.4 $PtAu_3$ clusters on MgO/Ag (100)

Gas-phase $PtAu_3$ is a rhombus, Figure 8.2c.[7] There are two possible isomers, one with the Pt atom along the short diagonal, preferred, and a second one where Pt is on the long diagonal. Another low-lying isomer is a triangular piramid with Pt above a Au_3 triangle. On the MgO/Ag(100) film the planar rhombus is the preferred isomer, Figure 8.3f and g. The cluster is anchored to the surface via a direct Pt–O bond (2.15 Å) and keeps essentially the gas-phase structure. Two possible isomers exist depending on the orientation of the cluster plane along the (100) or the (110) directions. The binding energies computed with respect to gas-phase $PtAu_3$ are 2.97 eV for the (110)-aligned isomer and 2.94 eV for the (100) case. The small energy difference suggests a free rotation of the molecule around the Pt–O bond. Also in this case a flat lying $PtAu_3$ cluster is unstable. The attachment of a third Au atom to a pre-existing $PtAu_2$ complex to form the $PtAu_3$ supported species gives a cluster binding energy E_b = 1.20 eV (Table 8.1) and in this case Au atoms will hardly leave the cluster.

At variance with the gas-phase cluster, which has a magnetic moment close to 1 (the spin population is 0.75), by effect of the charge transfer the supported $PtAu_3$ cluster is diamagnetic and carries a net negative charge, Table 8.1.

8.4 Conclusions

As aforementioned, Pt atoms can act as nucleation centers for small PtAu bimetallic clusters on the surface of MgO/Ag(100) thin films. Pt atoms bind quite strongly to the O^{2-} surface sites, 2.45 eV, and we estimate a lowest diffusion path on the MgO flat terraces via hollow sites, whose energy is about 0.7 eV higher than the ground state. On the contrary, Au atoms exhibit very low diffusion barriers (0.1-0.2 eV) so that they usually experience long diffusion lengths even at moderately low temperatures. Small amounts of Pt atoms deposited on MgO thin films can in principle act as nucleation centers for small Pt_1Au_n clusters. According to this preliminary study, still in progress, these clusters become negatively charged and possibly more reactive than their neutral counterparts.

In the following table, the most relevant properties of the clusters studied so far are shown.

	PtAu	$PtAu_2$	Pt_2Au	$PtAu_3$
E_a,eV	2.79	2.30	3.17	2.97
E_b, eV	1.28	0.24	–	1.20
Spin population	0.0	0.72	0.65	0.0
Bader charge (total)	1.07	0.81	0.77	1.04
Bader charge (Pt)	0.74	0.37	0.32	0.26
Bader charge (Au)	0.33	0.23	0.14	0.26

Table 8.1: Properties of the most stable isomers of PtAu bimetallic clusters adsorbed on a two-layers MgO/Ag(100) film.

The results of this chapter are still work in progress.

Bibliography

[1] G. Pacchioni, L. Giordano, M. Baistrocchi, *Phys. Rev. Lett.* **94** (2005), p. 226104.

[2] K. Honkala, H. Häkkinen, *J. Phys. Chem. C* **111** (2007), p. 4319.

[3] M. Sterrer, T. Risse, U. Martinez Pozzoni, L. Giordano, M. Heyde, H.-P. Rust, G. Pacchioni, H.-J. Freund, *Phys. Rev. Lett.* **98** (2007), p. 096107.

[4] W. Q. Tian, M. Ge, F. Gu, T. Yamada, Y. Aoki, *J. Phys. Chem. A* **100** (2006), p. 6285.

[5] G. Jian-Jun, Y. Ji-Xian, D. Dong, *J. Mol. Struct. THEOCHEM* **764** (2006), p. 117.

[6] J. B. Park, S. F. Conner, D. A. Chen, *J. Phys. Chem. C* **112** (2008), p. 5490.

[7] C. Song, C.; Q. Ge, L. Wang, *J. Phys. Chem. B* **109** (2005), p. 22341.

Publications

The results discussed in this thesis have been presented in the following publications:

- S. Sicolo, L. Giordano, G. Pacchioni, ADSORPTION OF LATE TRANSITION METAL ATOMS ON MGO/MO(100) AND MGO/AG(100) ULTRATHIN FILMS: A COMPARATIVE DFT STUDY, *J. Phys. Chem C* **113** (2009), p. 16694.

- S. Sicolo, L. Giordano, G. Pacchioni, CO ADSORPTION ON ONE-, TWO- AND THREE-DIMENSIONAL AU CLUSTERS SUPPORTED ON MGO/AG(001) ULTRATHIN FILMS, *J. Phys. Chem. C* **113** (2009), p. 10256.

- S. Sicolo, G. Pacchioni, CHARGING AND STABILIZATION OF PD ATOMS AND CLUSTERS ON AN ELECTRON-RICH MGO SURFACE, *Surf. Sci.* **602** (2008), p. 2801.

- G. Pacchioni, S. Sicolo, C. Di Valentin, M. Chiesa, E. Giamello, A ROUTE TOWARD THE GENERATION OF THERMALLY STABLE AU CLUSTER ANIONS SUPPORTED ON THE MGO SURFACE, *J. Am. Chem. Soc.* **130** (2008), p. 8690.

- L. Giordano, U. Martinez, S. Sicolo, G. Pacchioni, OBSERVABLE CONSEQUENCES OF FORMATION OF AU ANIONS FROM DEPOSITION OF AU ATOMS ON ULTRATHIN OXIDE FILMS, *J. Chem. Phys.* **127** (2007), p. 144713.

Where other sources of information have been used, they have been acknowledged.